Addis Ababa University

Addis Ababa Institute of Technology

School of Electrical and Computer Engineering

Performance Analysis and Optimization in Massive MIMO Systems

---

By: Amare Kassaw Yimer

Supervisor: Prof. Dr. -Ing. Abdelhak M. Zoubir

Co-Supervisor: Dr. -Ing. Dereje Hailemariam

A PhD Dissertation Submitted to the School of Electrical and Computer Engineering, Addis Ababa Institute of Technology, Addis Ababa University in Partial Fulfillment of the Requirements of the Degree of Doctor of Philosophy in Communication Engineering.

04 March, 2021

Approval Page

Addis Ababa University

Addis Ababa Institute of Technology

School of Electrical and Computer Engineering

Performance Analysis and Optimization in Massive MIMO Systems

By: Amare Kassaw Yimer

Approval by Examiners

Prof. Dr. -Ing. Abdelhak M. Zoubir	_____
Supervisor	Signature
Dr. -Ing. Dereje Hailemariam	_____
Co-Supervisor	Signature
Dr. Yalemzewd Negash	_____
Dean, SECE, AAiT	Signature
Dr. Beneyam Berehanu	_____
Internal Examiner	Signature
Prof. Dr. -Ing. Anja Klein	_____
External Examiner	Signature

Declaration

This PhD Dissertation is a presentation of my own research work and that any material used from other sources has been clearly identified, and properly acknowledged and cited.

Amare Kassaw Yimer 

Name Signature

Place: Addis Ababa

Date of Defense: 04 March, 2021

This PhD Dissertation has been submitted with the approval of my supervisors.

Prof. Dr. -Ing. Abdelhak M. Zoubir _____

Supervisor Signature

Dr. -Ing. Dereje Hailemariam _____

Co-Supervisor Signature

Abstract

Next generation networks are expected to support large volume of data traffic generated from emerging applications such as ultra high speed video streaming, machine-to-machine (M2M) communication and the Internet of things (IoT). To handle this large volume of data traffic, these networks should employ technologies that utilize broad spectrum, offer higher cell density and high spectral efficiency. The spectral efficiency can be improved by increasing the transmitter power; introducing additional processing (such as deploying multiple antenna systems and advanced modulation techniques) in transceiver pairs that help to harvest energy; minimize multiuser-interference; and implementing innovative wireless planning and operation strategies that save energy.

By deploying very large numbers of antennas at a base station (BS), which is called massive multiple input multiple output (MIMO), we can significantly improve the spectral efficiency of mobile networks. Besides, massive MIMO simplifies transmission processing, improves energy efficiency and reduces the required transmission power of the users. Due to those performance gains, massive MIMO has become an enabler for the deployment of 5G and beyond networks.

In this PhD research, we study and analyze channel modeling, resource allocation and optimization techniques in massive MIMO systems. For this, first we analyze recent works on signal processing, channel modeling, channel estimation, resource allocation and optimization techniques in massive MIMO systems. In this regard, fundamentals of massive MIMO systems including channel capacity, spectral efficiency and energy efficiency have been studied. Closedform lower bound expressions are derived for the spectral efficiency and energy efficiency. Then, simulation results are provided to validate the theoretical analysis. Besides, performance analysis is done for linear detection and precoding techniques and then computationally efficient inverse approximation techniques are proposed for linear detection and precoding in massive MIMO systems. Specifically, Truncated Neumann series-based matrix inversion approximation techniques are formulated and probability of

convergence, error of approximation and computationally complexity are analyzed.

Then, we analyze achievable spectral efficiency of massive MIMO systems in realistic propagation environment under perfect and imperfect channel state information (CSI) scenarios. In particular, the effects of major large scale and small fading parameters including pathloss, shadowing, multipath fading, spatial channel correlation and impact of channel estimation have been investigated. Spectral efficiency analysis is done for uplink massive MIMO system under Rician fading channel model. Besides, by applying non-central to central Wishart approximation, closedform lower bound achievable rate expressions are formulated for massive MIMO systems in Rican fading channel model.

Then, energy efficient power control and resource allocation algorithms have been proposed. For this, first by using large system analysis, analytical closedform lower bound expressions are derived for the achievable sum rate and appropriate power consumption model is formulated for the proposed massive MIMO systems. Then, by utilizing tools from fractional programming theory and sequential convex programming, energy efficient power control and resource allocation algorithms have been formulated. Further, the impacts of system and propagation parameters on energy efficiency have been evaluated. Particularly, the impacts of maximums transmitter power and minimum rate constraints of the users on global energy efficiency have been evaluated. The results show that the global energy efficiency increases with the maximum transmitter power constraint and decreases with the minimum data rate constraint.

Finally, we analyze the performance of multicell massive MIMO systems in spatially correlated channel model. First, we study and evaluate fundamentals of multicell massive MIMO systems. In this regard channel modeling, power allocation and spatial resource allocation in multicell massive MIMO systems are considered. Besides, we evaluate the impacts of spatial correlation and pilot contamination. Important trade-offs and considerations on design and optimization of multicell massive MIMO systems has been studied. The impacts of system and propagation parameters are evaluated theoretically and via numerical simulation. The results show that spatial channel correlation has a major impact on channel hardening, favorable propagation, channel estimation quality and spectral efficiency of the system.

Key Words: 5G, massive MIMO, spectral efficiency, energy efficiency, optimization, resource allocation.

List of Publications

The publications that emanated from this PhD research are listed below.

1. Amare Kassaw, Dereje Hailemariam, Michael Fauß, Abdelhak M. Zoubir, "Energy efficient power control in uplink massive MIMO systems: A fractional programming approach," under review, Elsevier Journal of Physical Communication.

2. Amare Kassaw, Fikiraddis Tazeb, Dereje Hailemariam, "Performance analysis of multicarrier modulation techniques for next generation networks," 8*th International Conference on the Advancements of science and technology (ICAST2020)*, Oct, 2020, Bahir Dar, Ethiopia.

3. Amare Kassaw, Dereje Hailemariam, Michael Fauß, Abdelhak M. Zoubir, "Fractional programming for energy efficient power control in uplink massive MIMO systems," 27*th European Signal Processing Conference (EUSIPCO2019)*, ACoruna, Spain, Sep, 2019.

4. Amare Kassaw, Dereje Hailemariam, Abdelhak M. Zoubir, "Review of energy efficient resource allocation techniques in massive MIMO systems," 9*th International Conference on Information and Communication Technology Convergence (ICTC2018)*, Korea, 2018.

5. Amare Kassaw, Dereje Hailemariam, Abdelhak M. Zoubir, "Performance analysis of uplink massive MIMO system over Rician fading channel," 26*th European Signal Processing Conference (EUSIPCO2018)*, Rome, 2018.

6. Amare Kassaw, Dereje Hailemariam, Abdelhak M. Zoubir, "Review of truncated Neumann series based detection in massive MIMO systems," *IEEE Wireless Africa Conference*, Addis Ababa, 2018.

7. Tewelgn Kebede, Amare Kassaw, Yihenew Wondie, Johannes Stenibrunn, "Joint evaluation of spectral efficiency, energy efficiency and transmission reliability in mas-

sive MIMO systems," 7*th International Conference on the Advancements of Science and Technology (ICAST2019)*, Bahir Dar-Ethiopia, August 2019.

8. Amare Kassaw, Dereje Hailemariam, Abdelhak M. Zoubir, "Performance analysis in massive MIMO systems," 6*th International Conference on the Advancements of Science and Technology (ICAST2018)*, Bahir Dar, Ethiopia, 2018.

9. Amare Kassaw, Zemene Matewos, Dereje Hailemariam, "Digital dividend and its opportunities for long term evolution mobile network: the case of Ethiopia," *IEEE AFRICON 2017*, Cape Town, 2017.

10. Amare Kassaw, Dereje Hailemariam, Abdelhak M. Zoubir, "Performance analysis of multiple antenna based blind spectrum sensing techniques for cognitive radio networks," 5*th International Conference on the Advancements of Science and Technology (ICAST2017)*, Bahir Dar, 2017.

Acknowledgment

First and foremost, I would like to extend my utmost gratitude and appreciation to my supervisor, Prof. Dr.-Ing. Abdelhak M. Zoubir. His excellent supervision with invaluable comments, suggestions and directions were very helpful to progress on my research. Prof. Zoubir also provided the necessary facilities and follow up during my research stay at Signal Processing Group, Technical University of Darmstadt. I also extend my gratitude to my co-supervisor Dr.-Ing Dereje Hailemariam. His advice and encouragement have increased my motivation over the years. The regular discussions and conversations were very vital and constructive that inspired me to think outside the box from multiple perspectives and helped to form a comprehensive and structured analysis and formulations. Dr. Dereje's supervision is not only limited to academics matters, it also spans on how to manage the family and life in general.

I would also extend my gratitude to my examiners Prof. Dr. -Ing. Anja Klein and Dr. Beneyam Berehanu for the willingness to review my work in this hard and busy time. The comments, suggestions and questions from them are very constructive, aspiring and technical. I would also like to extend my gratitude to Dr.-Ing. Michael Fauss at Technical University of Darmstadt, and Dr. Ephrem Teshale and Dr. Bisrat Derebssa at Addis Ababa Institute of Technology for the technical support, discussion and guidance. They contribute and help me a lot for the successful completion of this PhD study. Besides, I would also like to extend my appreciation to the Signal Processing Group at Technical University of Darmstadt and the Communication Engineering staff and PhD students at Addis Ababa Institute of Technology for the support, guidance and follow up.

I would also extend my gratitude to Addis Ababa Institute of Technology, Addis Ababa University and Bahir Dar Institute of Technology, Bahir Dar University for research funding and conference travel support. I also thank the German Academic Exchange Service (DAAD), Technical University of Darmstadt and the Ethiopian Ministry of Science and Higher Education for supporting and research funding.

Last but not least, I express my utmost gratitude to my families and friends who are my main source of motivation at any time and for every thing I do. Specifically, I express my utmost gratitude to my love, Meseret, who faced all the challenges alone in the last four years.

Contents

List of Figures

List of Tables

List of Acronyms

5G	Fifth generation
APP	A posteriori probability
BP	Belief propagation
BS	Base station
COMP	Coordinated multipoint
CSI	Channel state informaiton
ESPIRIT	Estimation of signal parameters via rotational invariance techniques
EVD	Eigenvalue decomposition
FBMC	Filter bank multicarrier
FDD	Frequency division duplex
GEE	Global energy efficiency
GFDM	Generalized frequency division multiplexing
HetNet	Hetrogenous networks
ICA	Independent component analysis
iid	Independent and identically distributed
IoT	Internet of things
IUI	Inter user interference
LS	Least squares
LSF	Large scale fading
LTE	Longterm evolution
M2M	Machine to machine
MCMC	Markov chain Monte Carlo
ML	Maximum likelihood
MMSE	Minimum mean square error
MRC	Maximum ratio combining

MRT	Maximum ratio transmission
MU-MIMO	Multiuser MIMO systems
MUSIC	Multiple signal classification
NOMA	Non-orthogonal multiple access
OFDM	Orthogonal frequency division multiplexing
PDA	Probabilistic data association
RAN	Radio acess network
RAT	Radio access technology
SAGE	Space alternating generalized expectation
SDMA	Space division multiple access
SDR	Semi-definite relaxation
SNR	Signal to noise ratio
SVD	SIngular value decomposition
TDD	Time division duplex
WMEE	Weighted minimum energy efficiency
WPEE	Weighted product energy efficiency
WSEE	Weighted sum energy efficiency
ZF	Zero forcing

List of Notations

a	Scalar value
$\mathbf{a}$	Vector value
$\mathbf{A}$	Matrix $\mathbf{A}$
$\mathbb{R}$	Set of real numbers
$\mathbb{Z}$	Set of integers
$\mathbb{C}$	Set of complex numbers
$\mathbb{Z}_+$	Set of strictly positive integers
$\mathbf{A}^{\mathrm{H}}$	Matrix conjugate transpose
$\mathbf{A}^{\mathrm{T}}$	Matrix transpose
$\mathbf{A}^*$	Conjugate of matrix
$\mathbf{A}^{-1}$	Inverse of matrix
$\mathrm{Tr}(\mathbf{A})$	Trace of a square matrix $\mathbf{A}$
$\mathbf{A}_{ij}$	ijth element of matrix $\mathbf{A}$
$r(\mathbf{A})$	Spectral radius of $\mathbf{A}$
$\mathbf{I}_N$	Identity matrix of size N
$\mathbb{E}\{.\}$	Expectation operator
$\|.\|$	Euclidean norm
$\mathbf{x} \sim \mathcal{CN}(\boldsymbol{\mu}, \boldsymbol{\Sigma}\,\mathbf{I})$	Circular symmetric complex Gaussian distributed random variable

Chapter 1

Introduction

1.1 Background

Next generation wireless networks are expected to support large number of devices and connections. The vision is to establish a connected society in which sensors, automobiles, drones, medical and wearable devices will use mobile networks to connect each other and to interact with humans [1, 2]. The number of connected devices grows exponentially and this results in massive mobile data traffic [4–6]. The increasing growth of the data traffic intern stimulates the Telecom industry to plan a head and design mobile networks that can support this massive data traffic [4, 7–10]. Hence, the Telecom industry is releasing successive technologies with new features [5]. The recent release is the Long Term Evolution (LTE) Advanced-pro (Release 14) [11] that aims to provide higher capacity with the implementation of carrier aggregation, spatial multiplexing, base station coordination and advanced relaying [5, 11].

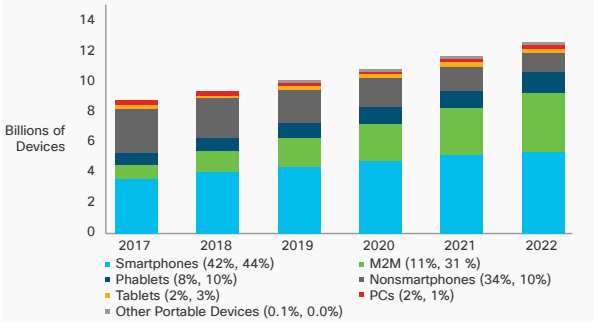

(a) Global mobile devices and connections growth.

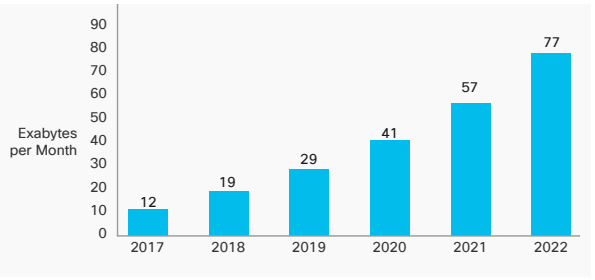

(b) Global mobile data traffic growth. More than seven times increase of mobile data traffice is expected from 2017 to 2022.

Figure 1.1: Cisco forcasts on growth of global mobile devices and associated data traffic [1].

Despite improvements achieve so far, increasing growth of the data traffic is forcing the development of fifth generation (5G) and beyond networks [4–9]. In addition to the current applications, these networks should support innovative services which were not possible due to capacity and latency constraints. Some examples of innovative services are ultra high video streaming, the Internet of Things (IoT), enhanced e-health and machine-to-machine (M2M) communications. To achieve the required capacity and performances, the 5G network working groups commonly recognize promising evolutions of current networks from three technical aspects; namely [8, 9]:

- high spectral efficiency that can be achieved by large scale antenna systems;
- broad spectrum that may need utilization of millimeter wave (mmWave) frequency bands;
- higher cell density that need small cells and heterogeneous deployment.

Considering these technical aspects, there are five requirements that have been taken into account during the 5G network design [8, 9]:

- **Area Capacity**: with the most recent forecasts, compared to the current LTE Advanced-pro networks, a thousand-fold capacity gains per area is needed [2, 12]. Hence, 5G networks could handle this large volume of mobile data traffic in the coverage area.
- **Data Rate**: in general, the data rates at the users should be higher than current networks. The idea is to deliver better quality of service (QoS) with respect to the user requests. 5G networks are expected to provide a data rate of at least 5 Gbps and 1 Gbps at 20% and 95% of the user locations from the BS, respectively. Users with poor coverage should also get a data rate of at least 100 Mbps in the downlink and 20 Mbps in the uplink [12].
- **Energy Efficiency**: the vision of next generation networks is to be more energy efficient at the device, site and network levels. This requires the usage of efficient components, energy harvesting technologies, network planning and deployment techniques, and optimal resource allocation algorithms [2].
- **Connectivity**: 5G systems are expected to support large number of connected devices at the same time with different services and requirements. Scenarios, such as

crowded places with massive deployment of sensors and other devices must be addressed in terms of connectivity. The target is to deploy a 100× gain on the number of simultaneously connected devices and provide up to 20 Mbps in the worst case scenarios [4].

- **Network Latency**: the latency over the radio access network (RAN) should be less than 1 ms which is five times less as compared to LTE Advanced-pro networks [4]. This would enable the possibility of applications such as augmented reality and real-time control of industrial processes.

As seen in the points described above, 5G networks are expected to have many gains compared to current LTE Advanced-pro networks. A viable option to achieve these gains is the combined use of technologies that provide broad spectrum, high spectral efficiency and high network density [2]. Improvements in these directions could help to fulfill the desired goals. Thus, by using the three degrees of freedom, the area throughput is given by [2]

$$\underbrace{\text{Area Throughput}}_{\text{bits/sec/area}} = \underbrace{\text{Available Spectrum}}_{\text{Hz}} . \underbrace{\text{Cell Density}}_{\text{cell/area}} . \underbrace{\text{Spectral Efficiency}}_{\text{bits/sec/Hz/cell}} . \tag{1.1}$$

An illustration for (1.1) is shown in Figure 1.2 which includes some of the candidate key technologies that could be implemented in 5G networks to achieve the proposed area throughput [5].

1.1.1 Candidate Technologies to Achieve the Area Throughput in Mobile Networks

Some of the enabling technologies for 5G network deployment are described as follows [2, 3, 8].

- **Massive MIMO**: multiple-input multiple-output (MIMO) systems with multiple antennas at the transmitter and/or receiver are used to achieve high capacity and link reliability by exploiting spatial multiplexing and diversity gains. In order to achieve the required capacity in 5G and beyond networks, employing very large number of antennas at the BS, which is called massive MIMO, is become a reality. Massive MIMO provides large spectral efficiency and energy efficiency while serving many users under the same time-frequency resources. In addition, massive MIMO simplifies

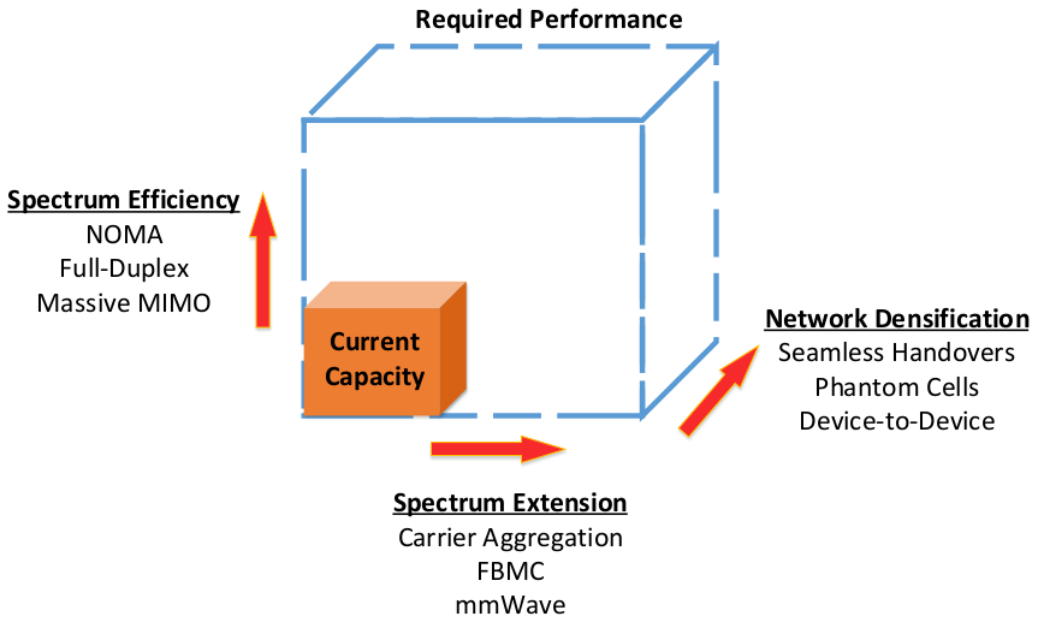

Figure 1.2: Possible paths to attain the required network capacity and candidate technologies for implementation [2].

the signal processing complexity and reduces the required transmission power of the users [2, 3, 10, 13–16]. The main benefits and challenges of massive MIMO systems are provided in Chapter 2.

- **Network Densification**: network densification enables networks to handle the required increase in capacity. It improves the network capacity via the introduction of low power nodes in high traffic areas. Small cells operate at high frequencies to improve the network throughput. The control signaling and handover management can be done by the macro cell that operate at low frequencies [2, 4]. Together, they form a heterogeneous network that consist of the hotspot tier and the coverage tier, respectively [2]. The hotspot tier mainly consists of indoor base stations that offer high throughput in small local areas to few users; whereas the coverage tier consist of outdoor cellular base stations that provide wide-area coverage, mobility support and multiplex many users [14, 17].

- **Waveform Design**: 5G networks are expected to use different spectrum bands that require different propagation conditions and modulation requirements. Thus, apart from orthogonal frequency division multiplexing (OFDM), other alternative multicarrier waveforms such as filter bank multicarrier modulation (FBMC), universal filter multicarrier modulation (UFMC), filtered-OFDM, generalized frequency divi-

sion multiplexing (GFDM) and non-orthogonal multiple access (NOMA) techniques are proposed [15,18]. NOMA is proposed to transmit data from different users in the same slot (time and frequency) and by exploiting the power domain, advanced successive interference cancellation schemes is used to decode the transmitted data [15].

- **mmWave Communication**: the use of millimeter wave (mmWave) frequency provides more bandwidth to support high data rates [19]. Still now, this band was not used for cellular communications due to high propagation losses. However, if network density is increased, distance between users and serving BS is reduced which enable the use of mmWave frequency bands [19]. But, high densification may lead to high levels of interference that significantly reduce the throughput [19]. Hence, a careful network planning is mandatory. Besides, conventional modulation and waveform synthesis techniques may not be convenient at these frequency bands. Hence, new waveform design may be needed [19].

- **Full Duplex Communication**: Implementing a software defined radio (SDN) system provides flexibility interms of utilized carrier frequency and duplex scheme. The combined use of time division duplex (TDD) and frequency division duplex (FDD) schemes, along with dynamic subcarrier selection plays a key role in 5G radio access technology (5G-RAT) [8]. A full-duplex (FD) system simultaneously transmits and receives signals over the same frequency band, providing the potential of doubling the capacity compared to conventional half-duplex systems and sustaining the evolution of 5G technologies within limited spectrum. It is a promising technology that can be employed in the next-generation wireless networks [20].

In general, the above candidate technologies help to increase either the bandwidth, spectral efficiency or cell density. The combined use of them can provide the expected network capacity to support large number of users. Based on the above background information, the main focus of this PhD research is performance analysis and optimization in massive MIMO systems. In this regard, the main questions to be addressed in this PhD research are to study signal processing, channel modeling and estimation, resource allocation and optimization algorithms in massive MIMO systems.

1.2 Statement of the Problem

While massive MIMO system can provide many gains for the capacity requirements, it has also many problems and challenges. These include challenges on channel modeling and channel state acquisition, complexity of inverse operation in signal detection and precoding, multiuser interference and user scheduling, power control and resource allocation, multicell operation and pilot contamination and complexities on deployment scenarios. These challenges are directly or indirectly related to the following parameters of the massive MIMO systems [2, 3, 14, 21].

- large number of antennas and RF chains at the base station;
- large number of scheduled users in the system;
- allocated bandwidth and power for transmission;
- types of radio propagation channel model.

Thus, the researches in massive MIMO systems focuses on developing efficient algorithms for signal processing, channel estimation, power control, resource allocation and optimization [14, 21, 22]. Based on the literature review, we identified that there are still gaps on driving closedform lower bound achievable rate expressions in mixed line-of-sight and non-line-of-sight propagation environments, on developing computationally efficient matrix inverse approximation techniques for detection and precoding, and on developing energy efficient power control and resource allocation algorithms. In line with these facts, the main goal of this PhD research is to study signal detection and precoding, channel estimation and channel state information acquisition, resource allocation and optimization algorithms in massive MIMO systems. Specifically, we derive closedform lower bound achievable rate of massive MIMO systems in mixed line-of-sight and non-line-of-sight propagation environments; formulate computationally efficient inverse approximation techniques for linear detection and linear precoding in massive MIMO systems; derive energy efficient power control and resource allocation algorithms in massive MIMO systems; and analyze the performance of multicell massive MIMO systems in spatially correlated fading channel model. In line with these, the objectives of this PhD research are outlined in next section.

1.3 Objectives of the Research

1.3.1 General Objective

The main objective of the research is to study channel modeling, signal processing, resource allocation and optimization algorithms in massive MIMO systems.

1.3.2 Specific Objectives

The above general objective is accompanied by the following specific objectives and activities.

- Review the fundamentals of massive MIMO systems.
- Study state of the art channel models for massive MIMO systems.
- Assuming the channel state information (CSI) is unknown at the BS, drive minimum mean square error (MMSE) based estimate of the channel and analyze the variance of the channel estimate.
- Analyze performance and complexity of linear detection and precoding techniques in massive MIMO systems.
- Formulate computationally efficient matrix inverse approximation techniques for linear detection and precoding.
- Analyze the spectral efficiency and energy efficiency of massive MIMO systems under Rayleigh and Rician fading channel models.
- Derive analytical closedform lower bounds for the spectral efficiency and formulate appropriate power consumption model that accounts for both the radiated power and circuit power consumption in massive MIMO systems.
- Formulate energy efficient power optimization and resource allocation algorithms.
- Analyze performances of multicell massive MIMO systems in spatially correlated channel model.
- Evaluate the impacts of system parameters, line of sight propagation, channel estimation, pilot contamination and spatial channel correlation in massive MIMO systems.

1.4 Methodology

The methodology used to conduct this PhD research comprises of three major steps as shown in Figure 1.3.

- **Literature Review**: the first step encompasses the study of the state-of-the-art works and algorithms closely related to the PhD research in order to acquire an in-depth understanding of the relevant areas and open problems. In this step, the fundamentals of massive MIMO systems including the spectral efficiency and energy efficiency, detection and precoding techniques, channel modeling, resource allocation and optimization algorithms are reviewed.

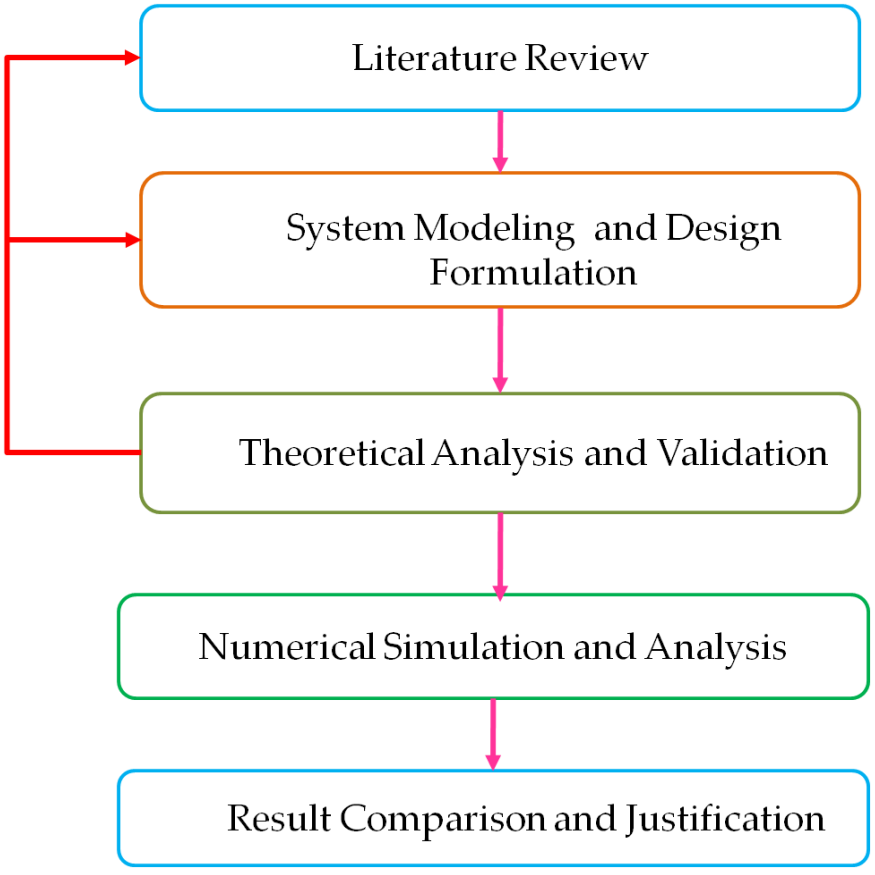

Figure 1.3: Summary of the research methodology.

- **System Modeling and Designing**: At this stage the massive MIMO system is modeled based on selected algorithms. Then, the system is analyzed mathematically and theoretical justification is provided.

- **Numerical Simulation and Analysis**: In this stage, the proposed channel mod-

eling and resource allocation algorithms are tested through simulation to check their validity and reliability. Further, the performance of the proposed system is analyzed at different system and propagation parameters. Then, the results are analyzed and conclusions are drawn.

1.5 Contributions of the Research

The research work incorporates advanced mathematical models and algorithms for solving complex signal detection, parameter estimation, resource allocation and optimization algorithms in massive MIMO systems. This shows the importance of mathematical models and optimization to the design of wireless communication.

Generally, we can subdivide the contributions of this research as two-fold, such as the theoretical contributions and the contributions to field of multi-antenna signal processing for wireless communication. Theoretically, we contribute to the field of estimation and optimization theory by formulating the detection, estimation and resource allocation algorithms. Besides the theoretical analysis, we also proposed analytical closedform lower bound spectral efficiency and energy efficiency formulations for multiuser massive MIMO systems. Further, energy efficient power control and resource allocation algorithms are formulated. In line with these, several peer reviewed conference and journal papers are published.

Thus, the above justification and achieved publications show that the PhD research work is relevant to create a research platform for Ethiopian universities on signal processing in wireless communication, and to provide fundamental knowledge on upcoming massive MIMO and 5G networks to the Telecom sectors in Ethiopia.

1.6 Organization of the Dissertation

This Dissertation contains eight chapters. The first chapter provides the background, motivation of the research and statement of the problem. Other information presented in this chapter includes the objectives and significant of the research. Chapter two provides the fundamentals on massive MIMO systems. Specifically, the chapter provides an in-depth review on signal processing, channel modeling, channel estimation, resource allocation and optimization techniques in massive MIMO systems.

The third chapter focuses on analyzing the performance and complexity of linear detection and precoding techniques in massive MIMO systems. Besides, computationally efficient matrix inverse approximation techniques are reviewed and Truncated Neumann series based matrix inversion approximation is proposed. Performance analysis of massive MIMO systems in Rician fading channel model is provided in Chapter four. Specifically, the achievable spectral efficiency and energy efficiency of massive MIMO systems under Rician fading channel model are analyzed.

The fifth and six chapters focus on energy efficient power optimization and resource allocation in massive MIMO systems. Energy efficient power control algorithms for uplink massive MIMO systems are proposed in Chapter five. Then, in Chapter six, joint energy efficient resource allocation algorithm is proposed to select the optimal number of users, number of BS antennas and transmit power of the massive MIMO systems.

In Chapter seven, performance analysis of multicell massive MIMO systems is provided. Finally, Chapter eight summarizes the dissertation based on the theoretical analysis and simulation results. Besides, conclusions and recommendations are presented based on the findings.

Chapter 2

Fundamentals of Massive MIMO Systems

2.1 Introduction

Multiuser multiple input multiple output (MU-MIMO) systems have been used to provide substantial spatial multiplexing and diversity gains. In MU-MIMO systems, many single-antenna users communicate to a BS equipped with multiple antennas under the same time-frequency resources. MU-MIMO systems have nearly equal number of BS antennas and users; and they are designed to work both in TDD and FDD mode. Due to frequency selective and small scale fading, the propagation channel varies over time and frequency. To account the channel variations, resource allocation algorithms could change rapidly. Besides, to achieve the required spectral efficiency, it needs to implement complex signal processing algorithms both at the BS and the users. Further, in downlink communication both the BS and the users must know the CSI and that require transmission of pilots in both directions. Due to these challenges, conventional MU-MIMO is not scalable with respect to the number of BS antennas and scheduled users [3, 17].

Massive MIMO is a scalable version of MU-MIMO in which the BS is equipped with large number of antennas to serve many users as shown in Figure 2.1 [2, 3]. The figure shows a massive MIMO system with BS antennas, detection and precoding blocks, and scheduled users. In massive MIMO systems, the number of antennas at the BS is much greater than the number of users (for instance a BS with 100 antennas can support 10 or more users in the same time-frequency resources [14]) [3]. Massive MIMO operates in TDD mode to exploit channel reciprocity. Thus, CSI acquisition is done by sending uplink pilots and exploiting channel reciprocity. In massive MIMO systems, deploying large number of antennas at the BS focuses the transmit energy into smaller regions. This brings high improvement in spectral efficiency and radiated energy efficiency. The spectral

efficiency improvement results from spatial multiplexing gains and the improvement in energy efficiency is obtained due to concentration of energy in small regions [17, 23]. Thus, massive MIMO is expected to increase the spectral efficiency in the order of 10× and simultaneously improve the radiated energy efficiency in the order of 100× [17, 23].

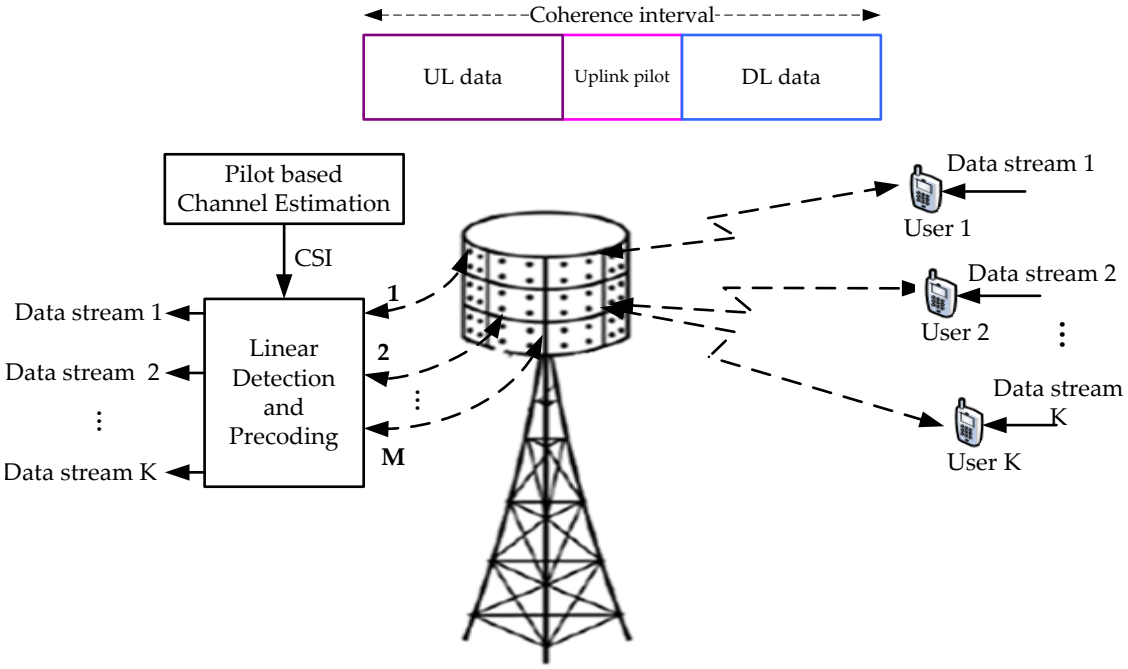

Figure 2.1: Massive MIMO system architecture [3].

Besides, when the number of BS antennas are much larger than the number of users, large number of degrees of freedom are available and this can be used to shape the transmitted signals and to null interference [3]. Hence, the effects of uncorrelated noise and small-scale fading are averaged out and the required transmit power to cover the cell is decreased. Furthermore, linear signal processing techniques such as maximum ratio transmission (MRT) and zero forcing (ZF) can be employed to achieve near optimal performance [17, 23]. For instance, it is shown in [14] that under realistic propagation conditions, a massive MIMO system with 100 BS antennas and equipped with MRT processing could achieve a data rate of 17 Mbps for 40 users in 20 MHz channel in both the uplink and downlink.

Generally, the main benefits of massive MIMO systems are summarized as follows [3, 10, 13, 14].

- **High Spectral Efficiency and Communication Reliability**: in massive MIMO systems with M-antennas at the BS and K-users, we can achieve a diversity order of M and multiplexing gain of K [17, 23]. Hence, by increasing both M and K, we

can obtain high spectral efficiency and communication reliability [3, 23].

- **High Energy Efficiency**: the gain in energy efficiency enables massive MIMO systems to operate with low radiated power as compared to current mobile networks. This helps to reduce the energy consumption by cellular systems and to save energy. In addition, networks that consume low power could be powered by green energy sources such as solar and wind energy [24]. Thus, they can be deployed where no electricity grid is available. Besides, it is shown in [14] that the users uplink transmit power can be scaled down proportional to the number of BS antennas. This helps to elongate the battery life of user terminals [14].

- **Simplify Signal Processing Complexity**: the use of large number of antennas at the BS helps to obtain favorable propagation condition where the channel vectors between the users and the BS become pair wisely orthogonal. Under favorable propagation[1] [25], the effect of interuser interference and noise can be eliminated with simple signal processing techniques. Hence, linear processing techniques such as liner precoding in the downlink and linear detection in the uplink can be employed to get near optimal performance [3, 17, 23].

- **Obey Channel Hardening in Large Dimension**: when the number of antennas at the BS are very large, the effect of small scale fading is averaged out and the channel becomes nearly deterministic. That is, when the channel matrix is large, the distribution of the eigenvalues becomes less sensitive to the actual distribution of the channel. This property is termed as channel hardening[2] [26]. Channel hardening provides several advantages in massive MIMO systems. Channel hardening allows simple linear detection and precoding algorithms to achieve near optimal performance in large dimensions. Thus, user scheduling, power control, optimization and resource allocation can be done in large-scale fading (that is large time scale) instead of the small-scale fading (that is small time scale). This simplifies the signal processing complexity [3, 14, 27].

Combining all the above explanations, a highly spectral efficient massive MIMO systems employ space division multiple access (SDMA) to achieve multiplexing gains, deploy large

[1]Favorable propagation describes orthogonality between the user channels. It is the key properties of the radio channel that is exploited in massive MIMO systems [25].

[2] Mathematical formulations for channel hardening and favorable condition in massive MIMO systems are shown in [3, 26] and there impacts are analyzed in Chapter 7 of this dissertation.

number of BS antennas to suppress interuser interference (IUI) and to achieve channel hardening, operate in asynchronous TDD mode to limit CSI acquisition, and use linear processing to reduce signal processing complexity.

2.2 Design Challenges of Massive MIMO Systems

While massive MIMO systems can provide many gains to the current capacity demand, it has also many technical challenges [3,10]. These include challenges on channel modeling and channel state acquisition, complexity of inverse operation in linear processing, multiuser interference and user scheduling, complex power control and resource allocation algorithms, multicell operation and pilot contamination and complexities on deployment scenarios. These technical challenges should be solved effectively to fully realize the benefit of massive MIMO systems. The detail of these challenges are summarized as follows.

- **Channel Modeling and CSI Acquisition**: in order to achieve high spatial multiplexing gains, the BS needs to process the received signals coherently. This requires perfect knowledge of the channel state information. But, channel modeling and channel estimation may be challenging in large systems, especially in high mobility scenarios and when there is a line of sight propagation [3]. We analyze this challenge in [28, 29] and Chapter 4 of the dissertation.

- **Complexity of Inverse Operation in Linear Processing**: for massive MIMO systems, linear processing (linear detection and precoding) techniques achieve near optimal performance with low signal processing complexity. Hence, they are proposed to be the candidate detection and precoding techniques for massive MIMO systems. When the number of supported users increase, due to large matrix inversion operation, the computational complexity of linear processing techniques become very high. To reduce the computational complexity from large matrix inversion, several approximation approaches are proposed to avoid complex matrix inversion operation. We propose truncated Neumann series based matrix inversion approximation for massive MIMO systems in [30] and Chapter 3 of the dissertation.

- **Power Control and Resource Allocation**: in massive MIMO systems, issues related to power control, user selection, interference management, resource allocation and optimization creates new challenges on practical deployment. The challenges

on spectrally efficient and energy efficient power control and resource allocation is studied in [31–33] and Chapters 5 and 6 of the dissertation.

- **Multicell Operation and Pilot Contamination**: practical massive MIMO systems consist of many cells. In multicell massive MIMO systems, due to the limitation of the channel coherence interval, we cannot assign orthogonal pilot sequences for all users in all cells [3]. Hence, pilot sequences have to be reused from cell to cell. Therefore, the channel estimate obtained in a given cell contaminates by pilots transmitted by users in other cells. This effect is called pilot contamination. It reduces the system performance and is the major limitation of massive MIMO systems [3]. Considerable efforts have been made to mitigate the effect of pilot contamination. We analyze the performance of multicell massive MIMO systems and evaluate the impacts of channel estimation, spatial channel correlation and pilot contamination in Chapter 7 of the dissertation.

All in all, design and development of low complexity signal processing algorithms for linear processing, channel estimation, resource allocation and optimization are the key to practical implementation of massive MIMO systems [21, 26, 34–36]. Since several users are served in the same time-frequency resources, scheduling schemes that optimally select the optimal number of users depend on the precoding and detection techniques, CSI knowledge and resource allocation algorithms [3].

In the remaining section of this chapter, we analyze the performance of single cell massive MIMO systems equipped with linear processing techniques and assuming imperfect CSI at the BS. For this, the system and channel models are defined. Minimum mean square error (MMSE) based channel estimation is done. Then, spectral efficiency and energy efficiency expressions are formulated. Closedform lower bound spectral efficiency and energy efficiency expressions are derived. Numerical simulation is done to validate the theoretical analysis. In line with these points, the main contributions of this chapter is summarized as follows [18, 29, 31, 37–39].

- Study benefits and challenges of massive MIMO systems.
- Drive MMSE-based estimate of the channel and analyze variance of the channel estimation.
- Drive analytical closedform lower bounds for the spectral efficiency.

- Formulate appropriate power consumption model and study energy efficiency of the system.
- Evaluate impacts of system and propagation parameters on the spectral efficiency and energy efficiency.

2.3 The Massive MIMO System and Channel Models

We consider a single cell uplink massive MIMO system shown in Figure 2.1, where the BS is equipped with M-antennas to support K-single-antenna users in the same time-frequency resource. Since K-users share the same time-frequency resources, the received signal at the BS is a combination of signals transmitted from all users. If $\mathbf{x}$ denotes the complex valued $K \times 1$ transmit signal from all users, then the $M \times 1$ received signal at the BS is given by [3]

$$\mathbf{y} = \sqrt{p_u}\mathbf{G}\mathbf{x} + \mathbf{n} \tag{2.1}$$

where $\mathbf{G}$ represents an $M \times K$ channel matrix between the BS and the K-users with $g_{mk} \triangleq [\mathbf{G}]_{mk}$ is the channel coefficient between the mth antenna of the BS and the kth user, $\sqrt{p_u}\mathbf{x}$ is the $K \times 1$ vector of simultaneously transmitted signals by the K-users and p_u is the average transmitted power of each user. $\mathbf{n}$ is additive white Gaussian noise vector at the BS with zero mean and unit variance elements. From the received signal vector $\mathbf{x}$ together with knowledge of CSI, the BS coherently detects the signals transmitted from the K-users [10]. To facilitate our analysis we first define and explain the propagation channel model.

2.3.1 Uplink Propagation Channel Model

The propagation channel between a user and the BS antennas is subjected to pathloss, shadowing and multipath fading effects. By accounting these propagation parameters, the channel model for uplink massive MIMO system is expressed as [3, 40]

$$\mathbf{G} = \mathbf{H}\mathbf{D}^{\frac{1}{2}} \tag{2.2}$$

where $\mathbf{D} = \text{diag}\{\beta_1, \beta_2, \cdots, \beta_K\} \in \mathbb{R}^{K \times K}$ is a diagonal matrix which represents the large scale fading (LSF) effect that includes pathloss and shadowing effects with elements $\beta_k =$

$d_k^{-v}\psi_k$; d_k is the Euclidean distance between the BS antennas and the kth user; v is the pathloss exponent and ψ_k represents a log-normal shadowing with $10\log_{10}\psi_k \sim \mathcal{N}(0, \sigma_{\text{sh}}^2)$ where σ_{sh} is the standard deviation of the shadow fading model [3]. The matrix $\mathbf{H} \in \mathbb{C}^{\text{M}\times\text{K}}$ represents the multipath fading effect. It can be modeled with the Rayleigh or Rician distribution [21]. In this chapter, we consider a Rayleigh fading channel model in which the elements of $\mathbf{H}$ are assumed to be independent and identically distributed (iid) random variables with $\mathcal{CN}(0,1)$ elements. In real-world scenarios, perfect knowledge of $\mathbf{G}$ is not possible [3, 21]; hence, in this PhD research MMSE based channel estimation is considered at the BS as reported in subsequent sections.

2.3.2 MMSE-based Channel Estimation

In real world scenarios, the true channel matrix is unknown and should be estimated at the BS. Massive MIMO systems assumed to operate in TDD mode and the channel is estimated periodically at the BS [3]. The most common approaches to channel estimation include pilot-based, blind and semi blind channel estimation techniques [41–44]. In pilot based channel estimation, predetermined pilot signal sequences selected from known periodic patterns are sent before the transmission of the data. The BS receives the pilot signal sequences and uses one of the estimation techniques to estimate the channel. MMSE is among the common pilot-based channel estimation techniques.

For analysis purpose, most works assume that the large scale fading channel coefficients are perfectly known both at the BS and users [2, 3, 21, 28]. Thus, estimation is performed only for small scale fading channel coefficients. This assumption is reasonable for massive MIMO systems since the LSF channel coefficients change very slowly as compared to small scale fading (SSF) channel coefficients and they can be estimated reliably [2, 3]. In this case, the estimate of $\mathbf{G}$ can be expressed as

$$\hat{\mathbf{G}} = \hat{\mathbf{H}}\mathbf{D}^{\frac{1}{2}} \tag{2.3}$$

where $\hat{\mathbf{H}}$ represents the estimate of the random component of the channel [21]. In pilot based channel estimation, let $\tau_c = T_c B_c$ be the length of the coherence interval where T_c is the coherence time and B_c is the coherence bandwidth and let τ_p be the number of symbols used for pilots. During the training part of the coherence interval, all users simultaneously transmit mutually orthogonal pilot sequences of length τ_p symbols. The pilot sequences of K-users can be represented by a $\tau_p \times K$ matrix of $\sqrt{p_p}\mathbf{\Phi}$ which satisfies $\mathbf{\Phi}^{\text{H}}\mathbf{\Phi} = \mathbf{I}_K$ and

p_p is the transmit pilot power. Then, the $M \times \tau_p$ received pilot matrix at the BS is given by [2, 21]

$$\mathbf{Y}_p = \sqrt{p_p}\mathbf{G}\mathbf{\Phi}^T + \mathbf{N} \tag{2.4}$$

where $\mathbf{N}$ is $M \times \tau_p$ additive white noise matrix with iid $\mathcal{CN}(0,1)$ elements. By using MMSE based channel estimator, we get the channel estimate as shown in the following theorem.

Theorem 2.3.1 *Given a $\tau_p \times K$ pilot matrix $\sqrt{p_p}\mathbf{\Phi}$ which satisfies $\mathbf{\Phi}^H\mathbf{\Phi} = \mathbf{I}_K$ and $p_p = \tau_p p_u$ is the transmit pilot power, the MMSE based estimate of the Rayleigh fading channel model in (2.2) from the received pilot matrix $\mathbf{Y}_p$ is given by*

$$\hat{\mathbf{G}} = \mathbb{E}\{\mathbf{G}|\mathbf{Y}_p\} = \frac{1}{\sqrt{p_p}}\mathbf{Y}_p\mathbf{\Phi}^*\tilde{\mathbf{D}} = \left(\mathbf{G} + \frac{1}{\sqrt{p_p}}\mathbf{W}\right)\tilde{\mathbf{D}} \tag{2.5}$$

where $\mathbf{W} = \mathbf{N}\mathbf{\Phi}^*$ and $\tilde{\mathbf{D}} = \left(\frac{1}{p_p}\mathbf{D}^{-1} + \mathbf{I}_K\right)^{-1}$. With $\mathbf{\Phi}^H\mathbf{\Phi} = \mathbf{I}_K$, $\mathbf{W}$ has iid $\mathcal{CN}(0,1)$ elements.

The error due to channel estimation is given by $\tilde{\mathbf{G}} = \mathbf{G} - \hat{\mathbf{G}}$. Owing to the property of MMSE estimation, the estimation error is uncorrelated with both the channel estimate and the received pilot signal, and it is jointly Gaussian with the channel estimate [2, 21]. With MMSE based channel estimation, the kth user channel, $\mathbf{g}_k \in \mathbb{C}^{M\times 1}$, is given by [3]

$$\mathbf{g}_k = \hat{\mathbf{g}}_k \pm \tilde{\mathbf{g}}_k \tag{2.6}$$

where $\hat{\mathbf{g}}_k$ represents the channel estimate and $\tilde{\mathbf{g}}_k$ represents the channel estimation error. For massive MIMO systems, the elements of $\hat{\mathbf{g}}_k$ and $\tilde{\mathbf{g}}_k$ are also modeled as complex Gaussian distributed as [3]

$$\begin{aligned} \hat{\mathbf{g}}_k &\sim \mathcal{CN}(0, \hat{\beta}_k\mathbf{I}) \\ \tilde{\mathbf{g}}_k &\sim \mathcal{CN}(0, \tilde{\beta}_k\mathbf{I}) \end{aligned} \tag{2.7}$$

where $\hat{\beta}_k = \frac{\tau_p p_p \beta_k^2}{1+\tau_p p_p \beta_k}$ is the variance of the channel estimate, $\tilde{\beta}_k = \frac{\beta_k}{1+\tau_p p_p \beta_k}$ is the variance of the channel estimation error, $\tau_p \geq K$ is the pilot symbol length of orthogonal pilot sequences transmitted by users per coherence interval [3] and p_p represents the transmit power of the pilot symbol [2, 3]. The statistical properties of the channel estimate and the channel estimation error is summarized as follows.

- **Variance of the Channel Estimate**: based on large system analysis when M is very large, the inner product of the channel estimate in (2.5) converges as

$$\frac{1}{M}\hat{\mathbf{G}}^{\mathrm{H}}\hat{\mathbf{G}} \rightarrow \mathrm{diag}\{\frac{\tau_p p_p \beta_k^2}{1+\tau_p p_p \beta_k}\} \tag{2.8}$$

  where diag represents the diagonal matrix.

- **Variance of the Channel Estimation Error**: for the channel estimate in (2.5), the variance of the elements of the channel estimation error is given by

$$\mathbb{E}\{|\tilde{\mathbf{G}}_{mk} - \mathbb{E}\{\tilde{\mathbf{G}}_{mk}\}|^2\} = \frac{\beta_k}{1+\tau_p p_p \beta_k} \tag{2.9}$$

  for $m = 1, 2, \cdots, M$ and $k = 1, 2, \cdots, K$.

The proof of (2.5), (2.8) and (2.9) are shown in Appendix 2.1. Equation (2.8) and (2.9) shows that for massive MIMO systems, the variance of the channel estimate and channel estimation error is converged to a deterministic value that depends on the LSF.

2.4 Spectral Efficiency in Massive MIMO Systems

Depending on the employed precoding and decoding techniques, the channel between the BS antennas and the users can support many different possible spectral efficiencies. But the largest achievable spectral efficiency is the key importance when designing wireless communication systems [2, 3, 21]. The maximum spectral efficiency is determined by the channel capacity which is defined by Claude Shannon [45] and for massive MIMO systems, it is formulated as [22]

$$\mathbf{C} = \log_2 \det\left(\mathbf{I} + \frac{\rho}{K}\mathbf{G}\mathbf{G}^{\mathrm{H}}\right) \tag{2.10}$$

where ρ is the received signal-to-noise-ratio (SNR) and $\mathbf{G}$ is the channel matrix from the BS to the users. When the channel coefficient is normalized to give $\mathrm{tr}(\mathbf{G}\mathbf{G}^H) = MK$ where $\mathrm{tr}(.)$ is the trace of the matrix, the upper and lower bound channel capacity is given by [22]

$$\log_2\left(1+\rho M\right) \leq \mathbf{C} \leq \min(M,K)\log_2\left(1+\frac{\rho \max(M,K)}{K}\right). \tag{2.11}$$

The actual achievable rate depends on the distribution of eigenvalues of $\mathbf{G}\mathbf{G}^{\mathrm{H}}$. It is shown in [22] that the channel with equal eigenvalues achieve the highest spectral efficiency whereas those with only one nonzero eigenvalues achieve the lowest [21, 22].

The spectral efficiency of single-cell and multicell uplink massive MIMO systems are analyzed in [21, 46, 47]. They derive bounds on the achievable sum rate and provide asymptotic performance results when the number of BS antennas grows without bound. A unified analysis of uplink and downlink performance of linear processing in multicell systems when both the number of BS antennas and number of users become large with a fixed ratio is provided in [48]. In [49], the spectral efficiency of massive MIMO systems is analyzed in both centralized and distributed configurations.

Based on the above background information in this section, we derive general formulation of the achievable rate of massive MIMO systems equipped with linear receivers, Rayleigh channel model and imperfect channel state information (CSI) at the BS. With MMSE-based channel estimation at the BS, the linear receiver matrices are given by [3]

$$\mathbf{A} = \begin{cases} \hat{\mathbf{G}} & \text{MRC} \\ \hat{\mathbf{G}}(\hat{\mathbf{G}}^{\mathrm{H}}\hat{\mathbf{G}})^{-1} & \text{ZF} \\ \hat{\mathbf{G}}(\hat{\mathbf{G}}^{\mathrm{H}}\hat{\mathbf{G}} + \frac{\sigma^2}{p_u}\mathrm{I}_K)^{-1} & \text{MMSE} \end{cases} \tag{2.12}$$

where $\mathbf{A}$ is the linear receiver matrix. The output signal from these linear receivers have the form $\mathbf{A}^{\mathrm{H}}\mathbf{y}$ where $\mathbf{A}^{\mathrm{H}}$ represents the complex conjugate transpose of $\mathbf{A}$ and $\mathbf{y}$ is the received signal in (2.1). Thus, the output data stream from these linear receivers is given by [21]

$$\mathbf{r} = \mathbf{A}^{\mathrm{H}}\mathbf{y} = \sqrt{p_u}\mathbf{A}^{\mathrm{H}}\left(\sqrt{p_u}\hat{\mathbf{G}}\mathbf{x} - \sqrt{p_u}\tilde{\mathbf{G}}\mathbf{x}\right) + \mathbf{A}^{\mathrm{H}}\mathbf{n}. \tag{2.13}$$

Then, the kth component of the processed signal is given by

$$\begin{aligned} r_k &= \sqrt{p_u}\mathbf{a}_k^{\mathrm{H}}\left(\sqrt{p_u}\hat{\mathbf{G}}\mathbf{x} - \sqrt{p_u}\tilde{\mathbf{G}}\mathbf{x}\right) + \mathbf{a}_k^{\mathrm{H}}\mathbf{n} \\ &= \sqrt{p_u}\mathbf{a}_k^{\mathrm{H}}\hat{\mathbf{g}}_k x_k + \sqrt{p_u}\sum_{i\neq k}^{K}\mathbf{a}_k^{\mathrm{H}}\hat{\mathbf{g}}_i x_i - \sqrt{p_u}\sum_{i=1}^{K}\mathbf{a}_k^{\mathrm{H}}\tilde{\mathbf{g}}_i x_i + \mathbf{a}_k^{\mathrm{H}}\mathbf{n} \end{aligned} \tag{2.14}$$

where $\mathbf{a}_k, \hat{\mathbf{g}}_i$ and $\tilde{\mathbf{g}}_i$ are the ith columns of $\mathbf{A}, \hat{\mathbf{G}}$ and $\tilde{\mathbf{G}}$, respectively. The BS considers the channel estimate as the true channel and the part including the last three terms of (2.14) is considered as interference and noise. Therefore, the spectral efficiency of the kth user is given by

$$R_k = \mathbb{E}\left\{\log_2\left(1+\frac{p_{\mathrm{u}}\left|\mathbf{a}_k^H\hat{\mathbf{g}}_k\right|^2}{p_{\mathrm{u}}\sum_{i=1,i\neq k}^{K}\left|\mathbf{a}_k^H\hat{\mathbf{g}}_i\right|^2+p_{\mathrm{u}}\left\|\boldsymbol{a}_k\right\|^2\sum_{i=1}^{K}\frac{\beta_i}{\tau p_{\mathbf{u}}\beta_i+1}+\sigma^2\left\|\mathbf{a}_k\right\|^2}\right)\right\} \tag{2.15}$$

when the expectation is with respect to the random channel. Then, the total capacity per cell is the sum of the spectral efficiency from all users as [21]

$$R_s = B(1-\frac{\tau_p}{\tau_c})\sum_{k=1}^{K}R_k \tag{2.16}$$

where B is the bandwidth of the system, τ_c represents the coherence time of the channel and τ_p ($\tau_p \leq \tau_c$) is the symbol time required for pilot based channel estimation and σ^2 is the noise variance [21]. Based on the above formulations, we drive analytical closedform lower bound achievable rate of a user in massive MIMO system with linear receivers and under imperfect CSI assumptions.

2.4.1 Closedform Lower Bound Achievable Rate Formulation

For single cell uplink massive MIMO system under Rayleigh fading channel model and equipped with linear processing and imperfect CSI at the BS, a closedform lower bound achievable rate of the kth user is given by

$$R_k \approx \begin{cases} \log_2\left(1+\frac{\tau_p p_u(M-1)\beta_k^2}{(\tau p_u\beta_k+1)\sum_{i=1,i\neq k}^{K}\beta_i+(\tau_p+1)\beta_k+\frac{1}{p_u}}\right) & \text{MRC} \\ \log_2\left(1+\frac{\tau_p p_u^2(M-K)\beta_k^2}{(\tau_p p_u\beta_k+1)\sum_{k=1}^{K}\frac{p_u\beta_i}{\tau_p p_u\beta_{i+1}}+\tau p_{\mathrm{u}}\beta_k+1}\right) & \text{ZF} \\ \log_2\left(1+(\alpha_k-1)\,\theta_k\right) & \text{MMSE} \end{cases} \tag{2.17}$$

where

$$\begin{aligned} \alpha_k &= \frac{(M-K+1+(K-1)\mu)^2}{M-K+1+(K-1)\kappa} \\ \theta_k &= \frac{M-K+1+(K-1)\kappa}{M-K+1+(K-1)\mu}\omega\hat{\beta}_k \end{aligned} \tag{2.18}$$

where $\omega \triangleq \left(\sum_{i=1}^{K}\frac{\beta_i}{\tau_p p_u\beta_i+1}+\frac{1}{p_{\mathbf{u}}}\right)^{-1}$, $\hat{\beta}_k \triangleq \frac{\tau_p p_u\beta_k^2}{\tau_p p_u\beta_k+1}$, μ and κ are calculated from the following equations.

$$\begin{aligned} &\mu = \tfrac{1}{K-1}\textstyle\sum_{i=1,i\neq k}^{K}\frac{1}{M\omega\hat{\beta}_i\left(1-\frac{K-1}{M}+\frac{K-1}{M}\mu\right)+1} \\ &\kappa\left(1+\textstyle\sum_{i=1,i\neq k}^{K}\frac{\omega\hat{\beta}_i}{\left(M\omega\hat{\beta}_i\left(1-\frac{K-1}{M}+\frac{K-1}{M}\mu\right)+1\right)^2}\right) = \textstyle\sum_{i=1,i\neq k}^{K}\frac{\omega\hat{\beta}_i\mu+1/(K-1)}{\left(M\omega\hat{\beta}_i\left(1-\frac{K-1}{M}+\frac{K-1}{M}\mu\right)+1\right)^2} \end{aligned} \tag{2.19}$$

Part of the proof of Equation (2.17) is shown in Chapter 5. The result in (2.17) shows that when the number of BS antennas become very large, achievable rate depends only on the large scale fading channel coefficients and system parameters (BS antennas, users, transmit power and coherence interval). As a result, complicated calculations that involve large dimensional matrices from small scale fading channel coefficients are avoided.

2.5 Energy Efficiency in Massive MIMO Systems

Next generation wireless networks are expected to support large number of devices. The vision is to establish a connected society in which sensors, automotives, drones, medical and wearable devices use wireless networks to connect each other and to interact with humans. Trying to achieve this goal with current network architecture leads to an energy crunch with serious economic and environmental concerns [4, 5, 14, 50]. Besides, reducing energy consumption allows network operators to save electricity bills and minimize operational costs, and prolong the battery life of user equipments [50]. Based on these and other facts, in addition to data rate, throughput, quality of service and latency; energy efficiency is considered as the new parameters to design cellular systems. The main goal is to design innovative network architectures and technologies that achieve the required capacity with similar or lower energy consumption as current networks [21, 50, 50]. This requires to adopt new approaches on network design and operation such as efficient resource allocation, network planning and deployment, hardware solutions, energy harvesting and transfer technologies [50].

Energy efficiency of a wireless system is commonly defined as a benefit-cost ratio where the achievable sum rate is compared with associated energy consumption of the system as [2]

$$\text{Energy Efficiency (bits/Joule)} = \frac{\text{Achievable sum rate (bits/sec)}}{\text{Total power consumption (Joule/sec)}}. \tag{2.20}$$

Equation (2.20) shows that the energy efficiency is the ratio between the total amount of data that can be reliably transmitted per unit of time and the total amount of consumed power. For uplink massive MIMO systems, the total power consumption is given by the sum of radiated power and circuit power consumption as [22]

$$P_{\text{tot}} = P_{\text{tx}} + P_{\text{cp}} \tag{2.21}$$

where P_{tx} is the power consumed by the power amplifier. It accounts the power used for uplink pilot and data transmission which is expressed as

$$P_{\text{tx}} = \left(1 - \frac{\tau_p}{\tau_c}\right) \sum_{k=1}^{K} \frac{1}{\eta_k} p_k + \frac{\tau_p}{\tau_c} \frac{1}{\eta_k} K p_p \tag{2.22}$$

where $\eta_k \in (0, 1)$ is the power amplifier efficiency of user k. P_{cp} represents the circuit power consumption of the system given by

$$P_{\text{cp}} = \rho_a M + \sigma_{\text{sc}} R + \Theta_0 \tag{2.23}$$

where $\rho_a \triangleq \chi(P_{\text{TC}} + P_{\text{CE}} + P_{\text{LP}})$ denotes the circuit power consumption per BS antenna, χ represents the impacts of cooling and other effects at the BS, P_{LP} represents the power consumption for linear processing, P_{TC} accounts for the power consumption of transceiver chains and P_{CE} denotes the power consumption for channel estimation [2, 22]. The term $\sigma_{\text{sc}} R$ accounts for the power consumption that grows with the uplink data rate with scaling factor σ_{sc} which includes the power consumption for coding and decoding and backhaul transmission. To simplify our analysis, the rate dependent power consumption is assumed to be fixed [22]. Θ_0 shows a static circuit power consumption for control signaling and load independent base-band processing and it is mostly assumed as fixed [22]. Finally, plugging (2.24) and (2.25) in (2.23), the total system power consumption for uplink massive MIMO system is expressed as [51]

$$P_{\text{tot}}(\mathbf{p}) = \sum_{k=1}^{K} \mu_k p_k + P_0. \tag{2.24}$$

where $\mu_k = (1 - \frac{\tau_p}{\tau_c}) \frac{1}{\eta_k}$ and P_0 is the sum of the pilot power consumption and circuit power consumption of the system. The typical values of $\mu_k, \rho_a, \sigma_{\text{sc}}$ and Θ_0 depend on the types of cellular system such as macro cell, remote radio head and micro cell [50].

2.6 Modeling Energy Efficiency in Massive MIMO Systems

In massive MIMO systems, depending on the benefits and costs incurred by each individual links of the network, two approaches are used to formulate the energy efficiency such as global energy efficiency and multiobjective energy efficiency [50, 52]. In the next section, we describe the principle of these two approaches.

2.6.1 Global Energy Efficiency in Massive MIMO Systems

By using the achievable sum rate and total power consumption model, the global energy efficiency (GEE) is given by [2, 52]

$$\text{GEE} = \frac{\sum_{k=1}^{K} f(\gamma_k(\mathbf{p}))}{\sum_{k=1}^{K} \mu_k p_k + P_c} \tag{2.25}$$

where K is the number of scheduled users, $f(\gamma_k(\mathbf{p}))$ is the achievable rate function of user k, $\gamma_k(\mathbf{p})$ is the signal to interference-plus-noise-ratio (SINR), p_k is the radiated power of the users, μ is the inverse of the transmit power amplifier efficiency and P_c represents the power dissipated in the internal circuit of the system. Substituting the achievable sum rate and power consumption model of the proposed massive MIMO system in (2.16) and (2.24), the GEE is given by [53]

$$\text{GEE}(\mathbf{p}) = \frac{B\left(1 - \frac{\tau_p}{\tau_c}\right) \sum_{k=1}^{K} \log_2(1 + \gamma_k(\mathbf{p}))}{\sum_{k=1}^{K} \mu_k p_k + P_0}. \tag{2.26}$$

Equation (2.26) shows that the GEE is formulated as the ratio between the total amount of data that can be reliably transmitted per unit of time and the total amount of consumed power. The GEE is a sum-based performance metric, it tends to favor users with better propagation channels. Although it have strong physical interpretation, the GEE does not allow to tune individual energy efficiencies of the users [50]. This may be a challenge to optimize heterogeneous networks where terminals with different features and specifications coexist and possibly have different energy efficiency requirements. The GEE may also result unbalanced distribution of the energy efficiency and this many create unfair resource allocation among users. These challenges can be solved by formulating the energy efficiency based on multiobjective optimization approach that give more flexibility to choose the network operating point [50, 52].

2.6.2 Multiobjective Energy Efficiency in Massive MIMO Systems

In multiobjective formulation, the objective function is formulated to optimize the energy efficiencies of the K-users in the network. This leads to consider the network energy-efficiency region as the set of all feasible vectors $\{\text{EE}_k\}_{k=1}^{K}$ and to define the network energy efficiency as a performance measure whose maximization gives a point on the Pareto boundary of the energy-efficiency region. This results in a multiobjective resource allocation

scheme that maximize a combination of different energy efficiencies $\{\mathrm{EE}_k\}_{k=1}^{K}$ according to some increasing function $\mathbf{U}(\mathrm{EE}_1, \cdots, \mathrm{EE}_K)$ where $\mathbf{U}$ is the utility function. Several utility functions have been proposed such as weighted sum energy efficiency (WSEE), weighted product energy efficiency (WPEE), and weighted minimum energy efficiency (WMEE) that are formulated as [50, 52]

$$\mathrm{MOEE} = \begin{cases} \sum_{k=1}^{K} w_k \frac{f(\gamma_k(\mathbf{p}))}{\mu_k p_k + P_c} & \text{WSEE} \\ \prod_{k=1}^{K} \left(w_k \frac{f(\gamma_k(\mathbf{p}))}{\mu_k p_k + P_c} \right)^{w_k} & \text{WPEE} \\ \min\limits_{k \in \{1, \cdots, K\}} \left(w_k \frac{f(\gamma_k(\mathbf{p}))}{\mu_k p_k + P_c} \right) & \text{WMEE} \end{cases} \tag{2.27}$$

where w_k is the weighting parameter. The WSEE is a sum-based metric which tends to favor users with better propagation channels. The WPEE allows more balanced resource allocation and allows to assign priorities to individual energy efficiencies through the choice of weights [52]. The WMEE provides the max-min fairness energy efficiency for all nodes [50]. If the weights are all equal, maximizing the WMEE results equal energy efficiency to all nodes and which provides maximum fairness to the network. All the multiobjective energy efficiency functions are able to describe parts of the energy-efficiency on the Pareto boundary of the system [50, 52].

2.7 Simulation Results and Analysis

2.7.1 Simulation Setup and Simulation Parameters

We consider a single cell uplink massive MIMO system in which the BS is placed at the center of a circular cell. We assume that the users are distributed uniformly in a circular cell of radius $r_c = 500\,\mathrm{m}$ except for an exclusion zone ($r_h \leq 35\,\mathrm{m}$) near the BS. The exclusion zone is assumed to ensure that uplink and downlink communication is performed in the far field region of the transmitting antenna and plane waves can be assumed at the receiver [3]. The large scale fading is modeled as $\beta_k = z_k(\frac{r_k}{r_h})^{-v}$ where z_k is the log-normal shadow fading random variable with standard deviation $\sigma_{\mathrm{sh}} = 8\,\mathrm{dB}$, $v = 3.8$ is the path loss exponent and $r_k \in [r_c, r_h]$ denotes the Euclidean distance between the kth user and the BS antennas. The simulation is run for 2000 Monte-Carlo realizations where in each snapshot, the users are distributed randomly in the cell so that the large scale fading changes randomly. We use the standard system parameters proposed in [8] and [54]. Part

of the simulation parameters are shown in Table 2.1.

Table 2.1: Part of the simulation parameters.

Parameter	**Value**	**Parameter**	**Value**
τ_c	200	ρ_a	0.002 W
B	20 MHz	P_c	0.8 W
K	10	$\sigma_{\text{sc}}R$	0.4 W
τ_p	10	η_{BS}	0.39
p_p	30 dBm	η_{UE}	0.3
M	Variable	r_c	500 m

2.7.2 Impact of Number of BS Antennas on Spectral Efficiency

Figure 2.2 shows the achievable sum rate versus the number of BS antennas with linear detection techniques. The result shows that as the number of BS antennas increases, the achievable sum rate increases. For instance, the result shows that by going from 50 to 100 BS antennas, the spectral efficiency improves from 8.2 bps to 11.0 bps. This is achieved due to the array gain provided by multiple antennas and combining techniques. Thus, the spectral efficiency is increased logarithmically with the number of BS antennas and increases without limit as the BS antennas grows large. Besides, the result shows that when the BS antennas grows large, MMSE achieves better achievable sum rate than other detection techniques. But at large number of BS antennas, ZF detection gives nearly the same achievable sum rate to MMSE, because at large number of BS antennas, ZF detection can completely null-out interuser interference. The result also shows that the gaps between closedform lower bound approximation and simulated results are very small. Thus, in massive MIMO systems, it is quite reasonable to formulate the resource allocation and power allocation algorithms by using the closedform lower bound achievable sum rate approximations.

Next, we analyze the impact of increasing the number of BS antennas on transmit power of a user that is required to achieve a given target spectral efficiency. Figure 2.3 shows the normalized power required to achieve 1 bit/s/Hz per user as a function of the number of BS antennas. When the number of BS antennas is doubled, the required radiated power of the user is reduced by 3 dB and 1.5 dB for the cases of perfect and imperfect CSI, respectively. When the number of BS antennas becomes large, the difference in performance between

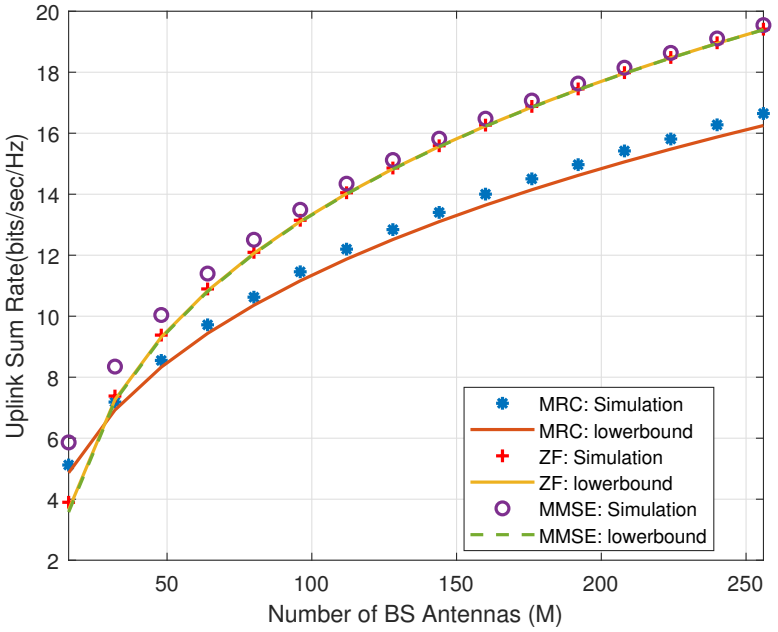

Figure 2.2: Spectral efficiency versus the number of BS antennas with linear processing techniques and imperfect CSI at the BS.

MRC, ZF and MMSE is less than 1 dB for the cases of perfect CSI and 3 dB for the case of imperfect CSI, respectively.

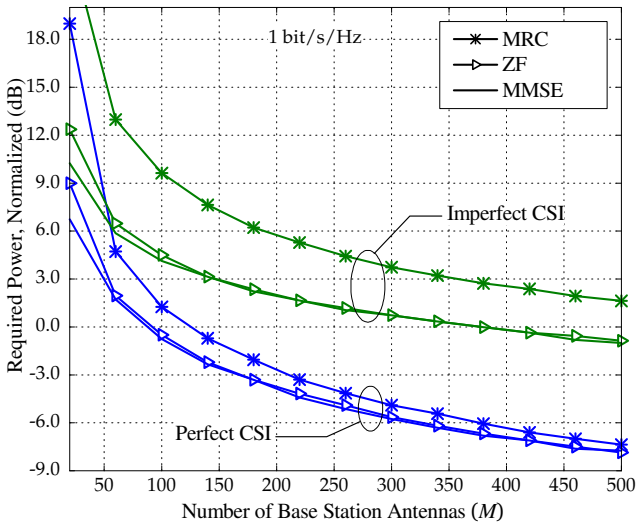

Figure 2.3: Required uplink transmit power of the user as a function of the number of BS antennas. We consider $K = 10$, linear processing, imperfect CSI and an achievable rate of 1 bit/s/Hz per user.

2.7.3 Impact of Number of BS Antennas on Energy Efficiency

Figure 2.4 shows the energy efficiency with the number of BS antennas. The result shows that energy efficiency increases until some number of BS antennas and then decreases with the number of BS antennas. This is because as shown in (2.25) when the number of BS antennas grows large, the internal circuit power consumption at the BS increases and this results in a lower energy efficiency. Thus, although increasing the number of BS antennas can help to reduce the radiated power for the system, it decreases the energy efficiency due to increment on internal power consumption. Hence, a design trade-off is required to obtain the optimal number of BS antennas that give near optimal spectral efficiency and energy efficiency simultaneously.

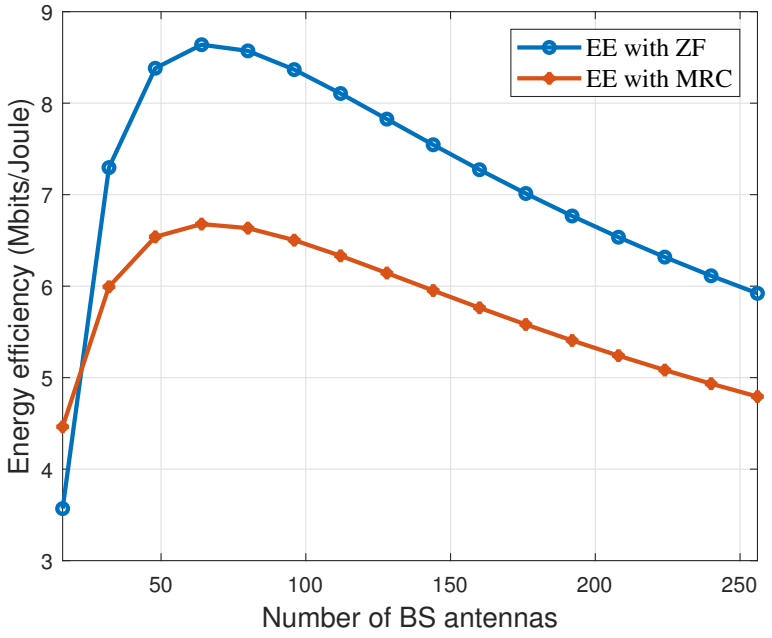

Figure 2.4: Energy efficiency versus the number of BS antennas.

Figure 2.5 shows energy efficiency versus the spectral efficiency in massive MIMO systems. The results shows that in lower spectral efficiency regime, when the spectral efficiency increases, the energy efficiency is also increased. Whereas at high spectral efficiency regime, the energy efficiency decreases. This is because, the spectral efficiency grows in logarithm function whereas the internal power consumption grows linearly and thus after a certain time the increment on the power consumption overtakes the spectral efficiency increment and the energy efficiency starts to decrease.

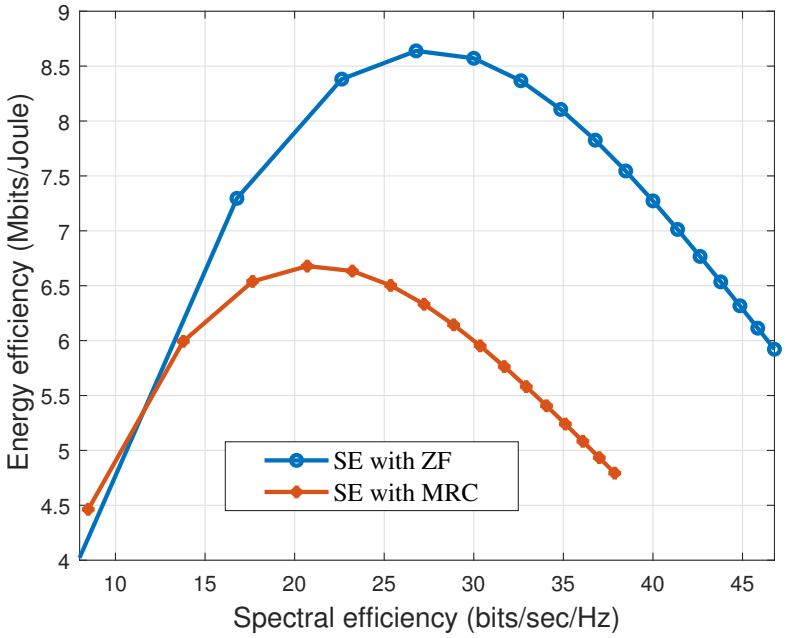

Figure 2.5: Spectral efficiency versus energy efficiency.

2.7.4 Impact of Transmitter Power on Spectral Efficiency

Figure 2.6 shows the spectral efficiency versus uplink transmit power of the users. The result shows that increasing the transmitter power can increase the spectral efficiency but the spectral efficiency could not increase indefinitely with the transmitter power. Hence, increasing the SNR by using more transmit power improves the spectral efficiency, but the positive effect quickly pushes the network into an interference-limited regime where no extraordinary spectral efficiency can be obtained. Thus, simple power-scaling approach cannot contribute much to achieve high spectral efficiency.

Figure 2.7 shows energy efficiency versus transmit power of a massive system at different internal power consumption [50]. The result shows that energy efficiency is a unimodal function with the transmit power [52]. Thus, it increases until some transmit power and then decreases above that power. This is a fundamental difference from traditional performance metrics that increase monotonically with the transmit power. Hence, the maximum value of the energy efficiency results a power level that is in general lower. This is the key feature which allows to save energy through energy efficient resource allocation. The results also show that increasing internal power consumption requires high transmitter power to achieve the maximum energy efficiency.

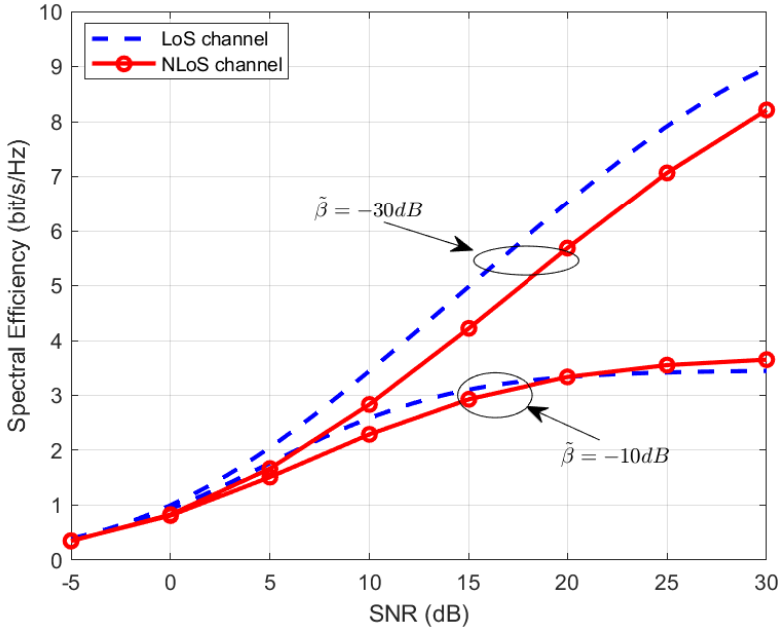

Figure 2.6: Spectral efficiency versus uplink transmitter power. Where $\tilde{\beta}$ is the ratio between intercell and intracell channel gains.

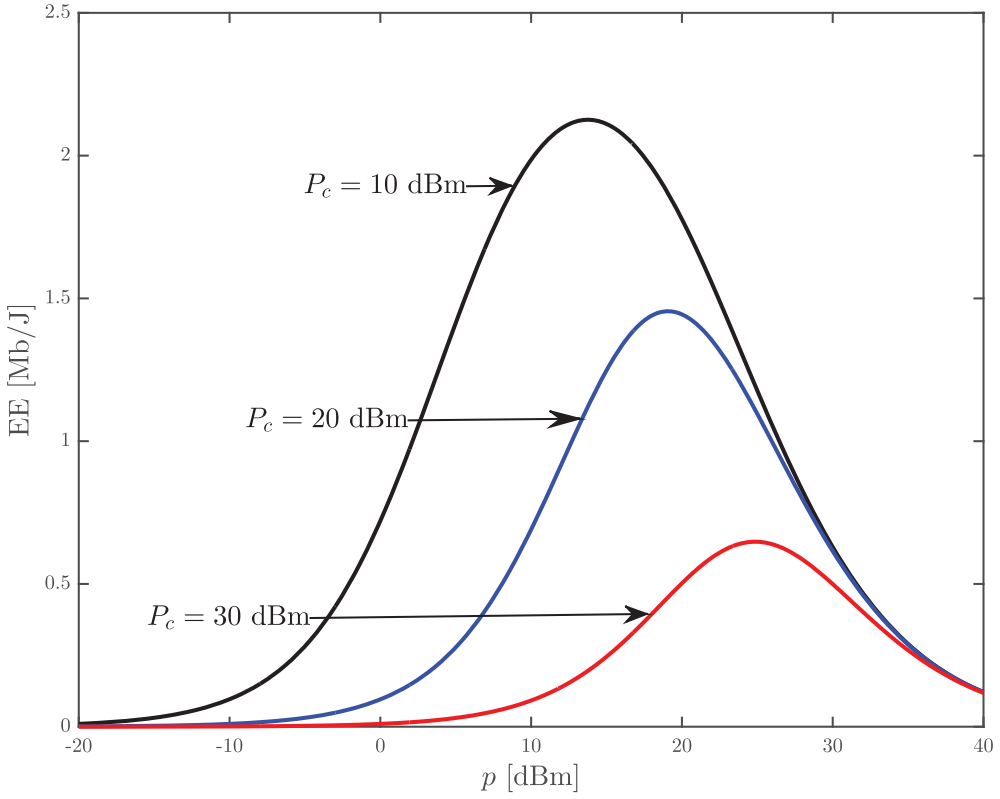

Figure 2.7: Energy efficiency of a wireless communication network. P_c denotes internal power consumption of the network.

2.7.5 Impact of Internal Power Consumption on Energy Efficiency

For analysis purpose, we consider a single cell massive MIMO system in Rayleigh fading channel model proposed in Figure 2.1 where the BS is equipped with M antennas, perfect channel station information is assumed. If we only assume one active user and with MRC, based on (2.15) the uplink achievable spectral efficiency is given by [3]

$$\mathrm{SE} = \log_2(1 + (M-1)\frac{p_u\beta}{\sigma^2}) \tag{2.28}$$

where p_u is the average transmitter power of the user, β is the channel gain of the user and σ^2 is the noise power. To understand the impacts of internal power consumption model, we analyze the energy efficiency under fixed and variable circuit power consumption scenarios. If we assume the circuit power is independent of the system parameters, the energy efficiency is given by

$$\mathrm{EE} = B\frac{\log_2(1 + (M-1)\frac{p_u\beta}{\sigma^2})}{\frac{1}{\eta}p_u + P_c} \tag{2.29}$$

where B is the bandwidth, $\frac{1}{\eta}p_u$ accounts for the transmission power, η is the power amplifier efficiency, P_c represents the fixed circuit power consumption. By using (2.28), the energy efficiency can be expressed as

$$\mathrm{EE} = B\frac{\mathrm{SE}}{(2^{\mathrm{SE}}-1)\frac{v_0}{M-1} + P_c} \tag{2.30}$$

where $v_0 = \frac{\sigma^2}{\eta\beta}$. Figure 2.8 shows the impacts of the number of BS antennas on the spectral efficiency and energy efficiency with $P_c = 10\,\mathrm{dB}, B = 100\,\mathrm{KHz}, \sigma^2/\beta = -6\,\mathrm{dB}, \eta = 0.4$. As expected, both the spectral efficiency and energy efficiency increases as M grows large. But, this is only valid when the internal power consumption does not account for additional power consumed due to multiple BS antennas. The blue line represents the points at each curve in which the energy efficiency achieves its maximum.

But, in practical systems, the impacts of the number of BS antennas on the internal circuit power consumption should be considered. This is particularly important in massive MIMO systems where the BS is equipped with M-antennas which require M-RF chains that contain many components. The circuit power consumption of such system is M-times higher than the circuit power consumption of a single-antenna transceiver [22]. In this case, the circuit power consumption can be expressed as [22]

$$P_{\mathrm{cp}} = P_c + MP_{\mathrm{BS}} \tag{2.31}$$

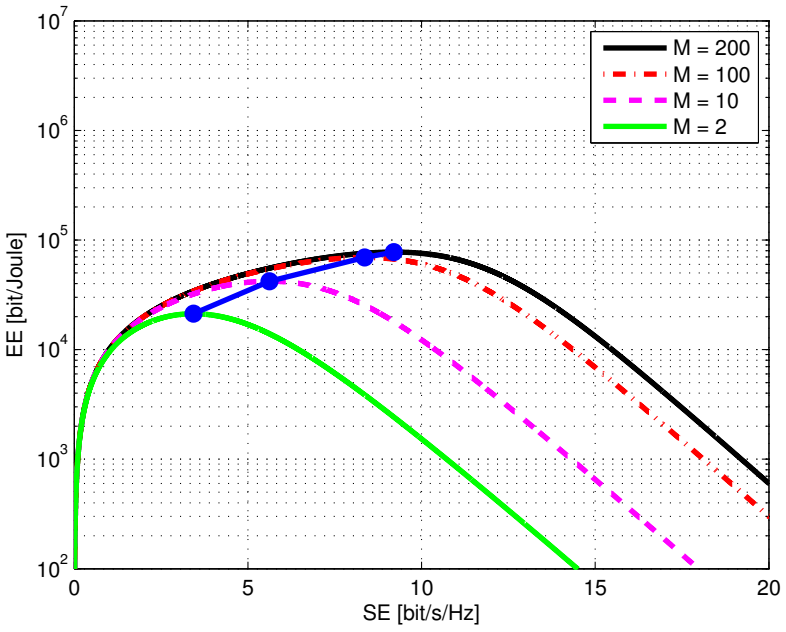

Figure 2.8: Spectral efficiency versus energy efficiency at various number of BS antennas and with fixed circuit power consumption model.

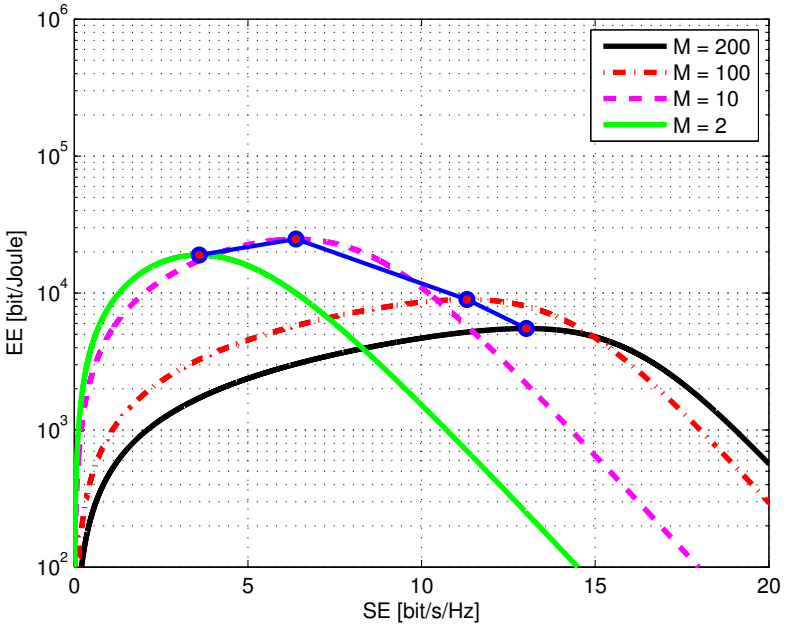

Figure 2.9: Spectral efficiency versus energy efficiency with variable internal circuit power consumption model.

where P_{BS} is the power consumed by the circuit components in each RF chains. By using (2.31), Equation (2.30) is modified as

$$\text{EE} = B\frac{\text{SE}}{(2^{\text{SE}}-1)\frac{v_0}{M-1} + P_c + MP_{\text{BS}}}. \tag{2.32}$$

Figure 2.9 shows the energy efficiency versus spectral efficiency with the same operating parameters as in Figure 2.8 when $P_{\text{BS}} = 0\,\text{dB}$. In contrast to Figure 2.8, the spectral efficiency-energy efficiency trade off does not increase unboundedly with the number of BS antennas. This is because each additional antenna increases the internal circuit power [2]. Hence, to find the optimal operating point for massive MIMO systems, appropriate model for the internal circuit power consumption is mandatory.

2.7.6 Impact of Scheduling Large Number of Users

Here, we evaluate the impact of deploying space division multiple access (SDMA) on sum spectral efficiency in massive MIMO systems. Figure 2.10 shows the sum spectral efficiency as function of the number of users. The result shows that at small number of BS antennas, the spectral efficiency increases slowly with the number of users. This is because the BS does not have enough spatial degrees of freedom to separate the users. But when the number of BS antennas are large (for instance $M > 100$), the sum spectral efficiency increases linearly with the number of users. Thus, nearly a K-fold spectral efficiency improvement is achieved as compared to a single user system.

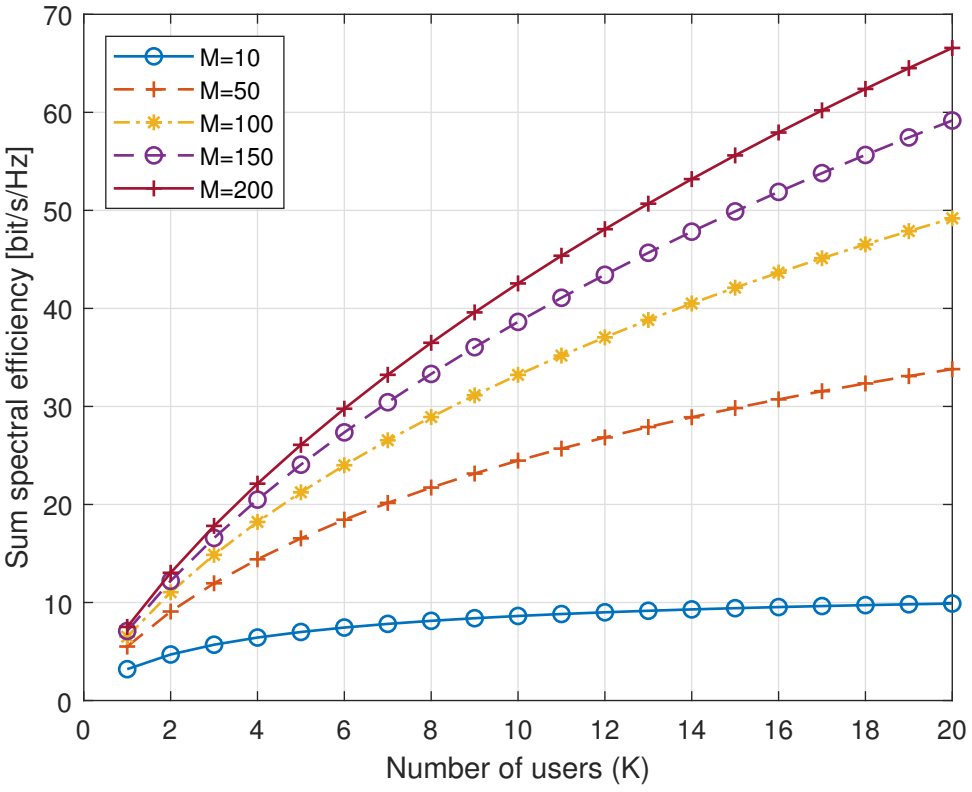

Figure 2.10: Spectral efficiency versus number of users. We assume SNR $= 0\,\text{dB}$.

We also evaluate the result where the number of BS antennas is increased proportionally with the number of users. This helps to suppress interuser interference that increase with the number of users. Figure 2.11 shows the sum spectral efficiency with the number of users. The result shows that the spectral efficiency grows linearly with the number of users in all cases. When M/K increases, the steepness of the curve increases since it becomes easier to suppress interference when $M \gg K$. The above results show that SDMA increases the sum spectral efficiency. This is achieved by serving K-users simultaneously and increasing the number of BS antennas to achieve an array gain that mitigate interuser interference.

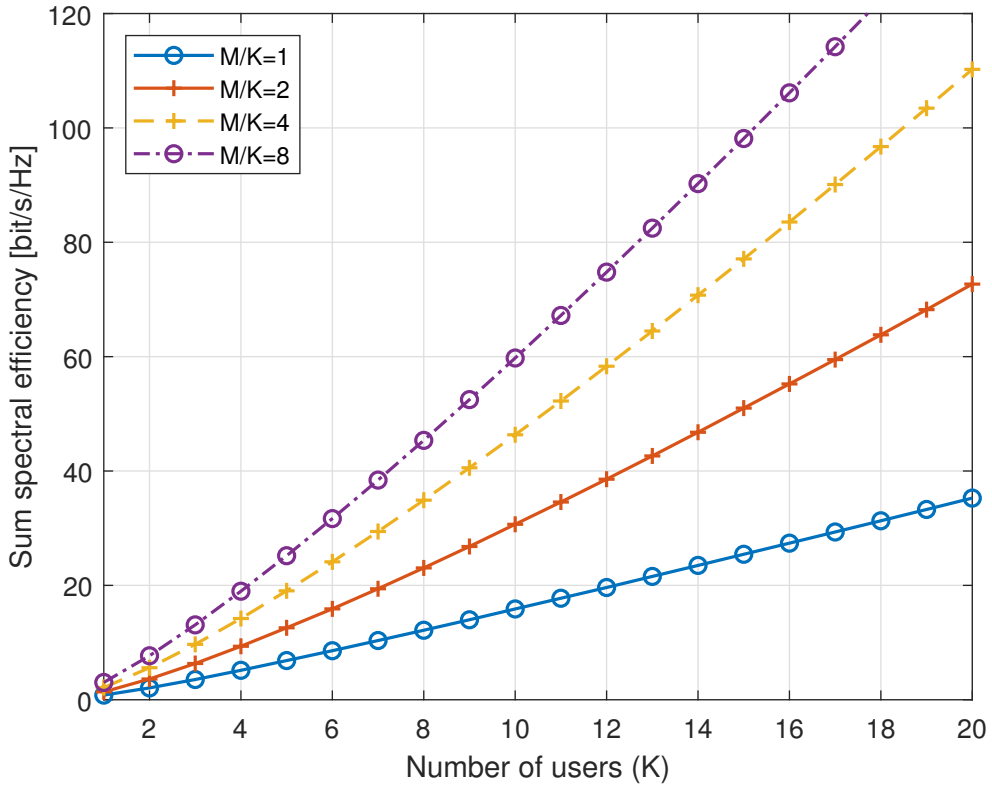

Figure 2.11: Spectral efficiency versus number of users per cell when the number of BS antennas increases with K with fixed M/K ratio.

2.8 Summary

Massive MIMO can increase the spectral efficiency in the order of 10× and simultaneously improve the radiated energy efficiency in the order of 100×. In addition, massive MIMO simplifies the transmission processing and reduces the required transmission power of the users. Besides, the analysis shows that when the number of BS antennas grows large,

the effects of uncorrelated noise and small-scale fading are average out, and the required transmitted energy is decreased. Furthermore, simple linear signal processing techniques can be employed to achieve near optimal performance.

In this chapter, the performance of massive MIMO systems are analyzed. MMSE based channel estimation is done and closedform lower bound achievable sum rate is derived. Besides, appropriate power consumption model which accounts for both the radiated power and internal circuit power is formulated. Then, analytical expression is formulated for the energy efficiency. The results from numerical simulation show that the achievable sum rate increases with the number of BS antennas and number of scheduled users. Whereas, the energy efficiency is increased up to some optimal number of BS antennas and decreased after that. This is because, when the number of BS antennas increases, internal circuit power is increased and this decreases the energy efficiency of the system.

Appendices

Appendix 2.1: Proof of Equation (2.5)

Given a $\tau \times K$ uplink transmitted pilot matrix $\sqrt{p_p}\mathbf{\Phi}$ which satisfies $\mathbf{\Phi}^{\mathrm{H}}\mathbf{\Phi} = \mathbf{I}_K$ where p_p is the pilot power, then an $M \times \tau$ received pilot signal at the BS is given by

$$\mathbf{Y}_p = \sqrt{p_p}\mathbf{G}\mathbf{\Phi}^T + \mathcal{N} \tag{2.33}$$

where $\mathcal{N}$ is an $M \times \tau$ noise matrix with iid $\mathcal{CN}(0,1)$ elements. The MMSE based estimate of $\mathbf{G}$ from $\mathbf{Y}_p$ is given by [55]

$$\hat{\mathbf{G}} = \frac{1}{\sqrt{p_p}}\mathbf{Y}_p\mathbf{\Phi}^*\tilde{\mathbf{D}} = \left(\mathbf{G} + \frac{1}{\sqrt{p_p}}\mathbf{W}\right)\tilde{\mathbf{D}} \tag{2.34}$$

where $\tilde{\mathbf{D}} \triangleq (\frac{1}{p_p}\mathbf{D}^{-1} + \mathbf{I}_{\mathrm{K}})^{-1}$ and $\mathbf{W} \triangleq \mathcal{N}\mathbf{\Phi}^*$. With $\mathbf{\Phi}^{\mathrm{H}}\mathbf{\Phi} = \mathbf{I}_K$, the elements of $\mathbf{W}$ are iid $\mathcal{CN}(0,1)$. Based on (2.34), the variance of the channel estimate of user k is given by

$$\hat{\beta}_k = \mathbb{E}\{|\hat{\mathbf{g}_k}|^2\} = \frac{\tau_p p_p \beta_k^2}{1 + \tau_p p_p \beta_k}. \tag{2.35}$$

The channel estimation error is given by $\tilde{\mathbf{G}} = \mathbf{G} - \hat{\mathbf{G}}$ and the variance of the channel estimation error of user k is

$$\tilde{\beta}_k = \mathbb{E}\{|\tilde{\mathbf{g}_k}|^2\} = \frac{\beta_k}{1 + \tau_p p_p \beta_k} \tag{2.36}$$

where β_k is the large scale fading coefficient of the kth user channel, τ_p is the pilot symbol length of user k and p_p is the transmit power of the pilot signal. Note that the detail steps for Equations (2.34), (2.35) and (2.36) are similar to the proof in Appendix 4.1 and 4.3.

Thus, the estimate of the channel to the kth user is an $M \times 1$ vector $[\hat{\mathbf{g}}_k]^T$ that can be expressed in normalized form as

$$\hat{\mathbf{g}}_k = \sqrt{\hat{\beta}_k}\, \mathbf{h}_k \tag{2.37}$$

where the elements of $\mathbf{h}_k$ are iid $\mathcal{CN}(0,1)$. Thus, the estimate of the K-users channel matrix can be formulated as

$$\hat{\mathbf{G}} = \mathbf{H}\mathbf{D}^{\frac{1}{2}} \tag{2.38}$$

where $\mathbf{D}$ is a diagonal matrix with diagonal element $\hat{\beta}_k$ and $\mathbf{H}$ is an $M \times K$ matrix with iid $\mathcal{CN}(0,1)$ elements. Generally, when both $(M,K) \to \infty$ with a finite ratio $\frac{M}{K} > 1$, the channel estimate and channel estimation error matrix can be reformulated as $\hat{\mathbf{G}} = \mathbf{H}_1\mathbf{D}_1$, $\tilde{\mathbf{G}} = \mathbf{H}_2\mathbf{D}_2$, respectively when $\mathbf{D}_l$ for $l = 1, 2$ are $K \times K$ diagonal matrices with diagonal elements d_{lk} is given by [56]

$$\begin{aligned} d_{1k} &= \sqrt{\frac{\tau_p p_p}{1 + \tau_p p_p \beta_k}}\beta_k \\ d_{2k} &= \sqrt{\frac{\beta_k}{1 + \tau_p p_p \beta_k}} \end{aligned} \tag{2.39}$$

where the matrices $\mathbf{H}_1$, $\mathbf{H}_2 \in \mathbb{C}^{M \times K}$ are independent and have iid $\mathcal{CN}(0,1)$ elements [56, 57].

Chapter 3

Efficient Detection Techniques in Massive MIMO Systems

3.1 Introduction

The goal of detection in massive MIMO systems is to estimate unknown transmitted signals from received signals, channel gains and knowledge of all the possible combination of the symbol alphabets of the transmitted signals [26, 58]. To get an optimal performance, maximum likelihood (ML) based signal detection techniques can be employed. But, due to its computational complexity, ML detection is not feasible for systems with large number of antennas or higher modulation schemes, which are practical scenarios for massive MIMO systems. To solve this challenge, alternative detection algorithms are proposed [26, 58, 59].

One option is to employ linear detection techniques such as MRC, ZF and MMSE based detection techniques [26, 35, 36, 60]. These algorithms give near optimal performance with low complexity. The other option for detection is to use algorithms and tools from optimization, heuristics, machine learning and artificial intelligence. These include detectors based on semi-definite relaxation (SDR), local search (LS), probabilistic data association (PDA), belief propagation (BP) and detection based on Markov Chain Monte Carlo (MCMC). Although, they have high computational complexity than linear detection techniques, these algorithms can achieve near optimal performance [26, 59].

As stated before, for massive MIMO systems, linear detection techniques such as MRC, ZF and MMSE give near optimal performance with low signal processing complexity [17, 21]. Various studies are conducted to analyze the performance and computational complexity of these detection techniques [3, 21, 34, 48, 61–63]. The studies show that despite very large number of BS antennas, the main complexity for practical system implementa-

tion emanates from the inverse operation of $K \times K$ matrix as shown in (3.4), where K is the number of users supported by the system [34, 61]. Although much smaller than the number of BS antennas, the number of scheduled users are quite large in massive MIMO systems [14]. Hence, computing the inverse of $K \times K$ matrix could result in very high computational complexity which may cause large processing delay [61].

To reduce the computational complexity from large matrix inversion, several approximation approaches are proposed. These include preconditioning of exact matrix inversion techniques [64], iterative techniques [65, 66], Truncated polynomial series expansion [17,61,62] and accelerator techniques [67,68]. A low complexity Richardson method is used in [69], but it has uncertainty parameter that affect convergence. Conjugate gradient method is applied in [68], but many divisions are involved in this method. Gauss-Seidel method is used in [65], but matrix inversion is not obtained directly which increase the complexity. Newton iteration method is used in [70] and the complexity can be controlled by number of iterations. It converges very fast. However, it requires complex calculation to get an initial matrix that ensure convergence [70].

Truncated Neumann series is proposed in [61, 62] to replace complex matrix inversion operation by matrix polynomial summation. It contains matrix addition and multiplication that are simple to implement in massive MIMO systems. Due to this, many recent works proposed Truncated Neumann series as the best alternative for large matrix inversion approximation [17, 34, 61, 62]. However, to implement Truncated Neumann series in massive MIMO systems, selecting appropriate initial matrix that speed up convergence is challenging [62]. Besides, thorough analysis is required to evaluate the performance-complexity trade-off, incurred error of approximation and the impacts of the ratio of number of BS antennas to number of users on convergence [62].

In this chapter, we analyze the performance and complexity of Truncated Neumann series-based matrix inversion approximation to linear detection in massive MIMO systems. Specifically, we analyze the performance with respect to the probability of convergence, complexity and error of approximation. Furthermore, we provide numerical simulation results that validate the theoretical analysis. In line with these points, the main contributions of this chapter are summarized as follows [30, 71, 72].

- Evaluate performance and complexity of linear detection and precoding techniques.
- Formulate Truncated Neumann series-based matrix inversion approximation algorithm for linear detection techniques.

- Analyze the performance and computational complexity of Truncated Neumann series-based matrix inversion approximation.
- Numerical simulation is done to validate the theoretical analysis.

3.2 The Massive MIMO System Model

We reconsider a single cell uplink massive MIMO system shown in Figure 2.1, where the BS is equipped with M-antennas to serve K-single antenna users under the same time-frequency resources. To simplify the analysis, we consider only the small scale fading

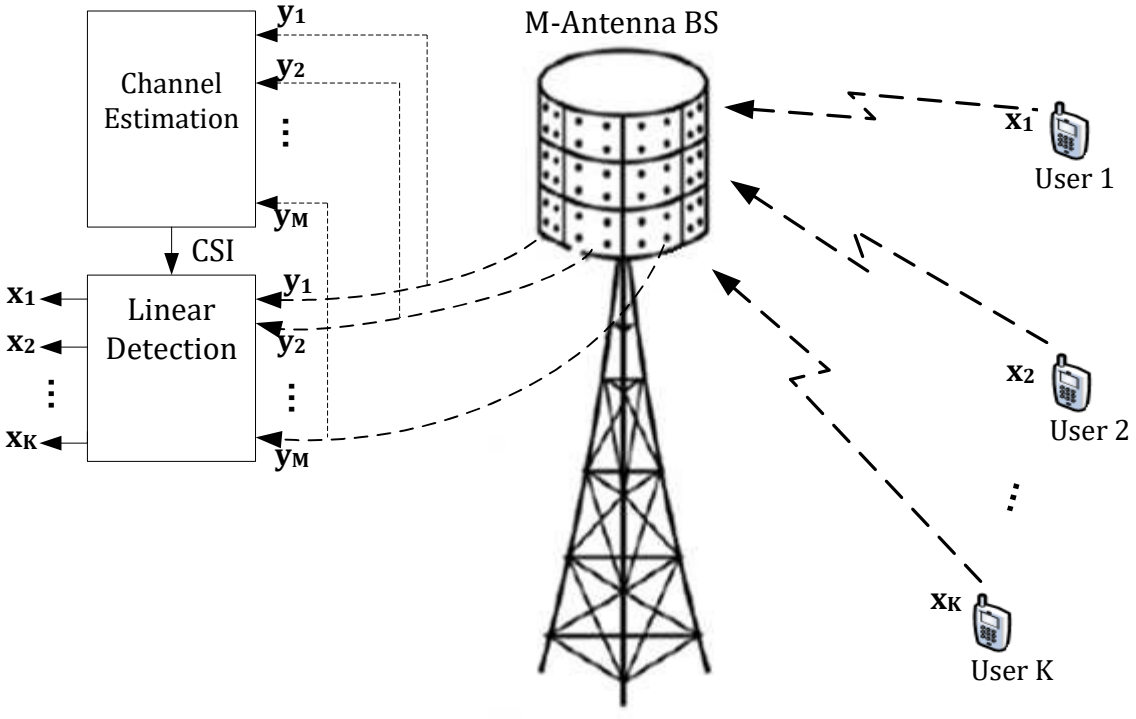

Figure 3.1: A single cell uplink massive MIMO system model.

channel coefficients. If $\mathbf{x}$ denotes the $K \times 1$ simultaneously transmitted signal vector from the K-users, then the $M \times 1$ received signal vector at the BS is given by [60]

$$\mathbf{y} = \mathbf{H}\mathbf{x} + \mathbf{n} \tag{3.1}$$

where $\mathbf{y} \in \mathbb{C}^M$ is the received signal at the BS antennas, $\mathbf{H} \in \mathbb{C}^{M \times K}$ represents the small scale fading channel gain matrix between the BS antennas and the K-users with $h_{mk} \triangleq [\mathbf{H}]_{mk}$ being the channel coefficient between the mth antenna and the kth user. We assume that the channel elements are uncorrelated, Rayleigh flat fading with independent and identically distributed (iid) zero mean and unit variance complex Gaussian random

variables. The channel gains are assumed to be perfectly known at the BS. $\mathbf{n}$ represents an $M \times 1$ additive white Gaussian noise vector observed at BS antennas with zero mean and variance σ^2 and it is assumed to be independent of $\mathbf{H}$. The average transmit power of each user is assumed to be unity. From the received signal vector $\mathbf{y}$ and knowledge of the CSI, the BS can detect signals transmitted from K-users [17, 60].

3.2.1 Detections in Massive MIMO Systems

Based on the received signal model in (3.1), the goal of massive MIMO detection is to estimate unknown transmitted signal vector $\mathbf{x}$, from received signal vector $\mathbf{y}$, channel gain $\mathbf{H}$, and knowledge of all the possible combination of the transmitted signal, $\mathcal{X}^K$ [60]. To achieve optimal performance, ML detection techniques can be employed [14]. With ML detection, the detector has to search all possible transmitted signal vectors and choose the best one that minimizes the distance between $\mathbf{y}$ and $\mathbf{Hx}$ as [60]

$$\hat{\mathbf{x}}_{\text{ML}} = \arg \min_{\mathbf{x} \in \mathcal{X}^K} \|\mathbf{y} - \mathbf{Hx}\|^2. \tag{3.2}$$

Solving (3.2) involves computing the objective function for all $\mathcal{X}^K$ and it results a complexity in the order of $|\mathcal{X}|^{\text{K}}$. For instance with 16 QAM and $K = 10$ users, it results one Trillion operation. Thus, ML detection is not feasible for massive MIMO systems that deploy large number of users and higher modulation orders [60].

3.2.2 Linear Detection Techniques in Massive MIMO Systems

It is shown in [21] that for massive MIMO systems where M is much larger than K (for instance $M = 200$ to support tens of users), linear detection techniques can give near optimal performance with low signal processing complexity. Linear detection techniques generate estimates of the transmitted symbols through linear transformation of the received signal as [21]

$$\hat{\mathbf{x}} = \mathbf{A}^{\text{H}}\mathbf{y} \tag{3.3}$$

where $\mathbf{A}^{\text{H}}$ the conjugate transpose of the linear transformation matrix that is given in (2.12). Assuming perfect CSI and removing the LSF part in (2.12), the linear transforma-

tion matrix is given by [21]

$$\mathbf{A} = \begin{cases} \mathbf{H} & \text{MRT} \\ \mathbf{H}(\mathbf{H}^{\mathrm{H}}\mathbf{H})^{-1} & \text{ZF} \\ \mathbf{H}(\mathbf{H}^{\mathrm{H}}\mathbf{H} + \frac{\sigma^2}{p_u}\mathbf{I}_{\mathrm{K}})^{-1} & \text{MMSE} \end{cases} \tag{3.4}$$

where $\mathbf{H} \in \mathbb{C}^{M \times K}$ represents the small scale fading channel matrix between the BS antennas and the users, σ^2 is the noise power and p_u is the power of uplink transmitted signal. As shown in (3.4), ZF and MMSE detectors incorporate complex matrix inversion operation. For massive MIMO systems, this inverse operation increase the computational complexity and may create a processing delay [61]. Thus, although much smaller than ML detection, the complexity is still high due to this matrix inversion. Besides, inversion operation is not feasible for practical hardware implementation. Hence, to avoid this matrix inversion operation, we propose Truncated Neumann series-based matrix inverse approximation for ZF detection in massive MIMO systems.

3.3 Truncated Neumann Series-based Matrix Inverse Approximation

Considering ZF detection and with Truncated Neumann series, the inverse of a $K \times K$ matrix $\mathbf{W} = \mathbf{H}^{\mathrm{H}}\mathbf{H}$ in (3.4) is transformed into sum of matrix polynomial series as [61, 62]

$$\mathbf{W}_N^{-1} \approx \sum_{n=0}^{N-1} (\mathbf{I}_K - \Theta\mathbf{W})^n \Theta \tag{3.5}$$

where N is the number of terms used in Truncated Neumann series approximation, Θ is a $K \times K$ initial matrix used in the approximation and $\mathbf{I}_K$ is identity matrix of size K. Inverse approximation with Truncated Neumann series is applied when the polynomial series in (3.5) is convergent. The polynomial series in (3.5) is convergent if-and-only-if (iff) the premise condition

$$\lim_{n \to \infty} (\mathbf{I}_K - \Theta\mathbf{W})^n \to \mathbf{0}_K \tag{3.6}$$

is satisfied [62]. Where $\mathbf{0}_K$ is the zero matrix. At given N, the speed of convergence and accuracy of the approximation in (3.5) depend on the size of the eigenvalues of $(\mathbf{I}_K - \Theta\mathbf{W})$.

When, the magnitude of the eigenvalues are small, the convergence is fast [73]. Besides, the probability of convergence and complexity of (3.5) is highly dependent on the initial matrix Θ [62]. Thus, finding an appropriate value of Θ is very critical to apply (3.5) in massive MIMO systems. Hence, in Section 3.3.1, we summarize different assumptions considered for the initial matrix.

3.3.1 Approximations for Initial Matrix, Θ

Based on eigenvalue based analysis and random matrix theory [57], we formulate and summarize assumptions for the initial matrix as

$$\Theta = \frac{1}{M+K}\mathbf{I}_K \tag{3.7a}$$

$$\Theta = \frac{\delta}{M+K}\mathbf{I}_K \tag{3.7b}$$

$$\Theta = \mathbf{D}^{-1} \tag{3.7c}$$

where $\delta\,(0 < \delta < 1)$ is an attenuation factor, $\mathbf{W} = \mathbf{D} + \mathbf{E}$ when $\mathbf{D}$ is a diagonal matrix including the diagonal elements of $\mathbf{W}$ and $\mathbf{E}$ is a hollow matrix including the off-diagonal elements of $\mathbf{W}$. The proof of (3.7a) is shown in Appendix 3.1.

Equation (3.7a) gives fast convergence when $M \gg K$ is very large. In this case, the M/K ratio is very large and this assumption can give performance close to the exact inverse with few iterations [34]. Whereas, for finite value of M and K, it may result a convergence failure in (3.6) as shown in Appendix 3.1. To solve the issue of convergence failure, an attenuation factor $\delta\,(0 < \delta < 1)$ is included as shown in (3.7b) to modify Θ [62]. It is shown in [62] that this approach provides better convergence to (3.5). But, it is difficult to chose an appropriate value of δ. If we choose large δ, the issue of non-convergence still exists; whereas if δ is small, the speed of convergence becomes very slow, hence N should be large to give good approximation. This increases the computational complexity. Thus, this assumption is not feasible for real system implementation.

The third approach is to use the diagonal element of $\mathbf{W}$ as shown in (3.7c). When $\mathbf{W}$ is a diagonal dominant matrix (DMM), (3.7c) gives better convergence for (3.6). $\mathbf{W}$ becomes a DDM when the magnitude of the diagonal elements of each row is larger than the sum of the magnitude of the off-diagonal elements in the same row as [61]

$$|\mathbf{W}_{ii}| > \sum_{j,\, j\neq i} |\mathbf{W}_{ij}|. \tag{3.8}$$

To further speed up the convergence, Newton iteration method is used in [70] to estimate Θ in an iterative way. Suppose $\mathbf{Z}_0$ is the original estimate of $\mathbf{W}^{-1}$ and if the premise condition $\|\mathbf{I}_K - \mathbf{W}\mathbf{Z}_0\| < 1$ is satisfied, the nth iteration estimate of $\mathbf{W}^{-1}$ is given by [70]

$$\mathbf{Z}_n = \mathbf{Z}_{n-1}(2\mathbf{I}_K - \mathbf{W}\mathbf{Z}_{n-1}). \tag{3.9}$$

Equation (3.9) is the modified Newton iteration method and it converges fast [70]. But the premise condition $\|\mathbf{I}_K - \mathbf{W}\mathbf{Z}_0\| < 1$ requires complex calculation to get an appropriate $\mathbf{Z}_0$. It is shown in [70] that substituting $\mathbf{D}^{-1}$ for $\mathbf{Z}_0$ satisfies the condition in (3.6). With this assumption, Θ can be replaced by $\mathbf{Z}_1$ where

$$\mathbf{Z}_1 = \mathbf{D}^{-1}(2\mathbf{I}_K - \mathbf{W}\mathbf{D}^{-1}). \tag{3.10}$$

By using (3.10), Truncated Neumann series-based inverse approximation in (3.5) is reformulated as

$$\mathbf{W}_N^{-1} \approx \sum_{n=0}^{N-1} (\mathbf{I}_K - \mathbf{Z}_1\mathbf{W})^n \mathbf{Z}_1. \tag{3.11}$$

By using the above approximations for the initial matrix, we analyze the performance of Truncated Neumann series-based inverse approximation.

3.4 Performance Analysis of Truncated Neumann Series-based Inverse Approximation

3.4.1 Conditions for Convergence

As it is stated in Section 3.3, Truncated Neumann series based matrix inverse approximation could be practical iff the premise condition in (3.6) is satisfied. Hence, we first analyze the convergence of (3.6) with the proposed initial matrix in Section 3.3.1. Based on the theory of matrix power series, the series $\mathbf{B}^N$ of a $K \times K$ matrix $\mathbf{B}$ converges to a zero matrix iff the spectral radius of $\mathbf{B}$ ($\rho(\mathbf{B})$) is less than one [62]. Thus, for $\Theta = \mathbf{D}^{-1}$, the condition of convergence in (3.6) is satisfied when

$$\rho(\mathbf{I}_K - \mathbf{D}^{-1}\mathbf{W}) < 1. \tag{3.12}$$

We assumed that $\mathbf{H}$ has iid $\mathcal{CN}(0,1)$ elements and M is very large. Hence, with the law of large numbers, the diagonal elements of $\mathbf{D}$ converges to $M\,\mathbb{E}\{|\mathbf{h}_{kk}|^2\} = M$ [74]. Replacing

the diagonal matrix $\mathbf{D}$ by $M\mathbf{I}_K$, the convergence condition in (3.12) is simplified to

$$\begin{aligned} &|M - \lambda(\mathbf{W})| < M \\ &\Rightarrow 0 < \lambda(\mathbf{W}) < 2M \\ &\Rightarrow \lambda_{\max}(\mathbf{W}) < 2M. \end{aligned} \tag{3.13}$$

By using the limit expression from (3.7), we get

$$\begin{aligned} &M(1 + \frac{1}{\sqrt{\alpha}})^2 < 2M \\ &\Rightarrow \alpha > \frac{1}{(\sqrt{2}-1)^2} \geq 5.83 \end{aligned} \tag{3.14}$$

where $\alpha = M/K$. Equation (3.14) is the minimum lower bound on M/K ratio that guarantee the condition of convergence for Truncated Neumann series-based inverse approximation. With (3.14), maximum number of users supported by the BS that achieve the condition of convergence for (3.6) is calculated and plotted in Figure 3.2. With these

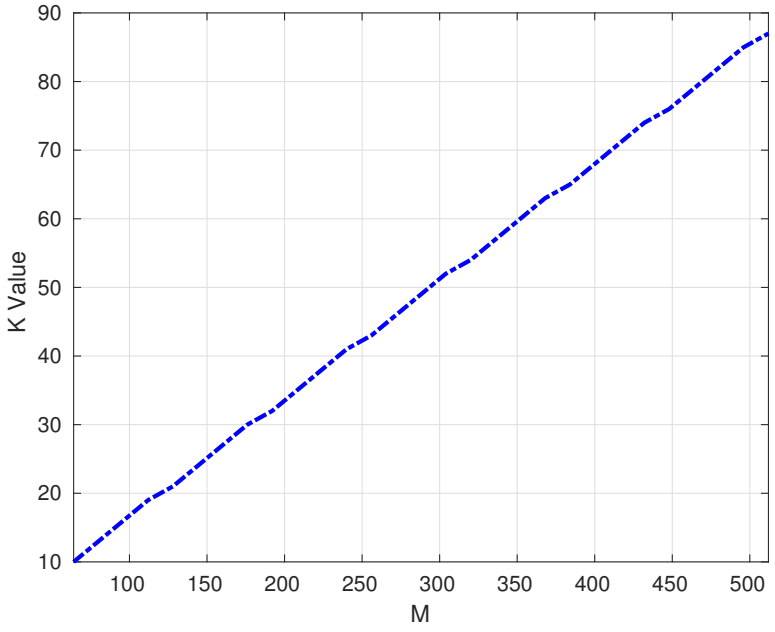

Figure 3.2: Maximum number of users supported by the system versus the number of BS antennas that satisfy (3.14).

users, the convergence probability of (3.6) based on the definition in (3.12) and approximate condition in (3.13) is shown in Figure 3.3. The result verifies that (3.13) is a good approximation for (3.12) and it gives high probability to guarantee the convergence condition in (3.6).

But, the condition in (3.13) does not give any information on the rate of convergence of (3.6). It may take many iterations to achieve the condition of convergence. Hence, to

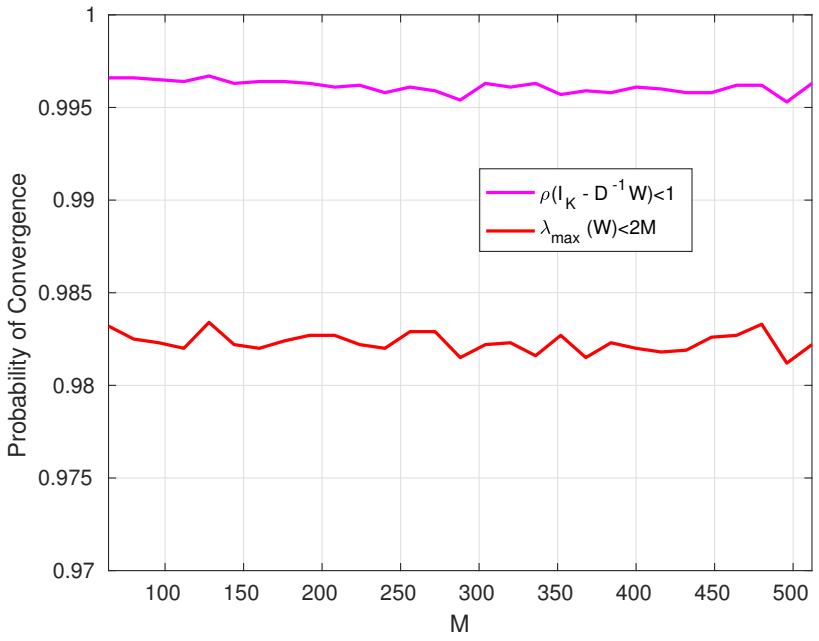

Figure 3.3: Convergence probability of (3.6) for the number of users in Figure 3.1.

assure convergence with few iterations, a strict lower bound on M/K ratio is proposed in [34] based on the diagonally dominant condition given in (3.8). If $\mathbf{h}_k$ denote the kth column vector of $\mathbf{H}$, the elements of $\mathbf{W}$ is calculated as [34]

$$\begin{cases} w_{ii} = \|\mathbf{h}_i\|^2 \\ w_{ij} = \mathbf{h}_i^H \mathbf{h}_j \qquad i \neq j. \end{cases} \tag{3.15}$$

When M is large, each w_{ii} approaches to M. In this case, the DMM condition in (3.8) can be approximated by [34]

$$\triangle_i = \sum_{i \neq j} |r_{ij}| < 1, \quad \forall_i \tag{3.16}$$

where r_{ij} is the normalized correlation coefficient between $\mathbf{h}_i$ and $\mathbf{h}_j$ and expressed by

$$r_{ij} = \frac{\mathbf{h}_i^H \mathbf{h}_j}{\|\mathbf{h}_i\| \|\mathbf{h}_j\|} \approx \frac{\mathbf{h}_i^H \mathbf{h}_j}{M}. \tag{3.17}$$

If we denote $x = |r_{ij}|$, the probability density function (pdf) of x is formulated in [34] as

$$f(x) = 2(M-1)x(1-x^2)^{M-2} \qquad 0 \leq x \leq 1. \tag{3.18}$$

With (3.18), the statistical parameters of x is calculated via Beta function approximation [34]. By using these statistical parameters, the lower bound on M/K ratio for $\mathbf{W}$ to be DDM is formulated as[1]

$$\alpha > \frac{M[\mathbb{E}(x) + \delta(x)]}{\mathbb{E}(x) + \delta(x) + 1} \tag{3.19}$$

[1]The proof is shown in Appendix 3.2

where $\mathbb{E}(x)$ is the mean of x and $\delta(x)$ is the standard deviation of x. With (3.19), maximum number of users supported by the BS that satisfy the convergence condition in (3.16) is calculated and plotted in Figure 3.4. With these K values, the condition for DDM is simulated based on the definition in (3.8) and approximated condition in (3.19) as shown in Figure 3.5. The figure shows that when M is large, it gives high probability for $\mathbf{W}$ to be diagonal dominant matrix. For instance at 128 number of BS antennas, the probability of convergence is 0.997. This verifies that (3.19) is a good approximation for (3.8) especially when M is large. Hence, the DDM condition in (3.19) is sufficient for the convergence condition in (3.12) and results faster convergence.

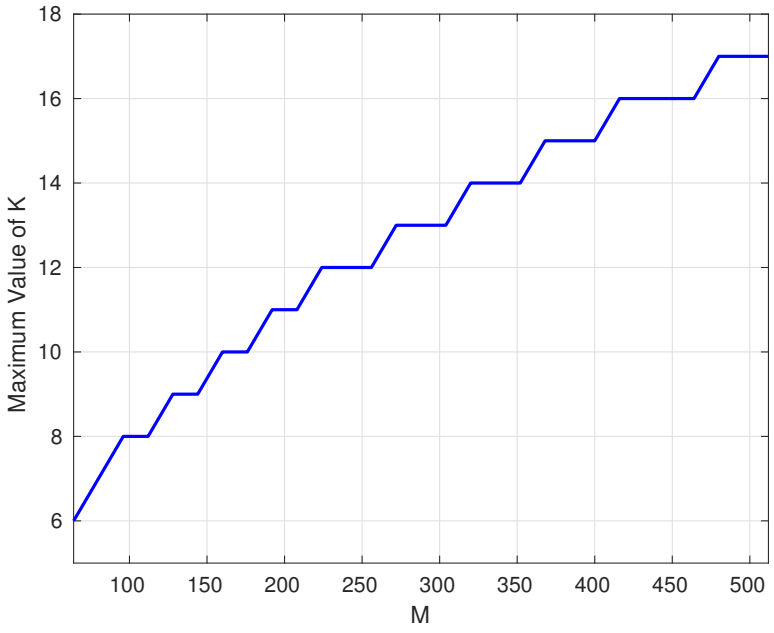

Figure 3.4: Maximum number of users supported by the BS that satisfy (3.19).

We further analyze the diagonal dominance condition of $\mathbf{W}$ by evaluating the condition number (λ_{ratio}) and diagonal dominance (DD) ratio expressed, respectively as [75]

$$\begin{aligned} \lambda_{\text{ratio}} &= \frac{\lambda_{\max}(\mathbf{W})}{\lambda_{\min}(\mathbf{W})} \\ \text{DD} &= \frac{\sum_{i=1}^{K} \mathbf{W}_{ii}}{\sum_{i=1}^{K} \sum_{j=1, j\neq i}^{K} |\mathbf{W}_{ij}|} \end{aligned} \tag{3.20}$$

where $\lambda_1, \lambda_2, \cdots, \lambda_K$ denote the eigenvalues of $\mathbf{W}$. If the condition number is close to one, the eigenvalues are less spread and convergence is very fast [73]. Figure 3.6 shows the condition number of $\mathbf{W}$ for $K = 10$ and $K = 40$. It is shown that for both values of K, the λ ratio converges to one when M becomes very large. Hence, to achieve the DDM condition, M should be very large.

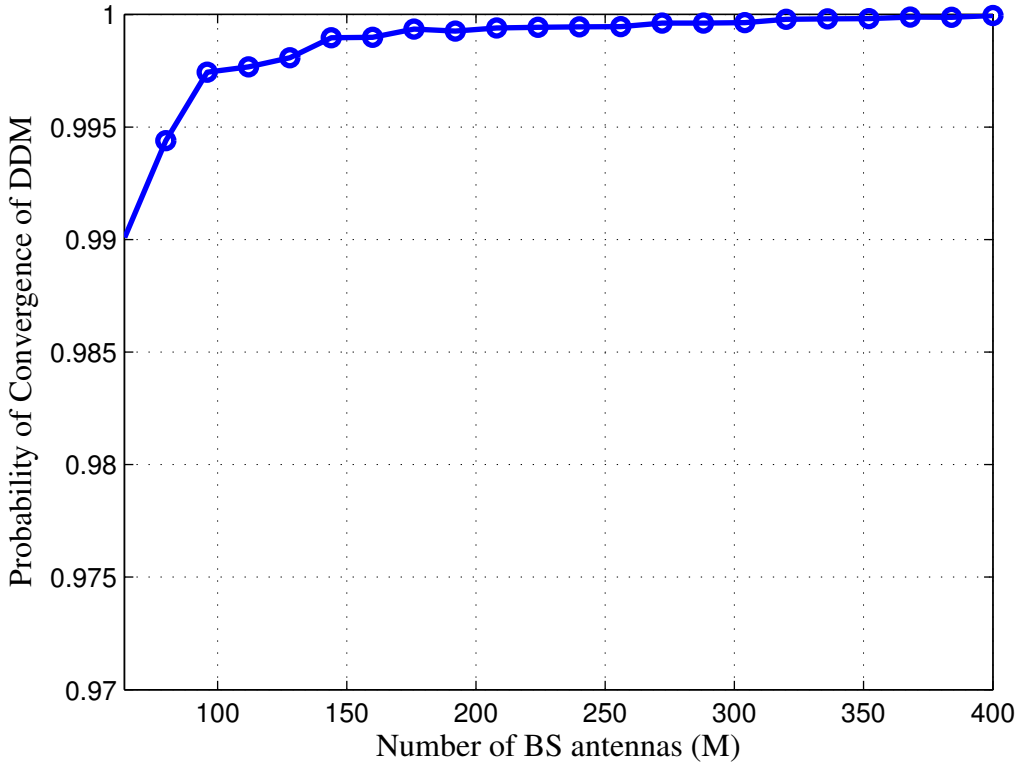

Figure 3.5: Diagonally dominant probability for the number of users in Figure 3.3.

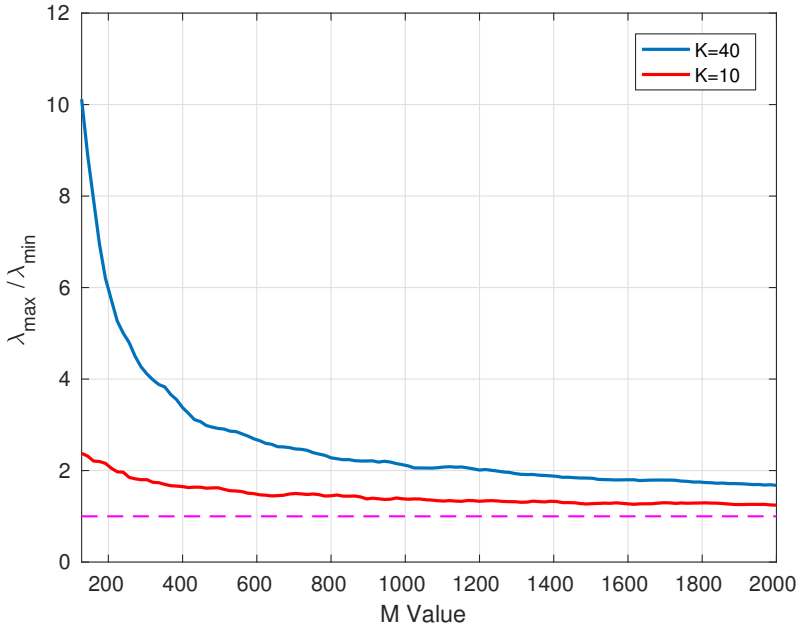

Figure 3.6: λ ratio versus M for $\mathbf{W}$.

Figure 3.7 shows the diagonal dominance ratio at fixed K and fixed M/K cases. The figure shows that at fixed K when M is large, $\mathbf{W}$ become highly diagonal dominant. This is because $\mathbf{W}$ has fixed dimension and the sum of the diagonal elements grows faster than

the off-diagonal elements. In contrast, when both M and K grows large, $\mathbf{W}$ becomes less diagonally dominant. This is because as the number of off-diagonal elements increases, their total contribution become quite significant.

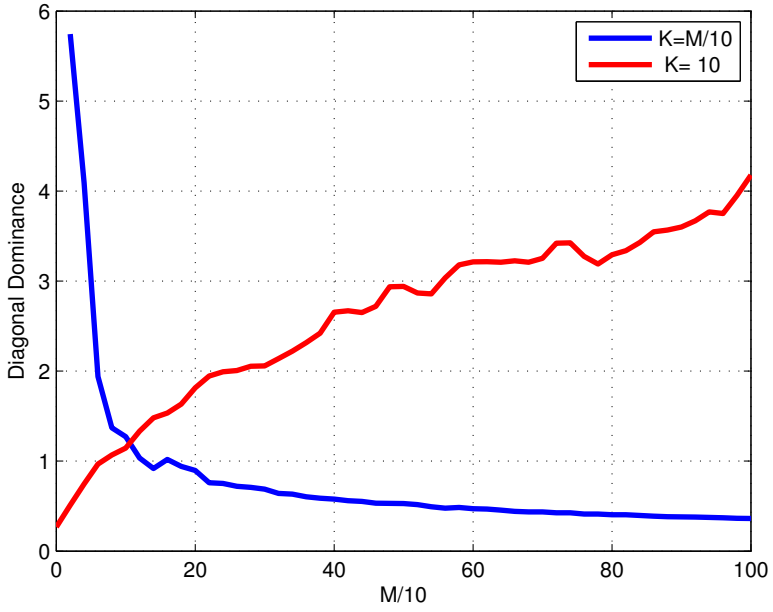

Figure 3.7: Test of channel diagonal dominance at fixed K and $\alpha = M/K$.

3.4.2 Analysis of the Approximation Error

The reduction in detection complexity with Truncated Neumann series results at the cost of approximation error. The error due to N-term approximation of the Neumann series is given by [62]

$$\triangle_N = (-\mathbf{D}^{-1}\mathbf{E})^N \mathbf{W}^{-1} \tag{3.21}$$

where $\mathbf{W}^{-1}$ denotes the exact inversion. Then, for ZF detection, the detected signal with Truncated Neumann series based inverse approximation is formulated as [62]

$$\hat{x}_{_N} = \mathbf{W}_N^{-1}\mathbf{H}^{\mathrm{H}}\mathbf{y} = \mathbf{W}^{-1}\mathbf{H}^{\mathrm{H}}\mathbf{y} - \triangle_N \mathbf{H}^{\mathrm{H}}\mathbf{y} \tag{3.22}$$

where $\triangle_{_N}\ \mathbf{H}^{\mathrm{H}}\mathbf{y}$ denotes the approximation error. As shown in Appendix 3.3, the norm of the approximation error is given by

$$\| \triangle_N \mathbf{H}^H\mathbf{y}\|_2 \leq \|(-\mathbf{D}^{-1}\mathbf{E})\|_2^N \ \ \|\mathbf{W}^{-1}\mathbf{H}^H\mathbf{y}\|_2. \tag{3.23}$$

From (3.23), it is clear that if the condition $\|\mathbf{D}^{-1}\mathbf{E}\| < 1$ is satisfied, the error approaches zero exponentially when N grows large. In this case, (3.13) is a sufficient condition for (3.5) to converge.

To analyze the error due to Truncated Neumann series approximation, we evaluate the the bit error rate (BER) performance of the system. For the simulation, we assume $M = 128$, $K = 8, 16$ and 16QAM is taken. Figure 3.8 shows the BER performance comparison between exact inversion and Truncated Neumann series-based inverse approximation. The result shows that Neumann series provides an efficient way to invert $\mathbf{W}$, especially when $N \geq 3$ and M/K ratio is large. For $K = 8$ and $N \geq 3$, Neumann series approximation and exact inversion gives nearly the same performance. When the number of scheduled users increases, the performance of Neumann series decreases. Because, as the number of users increases, $\mathbf{W}$ becomes less diagonal dominant and the condition in (3.12) is not necessarily satisfied [62].

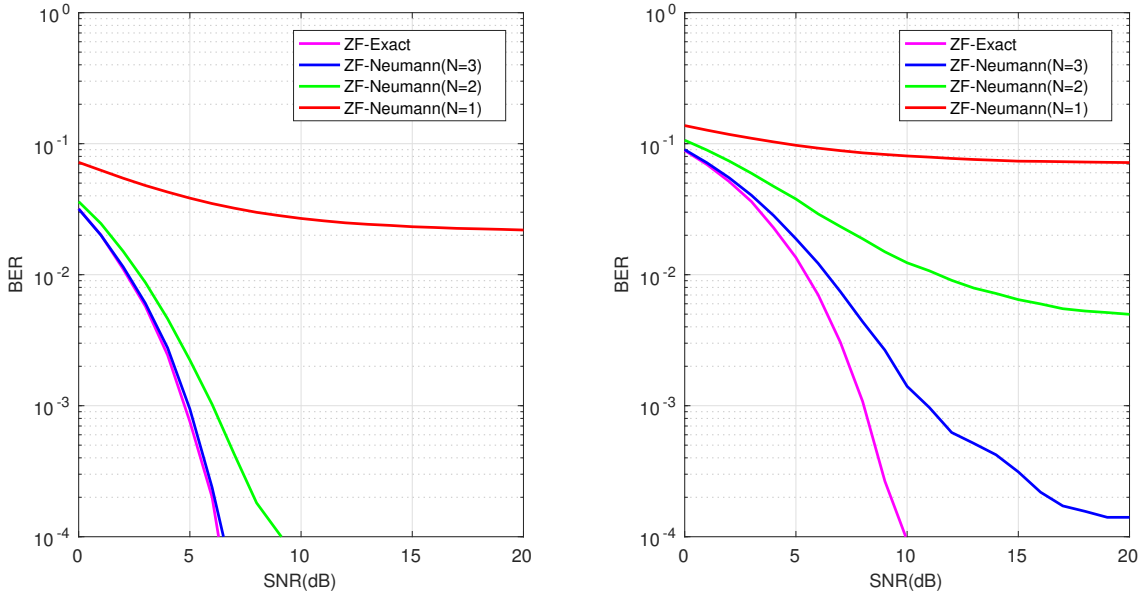

(a) For $K = 8$ users.

(b) For $K = 16$ users.

Figure 3.8: BER performance comparison between exact inversion and Truncated Neumann series approximation. We assume $M = 128$ and 16QAM is used.

Figure 3.9 shows the BER performance of Neumann series-based inverse approximation at different initial matrix, Θ. The result shows that if the diagonally dominant condition is satisfied, Newton iteration method gives better performance than other assumptions.

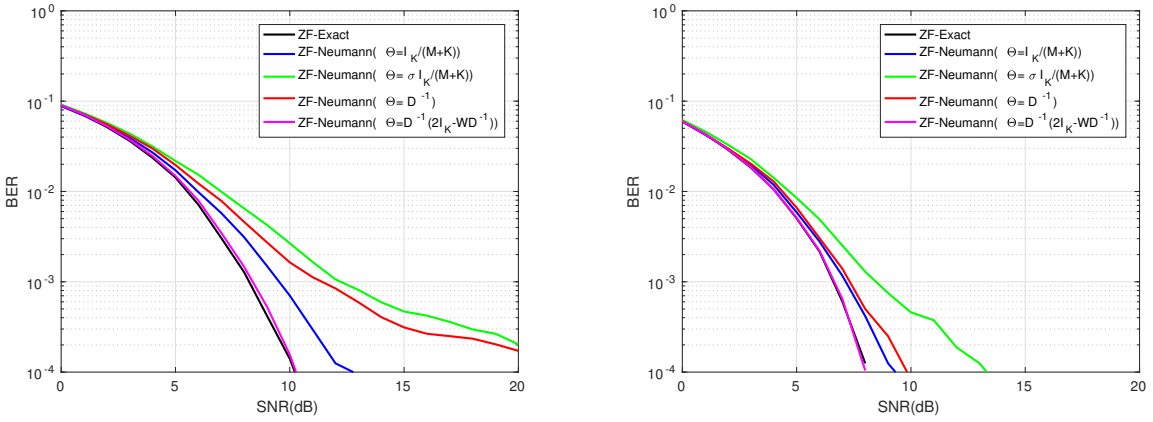

(a) For $K = 8$ users.

(b) For $K = 16$ users.

Figure 3.9: BER performance of Truncated Neumann series-based inverse approximation with different initial matrix, Θ. We assume $M = 128$, $N = 3$, $\delta = 0.25$. and 16QAM is used.

3.4.3 Computational Complexity Analysis

The computational complexity is calculated by sum of real valued addition, multiplication and division operations [62]. The required number of floating point operations on matrix inversion for various algorithms is calculated in [62] and shown in Table 3.1.

Table 3.1: Complexity comparison of a $K \times K$ matrix inversion techniques

Inversion Techniques		Multiplication*	Division	Square Root
Neumann Series	By using (3.7a)	$2(P-1)K^3$	K	0
	By using (3.7c)	$2(P-1)K^3 + K^2$	K	0
QR	Gram-Schmidt	$3K^3 + 2K^2$	$\frac{3}{2}K^2$	K
Gauss-Jordan		$K^3 + K^2$	$\frac{K^2+K}{2}$	0

*$P = \log_2(N+1)$

The result shows that exact inversion via Gauss-Jordan elimination requires few multiplications than other algorithms. But, its mathematical properties require complex floating point implementation in hardware [62]. Exact inversion via QR decomposition has complex operations including K^2 divisions and K square root. Compared to QR and Gauss-Jordan, inverse approximation using Truncated Neumann series-based inverse approximation re-

quires fewer division operations and has variable multiplication complexity based on the number of iteration [62].

We also calculate the floating point operations (FLOPS) with the number of users as shown in Figure 3.10. The result shows the computational complexity of exact inversion and Truncated Neumann series-based inverse approximation to reach a certain level of uplink achievable sum rate (for instance 90% of achievable rate with ZF detection). The result shows that when $N \leq 2$, the complexity of Truncated Neumann series-based inverse approximation is low even at large number of users. Because, all multiplications that involve diagonal matrices leads to low number of operations. For $N = 3$, one more matrix multiplication is required which increase the complexity. But, the complexity is still below QR decomposition. This shows that for $N \leq 3$, Neumann series require fewer computations and it can be implemented in hardware by using simple matrix multiplication [62].

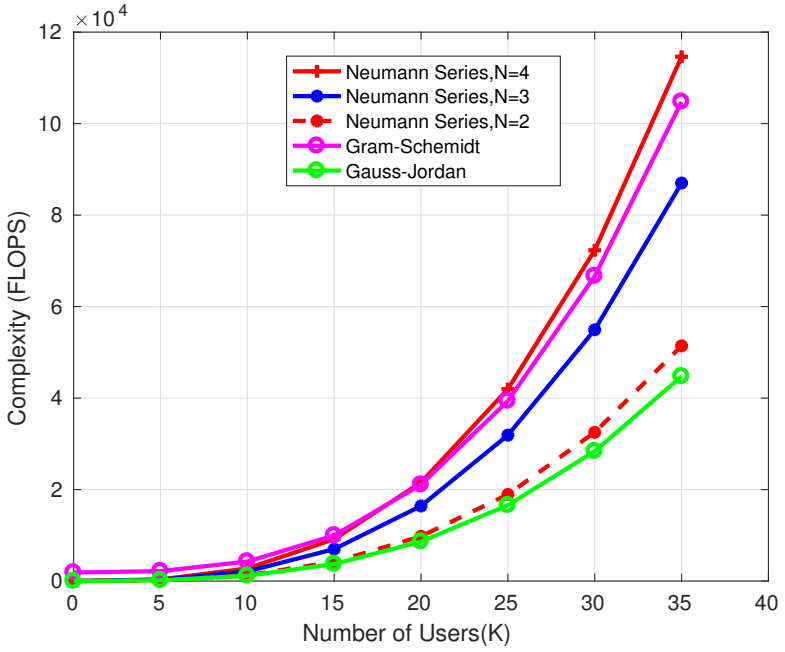

Figure 3.10: Algorithm complexity comparison to compute inverse of a $K \times K$ matrix.

3.5 Summary

In this chapter, the performance of Truncated Neumann series-based matrix inversion approximation is analyzed in massive MIMO systems. Various assumptions to choose the initial matrix for Truncated Neumann series-based matrix inversion approximation are reviewed. The performance and complexity of Truncated Neumann series-based inverse

approximation is thoroughly analyzed. Numerical simulation results are provided to validate the theoretical analysis. The results show that when the number of BS antennas become very large, the channel becomes more diagonal dominant and Truncated Neumann series-based inverse approximation converges fast and gives nearly the same performance as exact inversion techniques.

Appendices

Appendix 3.1: Proof of (3.7a)

If the elements of $\mathbf{H} \in \mathbb{C}^{M\times K}$ are iid $\mathcal{CN}(0,1)$ and let both M and $K \to \infty$ and $\alpha = M/K$; based on random matrix theory, the largest and smallest eigenvalues of $\mathbf{W}$ are converged to [74]

$$\begin{aligned} \lambda_{\max}(\mathbf{W}) &\to M(1+\frac{1}{\sqrt{\alpha}})^2 \\ \lambda_{\min}(\mathbf{W}) &\to M(1-\frac{1}{\sqrt{\alpha}})^2. \end{aligned} \tag{3.24}$$

If the initial matrix is formulated as

$$\Theta = \frac{1}{M+K} I_K \tag{3.25}$$

then, the extreme eigenvalues of the matrix product $\Theta\mathbf{W}$ is given by

$$\begin{aligned} \lambda_{\max}(\Theta\mathbf{W}) &\to (1+\frac{2\sqrt{\alpha}}{1+\alpha}) \\ \lambda_{\min}(\Theta\mathbf{W}) &\to (1-\frac{2\sqrt{\alpha}}{1+\alpha}). \end{aligned} \tag{3.26}$$

From (3.26), it is noteworthy that eigenvalues of $(\mathbf{I}_K - \Theta\mathbf{W})$ lie in the range of $[-2\sqrt{\alpha}/(1+\alpha), 2\sqrt{\alpha}/(1+\alpha)]$. For $\alpha \geq 1$, $2\sqrt{\alpha}/(1+\alpha) \leq 1$; thus, the convergence of (3.6) is satisfied with the choice of (3.25). Moreover, when α is large, $2\sqrt{\alpha}/(1+\alpha) \to 0$ which shows that (3.6) converges very fast. Hence, (3.5) can give performance close to the exact inverse with few iterations [34]. But, for finite value of M and K, eigenvalues of the matrix product $\Theta\mathbf{W}$ may lie outside $[-2\sqrt{\alpha}/(1+\alpha), 2\sqrt{\alpha}/(1+\alpha)]$. This results convergence failure in (3.6).

Appendix 3.2: Proof of (3.19)

For $x = |r_{ij}|$, with $0 \leq x \leq 1$, the pdf of x is given in [34] as

$$f(x) = 2(M-1)x(1-x^2)^{M-2}. \tag{3.27}$$

The mean and standard deviation of x is calculated via Beta function approximation [34], where the mean of x is

$$\mathbb{E}(x) = \int_0^1 xf(x)dx = (M-1)\beta(1.5, M-1) \tag{3.28}$$

when $\beta(a,b)$ is the Beta function defined by $\beta(a,b) = \int_0^1 t^{a-1}(1-t)^{b-1}dt$. Similarly

$$\mathbb{E}(x^2) = \int_0^1 x^2 f(x)dx = (M-1)\beta(2, M-1). \tag{3.29}$$

With (3.28) and (3.29), the standard deviation of x is

$$\delta(x) = \sqrt{\mathbb{E}(x^2) - \mathbb{E}(x)^2}. \tag{3.30}$$

For large K, $\triangle_i$ in (3.16) is mostly smaller than $(K-1)[\mathbb{E}(x) + \delta(x)]$ and can be approximated by [34]

$$(K-1)[\mathbb{E}(x) + \delta(x)] < 1. \tag{3.31}$$

Based on (3.31), the lower bound on the M/K ratio for $\mathbf{W}$ to be diagonal dominant is formulated as

$$\alpha > \frac{M[\mathbb{E}(x) + \delta(x)]}{\mathbb{E}(x) + \delta(x) + 1}. \tag{3.32}$$

Appendix 3.3: Proof of (3.21)

The error due to N-term approximation of the Neumann series is given by [62]

$$\begin{aligned} \triangle_N &= \mathbf{W}_\infty^{-1} - \mathbf{W}_N^{-1} \\ &= \sum_{n=N}^{\infty} (-\mathbf{D}^{-1}\mathbf{E})^n \mathbf{D}^{-1} \\ &= (-\mathbf{D}^{-1}\mathbf{E})^N \sum_{n=0}^{\infty} (-\mathbf{D}^{-1}\mathbf{E})^n \mathbf{D}^{-1} \\ &= (-\mathbf{D}^{-1}\mathbf{E})^N \mathbf{W}_\infty^{-1}. \end{aligned} \tag{3.33}$$

where $\mathbf{W}_\infty^{-1}$ denotes the exact inversion. For ZF detection, the detected signal with Truncated Neumann series inverse approximation is formulated as [62]

$$\hat{x}_{_N} = \mathbf{W}_N^{-1}\mathbf{H}^{\mathrm{H}}\mathbf{y} = \mathbf{W}_\infty^{-1}\mathbf{H}^{\mathrm{H}}\mathbf{y} - \triangle_N \mathbf{H}^{\mathrm{H}}\mathbf{y} \tag{3.34}$$

where $\triangle_N \ \mathbf{H}^{\mathrm{H}}\mathbf{y}$ denotes the approximation error and its norm is bounded as

$$\begin{aligned} \| \triangle_N \ \mathbf{H}^H\mathbf{y}\|_2 &= \|(\mathbf{D}^{-1}\mathbf{E})^N\mathbf{W}_\infty^{-1}\mathbf{H}^H\mathbf{y}\|_2 \\ &\leq \|(-\mathbf{D}^{-1}\mathbf{E})^N\|_2 \ \|\mathbf{W}_\infty^{-1}\mathbf{H}^H\mathbf{y}\|_2 \\ &\leq \|(-\mathbf{D}^{-1}\mathbf{E})\|_2^N \ \|\mathbf{W}_\infty^{-1}\mathbf{H}^H\mathbf{y}\|_2. \end{aligned} \tag{3.35}$$

Chapter 4

Achievable Rate of Massive MIMO Systems in Rician Fading Channel

4.1 Introduction

Various studies are done to analyze the possible propagation channel model of massive MIMO systems [14,17,21,48,76]. The studies show that the use of large number of antennas at the BS helps to obtain favorable propagation condition where channel vectors between the users and the BS antennas become pair wisely orthogonal. As stated in Chapter 2, under favorable propagation condition, the effect of interuser interference and noise can be minimized or eliminated [3, 17, 23, 25]. Besides, when the number of antennas at the BS are very large, the effect of small scale fading is averaged out and the channel becomes nearly deterministic. This effect is termed as channel hardening and thus, user scheduling, power control and resource allocation can be done in large-scale fading (that is large time scale) instead of the small-scale fading (that is small time scale). This simplifies the signal processing complexity [3, 14, 21, 27, 48].

However, most of the previous research works assume independent and identically distributed Rayleigh fading channel model, which does not take into account the line-of-sight (LOS) link that may be dominant in many realistic massive MIMO scenarios. For instance, cell densification makes the distance between the BS and the users more closer and the existence of LOS become more dominant. Previous works also assume the availability of perfect CSI at the BS. But, in real situations, the CSI of the true channel matrix is unknown and should be estimated at the BS [21]. Besides, most works do not account the combined effect of main propagation parameters such as path loss, shadowing, multipath fading and spatial correlation. Furthermore, the fundamental of placing massive number

of antennas in a confined space can be achieved by pushing the operating frequency in the millimeter wave (mmWave) bands that are typically modeled in Rician distribution due to the existence of dominant LOS components [77, 78].

In this chapter, we analyze the performances of massive MIMO systems in Rician fading channel. Major Rician fading channel parameters including pathloss, shadowing, multipath fading, LOS propagation and spatial channel correlation are considered. In this model, the multipath fading channel matrix has both a deterministic LOS component and a random non-line-of-sight (NLOS) component [76–80]. Assuming a Rician fading propagation model and linear receivers, we formulate the uplink achievable sum rate. Then, analytical closed-form lower bound achievable sum rate is derived and expressed as a function of system and propagation parameters. The impacts of system and propagation parameters on uplink achievable sum rate are evaluated. In line with these points, the main contributions of this chapter are summarized as follows [28]:

- Assuming the channel matrix is unknown at the BS, MMSE based channel estimation is done to derive the estimate of the Rician fading channel coefficients and variance of the channel estimation error;
- Derive analytical closedform lower bound achievable sum rate. To this end, closed-form lower bound achievable sum rate is formulated in-terms of system and propagation parameters. Furthermore, the impacts of these parameters are analyzed theoretically at large system regimes.
- Perform numerical simulations to validate theoretical analysis.

4.2 Massive MIMO Systems in Rician Fading Channel

We reconsider a single cell uplink massive MIMO system shown in Figure 3.1 where the BS is equipped with M-antennas to serve N-single antenna users in the same time-frequency resource. Let $\mathbf{x} = \sqrt{p_u}\,\mathbf{s}$ denotes the complex valued $N \times 1$ transmitted signal from N users. Then, an $M \times 1$ complex valued received signal $\mathbf{y}$ at the BS is given by [3, 21]

$$\mathbf{y} = \sqrt{p_u}\mathbf{G}\mathbf{x} + \mathbf{n} \tag{4.1}$$

where $\mathbf{G}$ represents an $M \times N$ Rician fading channel matrix between the BS antennas and the N users with $g_{mn} \triangleq [\mathbf{G}]_{mn}$ is the channel coefficient between the mth antenna of the BS and the nth user, p_u is the average transmitted power of each user. $\mathbf{s} = (s_1, s_2, \cdots, s_N)^T$ is the information bearing vector with $\mathbb{E}\{\mathbf{s}\mathbf{s}^H\} = \mathbf{I}_N$. The Vector $\mathbf{n}$ represents additive white Gaussian noise at the BS antennas with zero mean and covariance matrix $\sigma^2\mathbf{I}$ where $\mathbf{I}$ is the identity matrix [3, 21]. In the subsequent section, we further describe the uplink channel model.

4.2.1 Uplink Rician Fading Channel Model

The physical channel between a user and the BS antennas is subjected to pathloss, shadowing and multipath fading effects. Considering all these propagation effects, the channel model for uplink massive MIMO system is expressed as [3]

$$\mathbf{G} = \mathbf{H}\mathbf{D}^{\frac{1}{2}} \tag{4.2}$$

where $\mathbf{D} = \text{diag}\{\beta_1, \beta_2, \cdots, \beta_N\} \in \mathbb{R}^{N\times N}$ is a diagonal matrix and represents the large scale fading (LSF) effect that includes pathloss and shadowing effects with elements $\beta_n = \text{d}_n^{-v}\psi_n$, d_k is the Euclidean distance between the BS antenna and the nth user, v is the pathloss exponent and ψ_n represents a log-normal shadowing with $10\log_{10}\psi_n \sim \mathcal{N}(0, \sigma_{\text{sh}}^2)$ where σ_{sh} is the standard deviation of the shadow fading model [3]. The matrix $\mathbf{H} \in \mathbb{C}^{\text{M}\times\text{N}}$ represents the multipath fading effect. It can be modeled with the Rayleigh or Rician distribution [77].

We consider a Rician fading channel model in this chapter. In this model, the matrix $\mathbf{H}$ consists of two parts; a deterministic component that represent the LOS signals and a Rayleigh-distributed random component which accounts for the NLOS signals. It is formulated as [77]

$$\mathbf{H} = \bar{\mathbf{H}}\left(\frac{\Omega}{\Omega + \mathbf{I}_N}\right)^{\frac{1}{2}} + \mathbf{H}_r\left(\frac{1}{\Omega + \mathbf{I}_N}\right)^{\frac{1}{2}} \tag{4.3}$$

where $\bar{\mathbf{H}}$ is an $M \times N$ matrix that represents the deterministic component in which $[\bar{\mathbf{H}}]_{mn} = e^{-j(m-1)\frac{2\pi d}{\lambda}\sin(\theta_n)}$, when d is the spacing between BS antennas and λ is the transmission wave length, θ_n is the arrival angle of the nth user signal with respect to the BS antennas boresight direction, Ω is an $\text{N} \times \text{N}$ diagonal matrix with $[\Omega]_{nn} = \mathcal{K}_n$, $\mathcal{K}_n$ is the Rician factor of each user which shows ratio of the power of the deterministic component to the power of the scattered component [77] and $\mathbf{H}_r$ denotes the random NLOS component, the entries of

which are assumed to be iid Gaussian random variables with zero-mean and unit variance. Thus, by using (4.3), the channel model in (4.2) is modified as

$$\mathbf{G} = \bar{\mathbf{G}}\left(\frac{\Omega}{\Omega + \mathbf{I}_N}\right)^{\frac{1}{2}} + \mathbf{G}_r\left(\frac{1}{\Omega + \mathbf{I}_N}\right)^{\frac{1}{2}} \tag{4.4}$$

where $\bar{\mathbf{G}} = \bar{\mathbf{H}}\mathbf{D}^{\frac{1}{2}}$ denotes the LOS component of $\mathbf{G}$ and $\mathbf{G}_r = \mathbf{H}_r\mathbf{D}^{\frac{1}{2}}$ represents the random component of $\mathbf{G}$. We assume $\mathbf{G}$ to be unknown and MMSE based channel estimation is considered at the BS as reported in Section 4.2.2.

4.2.2 MMSE-based Rician Channel Estimation

In real-world scenarios, the true channel matrix $\mathbf{G}$ is unknown and estimated at the BS. To simplify the analysis, most works assume that the LSF channel coefficients, the deterministic LOS component and the the Rician-$\mathcal{K}$ factor are perfectly known both at the BS and users [2, 3, 21, 28]. Thus, estimation is performed only for the random NLOS component, $\mathbf{H}_r$. This assumption is reasonable since the LSF channel coefficients change very slowly as compared to small scale fading (SSF) channel coefficients and they can be reliably estimated [2, 3]. With this assumption, the MMSE based channel estimate of $\mathbf{G}$ can be expressed as [3]

$$\hat{\mathbf{G}} = \bar{\mathbf{G}}\left(\frac{\Omega}{\Omega + \mathbf{I}_N}\right)^{\frac{1}{2}} + \hat{\mathbf{G}}_r\left(\frac{1}{\Omega + \mathbf{I}_N}\right)^{\frac{1}{2}} \tag{4.5}$$

where $\hat{\mathbf{G}}_r = \hat{\mathbf{H}}_r\mathbf{D}^{\frac{1}{2}}$ represents the estimate of the random component of $\mathbf{G}$. It is shown in [3,21] that the channel can be estimated using uplink pilots. Let $\tau_c = B_c T_c$ be the length in time-bandwidth product of the coherence interval and let $\tau_p \leq \tau_c$ be the symbols used for uplink training. All users are assumed to simultaneously transmit the pilot sequences of τ_p-symbols. The pilot sequence of the N users is represented by a $\tau_p \times N$ matrix $\sqrt{p_p}\mathbf{\Phi}$ that satisfy $\mathbf{Z}^{\mathrm{H}}\mathbf{Z} = \mathbf{I}_N$ where $\mathbf{Z} \triangleq \mathbf{\Phi}[(\Omega + \mathbf{I}_N)^{-1}]^{\frac{1}{2}}$, and $p_p = \tau_p p_u$ is uplink transmit pilot power. Then, an $M \times \tau_p$ received pilot matrix at the BS is given by [3]

$$\mathbf{Y}_{\mathrm{p}} = \sqrt{p_p}\mathbf{G}\mathbf{\Phi}^T + \mathcal{N} \tag{4.6}$$

where $\mathcal{N}$ is an $M \times \tau_p$ noise matrix with iid $\mathcal{CN}(0, 1)$ elements. Removing the LOS component of $\mathbf{G}$ in (4.4), which is assumed to be known a-priori, and substituting the remaining terms into (4.6), the received pilot matrix become

$$\mathbf{Y}_{\mathrm{p},r} = \sqrt{p_p}\mathbf{G}_r(\frac{1}{\Omega + \mathbf{I}_N})^{\frac{1}{2}}\mathbf{\Phi}^T + \mathcal{N} = \sqrt{p_p}\mathbf{G}_r\mathbf{Z}^T + \mathcal{N}. \tag{4.7}$$

Then, channel estimation is done to estimate $\mathbf{G}_r$ from $\mathbf{Y}_{\mathrm{p},r}$. We derive the MMSE based channel estimation and summarize the proof in Theorem 4.2.1.

Theorem 4.2.1 *Given a $\tau_p \times N$ uplink transmitted pilot signal $\sqrt{p_p}\mathbf{\Phi}$ from all users that satisfy $\mathbf{Z}^H\mathbf{Z} = \mathbf{I}_N$ where $\mathbf{Z} \triangleq \mathbf{\Phi}[(\Omega + \mathbf{I}_N)^{-1}]^{\frac{1}{2}}$ and $p_p = \tau_p p_u$ is the transmit pilot signal power, then the MMSE based estimate of the random component of the Rician fading channel that are estimated from the received pilot matrix $\mathbf{Y}_{p,r}$ is given by*

$$\begin{aligned}\hat{\mathbf{G}}_r &= \frac{1}{\sqrt{p_p}}\mathbf{Y}_{p,r}\mathbf{Z}^*\tilde{\mathbf{D}} \\ &= (\mathbf{G}_r + \frac{1}{\sqrt{p_p}}\mathbf{W})\tilde{\mathbf{D}}\end{aligned} \tag{4.8}$$

where $\tilde{\mathbf{D}} \triangleq (\frac{1}{p_p}\mathbf{D}^{-1} + \mathbf{I}_N)^{-1}$ and $\mathbf{W} \triangleq \mathcal{N}\mathbf{Z}^*$. With $\mathbf{Z}^H\mathbf{Z} = \mathbf{I}_N$, the entries of $\mathbf{W}$ are iid Gaussian random variables with zero mean and unit variance. The proof is shown in Appendix 4.1.

4.2.3 Analysis of the Channel Estimation

Let $\tilde{\mathbf{G}} \triangleq \hat{\mathbf{G}} - \mathbf{G}$ denotes the error incurred due to channel estimation, owing to the properties of MMSE estimation [55], the channel estimation error is uncorrelated with both the channel estimate and the received pilot signal. Based on this factors, the statistical parameters of the elements of the channel estimation error is analyzed as follows.

- For the estimated channel matrix in (4.8), the channel estimation error is uncorrelated with both the channel estimate and the received pilot signal and has Gaussian distribution as

$$\tilde{\mathbf{g}}_{mn} \sim \mathcal{CN}(0, \tilde{\beta}_n) \tag{4.9}$$

  where $\tilde{\beta}_n$ is the variance of $\tilde{\mathbf{g}}_{mn}$ which is given by

$$\tilde{\beta}_n = \frac{\beta_n}{(1 + p_{\mathrm{p}}\beta_n)(\mathcal{K}_n + 1)} \tag{4.10}$$

  for $m = 1, 2, \cdots, M$ and $n = 1, 2, \cdots, N$.

- Applying the theory of large system analysis, it shown that when the number of BS antennas goes to large, the inner product of the estimated channel matrix is converged to [57]

$$\frac{1}{M}\hat{\mathbf{G}}^{\mathrm{H}}\hat{\mathbf{G}} \rightarrow \mathrm{diag}\Big[\frac{\beta_n}{\mathcal{K}_n+1}(\mathcal{K}_n+\eta_n)\Big] \tag{4.11}$$

  where diag represents the diagonal matrix and $\eta_n = \frac{p_p\beta_n}{1+p_p\beta_n}$.

The proof of Equations (4.10) and (4.11) is shown in Appendix 4.3. The result in (4.10) and (4.11) implies that when the number of BS antennas become large, the impacts of small scale fading is averaged out. And thus, the performances of the massive MIMO system depends only on the large scale fading parameters and the Rician $\mathcal{K}$-factor.

4.3 Achievable Sum Rate of Massive MIMO Systems with Linear Receivers

Let an $M \times N$ matrix $\mathbf{A}$ be the model for a linear detector which depends on $\hat{\mathbf{G}}$, then the BS processes the received signal by multiplying (4.1) with $\mathbf{A}^{\mathrm{H}}$ as [21]

$$\hat{\mathbf{x}} = \mathbf{A}^{\mathrm{H}}\mathbf{y} = \sqrt{p_u}\mathbf{A}^{\mathrm{H}}(\hat{\mathbf{G}}-\tilde{\mathbf{G}})\mathbf{x} + \mathbf{A}^{\mathrm{H}}\mathbf{n}. \tag{4.12}$$

From (4.12), the detected signal for the nth user is given by

$$\hat{x}_n = \mathbf{a}_n^{\mathrm{H}}\mathbf{y} = \sqrt{p_u}\mathbf{a}_n^{\mathrm{H}}\hat{\mathbf{g}}_n x_n + \sqrt{p_u}\sum_{i=1,i\neq n}^{N}\mathbf{a}_n^{\mathrm{H}}\hat{\mathbf{g}}_i x_i - \sqrt{p_u}\sum_{i=1}^{N}\mathbf{a}_n^{H}\tilde{\mathbf{g}}_i x_i + \mathbf{a}_n^{H}\mathbf{n}. \tag{4.13}$$

where $\mathbf{a}_n$ is the nth column of $\mathbf{A}$, and $\hat{\mathbf{g}}_i$ and $\tilde{\mathbf{g}}_i$ are the ith columns of $\hat{\mathbf{G}}$ and $\tilde{\mathbf{G}}$, respectively. The last three terms in (4.13) represents intracell interference, channel estimation error and noise, respectively. The BS treats the channel estimate as the true channel, and the last three terms in (4.13) is considered as interference and noise [3]. Thus, by employing the results from (4.10) and (4.11), the uplink achievable rate of the nth user with linear processing is given by

$$R_n = \mathbb{E}\left\{\log_2\left(1+\frac{p_u|\mathbf{a}_n^{\mathrm{H}}\hat{\mathbf{g}}_n|^2}{p_u\sum_{i=1,\,i\neq n}^{N}|\mathbf{a}_n^{\mathrm{H}}\hat{\mathbf{g}}_i|^2+\sum_{i=1}^{N}\|\mathbf{a}_n\|^2\frac{p_u\beta_i}{(1+p_p\beta_i)(\mathcal{K}_i+1)}+\|\mathbf{a}_n\|^2}\right)\right\}. \tag{4.14}$$

Finally, the uplink achievable sum rate of the system is given by [3]

$$R_s = (1-\frac{\tau_p}{\tau_c})\sum_{n=1}^{N}R_n \tag{4.15}$$

where τ_c the length of the coherence interval and τ_p the length of the pilot signal.

4.3.1 Uplink Achievable Rate with ZF Detector

Based on the achievable rate formulation in (4.14), we derive analytical closedform lower-bound expression for uplink achievable rate of ZF detector. For ZF detector with imperfect CSI at the BS, the detection matrix is given by $\mathbf{A} = \hat{\mathbf{G}}(\hat{\mathbf{G}}^{\mathrm{H}}\hat{\mathbf{G}})^{-1}$. When $M > N$, $\mathbf{A}^{\mathrm{H}}\hat{\mathbf{G}} = \mathbf{I}_N$ and thus, $\mathbf{a}_n^H\hat{\mathbf{g}}_i = 1$ for $n = i$ and zero otherwise [21]. With this assumption and by using (4.10) and (4.14), the achievable rate of user n is given by

$$R_n^{\mathrm{ZF}} = \mathbb{E}\Big\{ \log_2 \Big(1 + \frac{p_u}{\Big(\sum_{i=1}^{N} \frac{p_u\beta_i}{(1+p_p\beta_i)(\mathcal{K}_i+1)} + 1\Big)[(\hat{\mathbf{G}}^{\mathrm{H}}\hat{\mathbf{G}})^{-1}]_{\mathrm{nn}}}\Big)\Big\}. \tag{4.16}$$

We can see from (4.16) that when the Rician $\mathcal{K}$-factor become very large, the summation term decreases and thus, uplink achievable rate increases. Hence, unlike point to point MIMO, the LOS component has a positive impact in massive MIMO systems. But, (4.16) incorporates non-central Wishart distribution, $\hat{\mathbf{G}}^{\mathrm{H}}\hat{\mathbf{G}}$, which is difficult to evaluate analytically. Thus, to derive a closedform lower bound expression for the achievable rate in (4.16), we first calculate the approximate moments for the non-central Wishart distribution. To do this, we first introduce the approaches for non-central Wishart matrix approximation.

4.3.2 Basics on Non-central Wishart Matrix Approximation

Given a non zero mean Gaussian distributed matrix $\mathbf{H} \in \mathbb{C}^{M\times N}$ which is expressed as

$$\mathbf{H} = \bar{\mathbf{H}}\mathbf{A} + \mathbf{H}_r\mathbf{B} \tag{4.17}$$

where $\mathbf{A}$ and $\mathbf{B}$ are constant diagonal matrices, $\bar{\mathbf{H}}$ is a constant matrix and $\mathbf{H}_r \sim \mathcal{CN}(0,1)$, then the inner product $\mathbf{H}^{\mathrm{H}}\mathbf{H}$ results a non central Wishart distribution given by

$$\mathbf{H}^{\mathrm{H}}\mathbf{H} = \mathbf{W} \sim \mathcal{W}_N(M, \mathbf{P}, \mathbf{\Sigma}) \tag{4.18}$$

where M is the degree of freedom, $\mathbf{P}$ is the mean matrix of $\mathbf{H}$ and $\mathbf{\Sigma}$ is the covariance matrix of $\mathbf{H}$ given by

$$\begin{aligned} \mathbf{P} &= \mathbb{E}\{\mathbf{H}\} = \bar{\mathbf{H}}\mathbf{A} \\ \mathbf{\Sigma} &= \mathrm{cov}\{\mathbf{H}\} = \mathbf{B}^{\mathrm{H}}\mathbf{B} \end{aligned} \tag{4.19}$$

where cov denotes the covariance matrix.

This non-central Wishart matrix can be approximated to an equivalent central-Wishart matrix as

$$\hat{\mathbf{W}} \sim \mathcal{W}_N(M, \hat{\mathbf{\Sigma}}) \tag{4.20}$$

where $\hat{\mathbf{\Sigma}}$ is the approximated covariance matrix that is given by $\hat{\mathbf{\Sigma}} = \mathbf{\Sigma} + \frac{1}{M}\mathbf{P}^H\mathbf{P}$.

4.3.3 Closedform Lower Bound Achievable Rate of ZF Detector

Based on the above proof of concept, we derive analytical closedform lower bound expression for the uplink achievable rate in (4.16) as shown in Theorem 4.3.1.

Theorem 4.3.1 *The closedform lower bound achievable rate of a user under ZF detection and imperfect CSI at the BS can be approximated by*

$$R_n^{ZF} \approx \log_2\left(1 + \frac{p_u\beta_n(M-N)}{(\sum_{i=1}^{N}\frac{p_u\beta_i}{(1+p_p\beta_i)(\mathcal{K}_i+1)}+1)[\hat{\mathbf{\Sigma}}^{-1}]_{nn}}\right) \tag{4.21}$$

where

$$\begin{aligned}\hat{\mathbf{\Sigma}} &= \mathbf{\Sigma} + \frac{1}{M}[\Omega(\Omega+\mathbf{I}_N)^{-1}]^{\frac{1}{2}}\bar{\mathbf{H}}^H\bar{\mathbf{H}}[\Omega(\Omega+\boldsymbol{I}_N)^{-1}]^{\frac{1}{2}} \\ \mathbf{\Sigma} &= diag\{\frac{\eta_n}{\mathcal{K}_n+1}\} \qquad for\ n = 1, 2, \cdots, N.\end{aligned} \tag{4.22}$$

Proof: Noting the convexity of $\log(1+\frac{1}{x})$ and applying Jensen's inequality in (4.16), we get [21]

$$R_n^{\mathrm{ZF}} \approx \log_2\left(1 + \frac{p_u\beta_n}{(\sum_{i=1}^{N}\frac{p_u\beta_i}{(1+p_p\beta_i)(\mathcal{K}_i+1)}+1)\mathbb{E}\{[(\hat{\mathbf{H}}^{\mathrm{H}}\hat{\mathbf{H}})^{-1}]_{\mathrm{nn}}\}}\right) \tag{4.23}$$

where $\hat{\mathbf{H}}$ is the multipath fading part of the estimated channel matrix in (4.8). It is given by

$$\hat{\mathbf{H}} = \bar{\mathbf{H}}[\Omega(\Omega+\mathbf{I}_N)^{-1}]^{\frac{1}{2}} + (\hat{\mathbf{H}}_r + \frac{1}{\sqrt{p_p\beta_n}}\mathbf{W})\tilde{\mathbf{D}}[(\Omega+\mathbf{I}_N)^{-1}]^{\frac{1}{2}}. \tag{4.24}$$

It can be shown from (4.24) that $\hat{\mathbf{H}}$ follows a normal distribution with non-zero mean. Thus $\mathbf{W} \triangleq \hat{\mathbf{H}}^{\mathrm{H}}\hat{\mathbf{H}}$ follows a non-central Wishart distribution denoted by $\mathbf{W} \sim \mathcal{W}_N(M, \mathbf{P}, \mathbf{\Sigma})$ where $\mathbf{P} = \bar{\mathbf{H}}[\Omega(\Omega+\mathbf{I}_N)^{-1}]^{\frac{1}{2}}$ is the mean matrix of $\hat{\mathbf{H}}$ and $\mathbf{\Sigma} = (\Omega+\mathbf{I}_N)^{-1}\eta_n$ is the covariance matrix of the row vectors of $\hat{\mathbf{H}}$ [76]. This non-central Wishart distribution can be approximated by a central Wishart distribution as $\hat{\mathbf{W}} \sim \mathcal{W}_N(M, \hat{\mathbf{\Sigma}})$ where $\hat{\mathbf{\Sigma}} = \mathbf{\Sigma} + \frac{1}{M}\mathbf{P}^H\mathbf{P}$.

Now, let $\gamma_n = \frac{1}{[(\hat{\mathbf{H}}^{\mathrm{H}}\hat{\mathbf{H}})^{-1}]_{\mathrm{nn}}}$, under the above non central Wishart approximation, γ_n become a Chi-square random variable [76]. And, we proved in Appendix 4.2 that the first moment of the inverse Wishart distribution is given by

$$\mathbb{E}\{[(\hat{\mathbf{H}}^{\mathrm{H}}\hat{\mathbf{H}})^{-1}]_{nn}\} = \frac{[\hat{\mathbf{\Sigma}}^{-1}]_{nn}}{\text{M-N}}. \tag{4.25}$$

Finally, substituting (4.25) into (4.23), we get (4.21).

4.3.4 Achievable Rate at Large Rician $\mathcal{K}$-factor

When the Rician $\mathcal{K}$-factor grows large, the summation term in (4.21) and $\mathbf{\Sigma}$ in (4.22) goes to zero. Thus, the achievable rate in (4.21) converges to

$$\mathrm{R}_n^{\mathrm{ZF}} \approx \log_2\left(1+\frac{p_u\beta_n(M-N)}{[\hat{\mathbf{\Sigma}}^{-1}]_{\mathrm{nn}}}\right) \approx \log_2\left(1+\frac{p_u\beta_n(M-N)}{[(\frac{1}{M}\bar{\mathbf{H}}^{\mathrm{H}}\bar{\mathbf{H}})^{-1}]_{\mathrm{nn}}}\right). \tag{4.26}$$

The result shows that when the Rician $\mathcal{K}$-factor becomes large, the interference term vanishes and thus the achievable rate increases. Besides, the achievable rate in (4.26) is the same as the achievable rate of massive MIMO system over Rician fading channel with perfect CSI at the BS [81]. This shows that when the Rician $\mathcal{K}$-factor grows large, the approximation of the achievable rate converges to the same value regardless of the CSI quality [81]. In addition, when M grows large, $\frac{1}{M}\bar{\mathbf{H}}^{\mathrm{H}}\bar{\mathbf{H}}$ becomes asymptotically an identity matrix [77]. Thus, (4.26) converges to

$$\mathrm{R}_n^{\mathrm{ZF}} \approx \log_2\Big(1+p_u\beta_n(M-N)\Big). \tag{4.27}$$

This shows that when both the Rician $\mathcal{K}$-factor and the number of BS antennas become very large, the effects of small scale fading is completely averaged out and intra-cell interference disappears completely [77]. Thus, uplink achievable rate depends only on the number of BS antennas and large scale fading parameters.

4.3.5 Achievable Rate with MRC Detector

For MRC with MMSE based channel estimation at the BS, the detection matrix is given by $\mathbf{A}=\hat{\mathbf{G}}$ and thus, the detection matrix for each user is $\mathbf{a}_n=\hat{\mathbf{g}}_n$ [21]. Hence, starting from (4.14), the uplink rate of the nth user with MRC detector is given by

$$R_n^{\mathrm{MRC}} = \mathbb{E}\left\{\log_2\left(1+\frac{p_u\left\|\hat{\mathbf{g}}_n\right\|^4}{p_u\sum_{i=n,\ i\neq n}^{N}\left|\hat{\mathbf{g}}_n^H\hat{\mathbf{g}}_i\right|^2+\left[\sum_{i=1}^{N}\frac{p_u\beta_i}{(1+p_p\beta_i)(\mathcal{K}_i+1)}+1\right]\left\|\hat{\mathbf{g}}_n\right\|^2}\right)\right\}. \tag{4.28}$$

By using large system analysis, closedform lower bound approximation for the achievable rate in (4.28) is expressed as

$$R_n^{\mathrm{MRC}} \approx \log_2\left(1+\frac{p_u\beta_n\left[M^2\mathcal{K}_n^2+\left(2M\mathcal{K}_n+2M^2\mathcal{K}_n\right)\eta_n+\left(M+M^2\right)\eta_n^2\right]}{p_u\left(\mathcal{K}_n+1\right)\sum_{i=1,i\neq n}^{N}\beta_i\Delta_2+Mp_u\beta_n\frac{\mathcal{K}_n+\eta_n}{1+\beta_n p_p}+M\left(\mathcal{K}_n+1\right)\left(\mathcal{K}_n+\eta_n\right)}\right) \tag{4.29}$$

where $\Delta_2 = \left[\mathcal{K}_n\mathcal{K}_i\phi_{ni}^2+M\eta_n\left(\mathcal{K}_i+1\right)+M\mathcal{K}_n\right]/\left(\mathcal{K}_i+1\right)$ and $\phi_{ni} = \frac{\sin\left(\frac{M\pi}{2}[\sin(\theta_n)-\sin(\theta_i)]\right)}{\sin\left(\frac{\pi}{2}[\sin(\theta_n)-\sin(\theta_i)]\right)}$ that are formulated in [82].

The approximation in (4.29) is valid for any number of BS antennas and helps to analyze the impacts of the Rician $\mathcal{K}$-factor on the system performance. When the Rician $\mathcal{K}$-factor grows large (that is when $\mathcal{K}_n = \mathcal{K}_i \to \infty$), the achievable rate in (4.29) converges to

$$R_n^{\mathrm{MRC}} \approx \log_2 \left(1 + \frac{p_u \beta_n M^2}{p_u \sum_{i=1}^{N} \beta_i \phi_{ni}^2 + M} \right). \tag{4.30}$$

This shows that when the Rician $\mathcal{K}$-factor grows large, the uplink achievable rate with MRC detection and imperfect CSI approaches to a constant value regardless of the CSI quality at the BS. Whereas when the Rician $\mathcal{K}$-factor is zero (i.e $\mathcal{K}_n = \mathcal{K}_i = 0$), the achievable rate in (4.29) reduces to

$$R_n^{\mathrm{MRC}} \approx \log_2 \left(1 + \frac{\tau p_u^2 \beta_n^2 (M+1)}{p_u \left(\tau p_u \beta_n + 1\right) \sum_{i=1}^{N} \beta_i + (\tau + 1) p_u \beta_n + 1} \right). \tag{4.31}$$

The result in (4.31) is equivalent to the lower bound achievable rate with imperfect CSI and under Rayleigh fading channel model in [21].

4.4 Simulation Results and Analysis

We consider a single cell uplink massive MIMO system with cell radius of $r_{\mathrm{c}} = 1000$ meters. We assume N-users are distributed uniformly over the cell except for an exclusion zone around the BS ($r_{\mathrm{h}} \leq 100$ meter). The exclusion zone is assumed to ensure that uplink and downlink communication happens in the far field of the transmitting antenna and plane waves can be assumed at the receiver [21, 28]. The large scale fading is modeled as $\beta_n = z_n (\frac{r_n}{r_h})^{-\alpha}$ where z_n is the log-normal shadow fading random variable with standard deviation $\sigma_{\mathrm{sh}} = 8\mathrm{dB}$, $\alpha = 3.8$ is the path loss exponent, and $r_n \in [r_{\mathrm{c}}, r_{\mathrm{h}}]$ denotes the distance between the nth user and the BS [21]. To simplify the analysis, we assume that all users have the same Rician $\mathcal{K}$-factors. The system parameters are chosen according to the LTE standard [21] with $\tau_c = 200$ and $\tau_p = N$.

Figure 4.1 shows uplink achievable sum rate of a massive MIMO system in Rician fading channel model at different value of the Rician $\mathcal{K}$-factor. As it is shown from the figure, the achievable uplink sum rate increases with the Rician $\mathcal{K}$-factor. When the Rician $\mathcal{K}$-factor increases, channel estimation becomes more robust and the effects of the random component of the Rician fading channel is decreased and thus, the uplink achievable sum rate increases. Specifically, for very large M and Rician $\mathcal{K}$-factor, all the interference and noise can be ignored completely, which shows that the uplink sum rate in Rician fading channel model is higher than Rayleigh fading channel model.

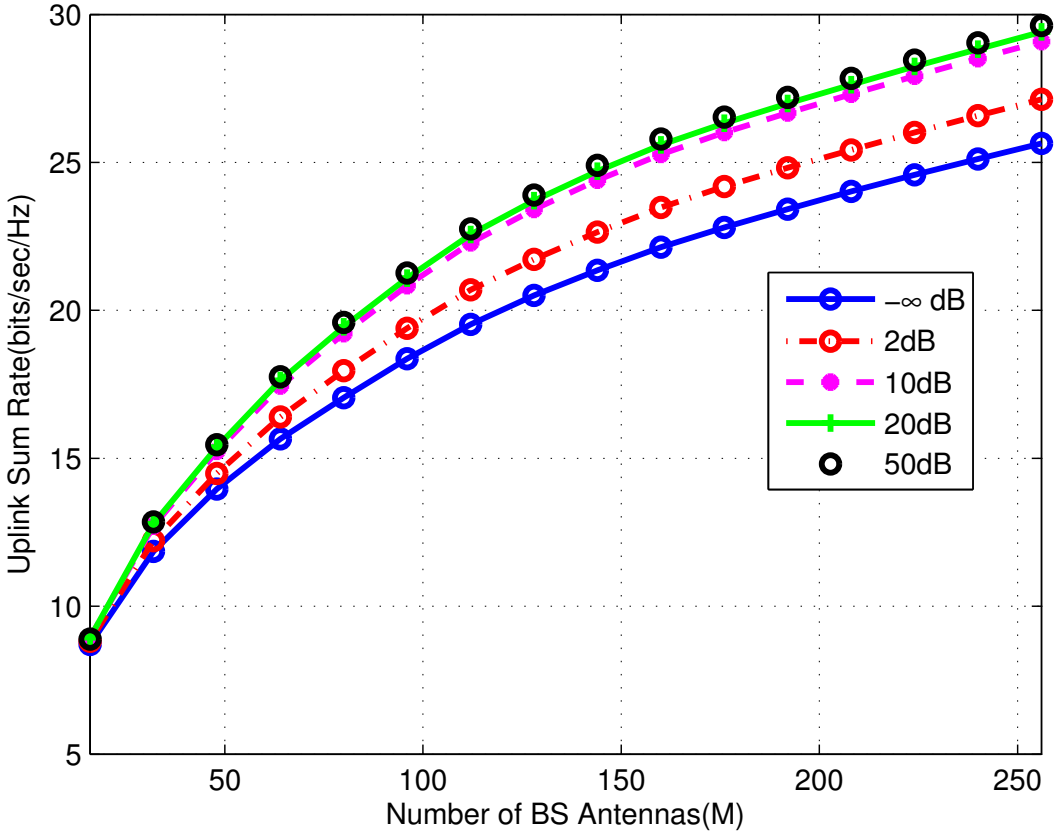

Figure 4.1: Uplink sum rate of massive MIMO system in Rician fading channel model with ZF detector and imperfect CSI. We assume $N = 10$, $p_u = 10$dB, $\tau = 10$, and 10^4 Monte-Carlo realization is used.

In Figure 4.2, we validate the feasibility and realization of Theorem 4.3.1. For this, we compare the simulated sum rates in (4.16) with the analytical approximations in (4.21) and (4.26) at different values of the Rician $\mathcal{K}$-factor. As shown in the Figure, the analytical approximations are fitted with the simulated results. This shows that the proposed approximation for the non-central Wishart distribution is very accurate and physically valid. Specifically, for both very large M and Rician $\mathcal{K}$-factor, channel estimation error decreases, the interference can be average out completely, and thus, the approximation of the achievable sum rate converges to the same value independent of the CSI quality.

4.5 Summary

In this chapter, the performance of massive MIMO systems over Rician fading channel is analyzed. Assuming imperfect CSI at the BS, MMSE based channel estimation is de-

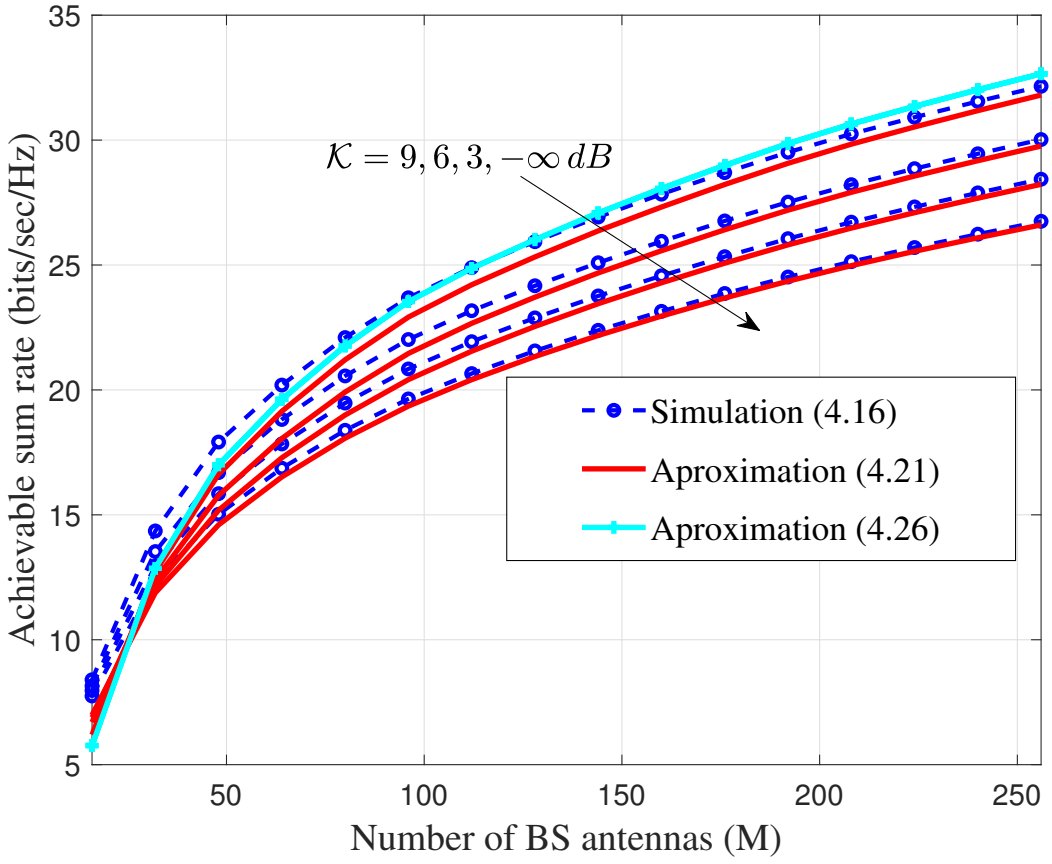

Figure 4.2: Comparison of approximated and simulated results of uplink sum rate of massive MIMO in a Rician fading channel model with a ZF detector and imperfect CSI. The number of users is $N = 10$, the transmit power per user is $p_u = 10$dB, the pilot symbol length is $\tau = 10$.

rived. Uplink achievable sum rate is formulated for ZF detectors. By approximating the non-central Wishart distribution to central Wishart distribution, closedform lower bound expression is derived for the uplink achievable sum rate. Detail analysis is done to understand the impact of system and propagation parameters on the achievable rate. The results show that when the Rician $\mathcal{K}$-factor increases, channel estimation becomes more robust and the effects of the random component of the Rician fading channel is decreased and thus, uplink achievable sum rate increases.

Appendices

Appendix 4.1

Proof of Theorem 4.2.1

To find the MMSE based estimator of the Rician channel in (4.5) from (4.7), first dispread the received noisy matrix in (4.7) by right multiplying with $(\mathbf{Z}^T)^H = \mathbf{Z}^*$ as

$$\begin{aligned}\mathbf{Y}' = \mathbf{Y}_{\mathrm{p},r}\mathbf{Z}^* &= \sqrt{p_p}\mathbf{G}_r\mathbf{Z}^T\mathbf{Z}^* + \boldsymbol{\mathcal{N}}\mathbf{Z}^* \\ &= \sqrt{p_p}\mathbf{G}_r + \boldsymbol{\mathcal{N}}\mathbf{Z}^*.\end{aligned} \tag{4.32}$$

Then, apply MMSE based estimator [55] on $\mathbf{Y}'$ to get $\hat{\mathbf{G}}_r$ as

$$\begin{aligned}\hat{\mathbf{G}}_r &= \mathbb{E}\{\mathbf{G}_r|\mathbf{Y}'\} \\ &= \frac{\mathbf{C}_{\mathbf{G}_r\mathbf{Y}'}}{\mathbf{C}_{\mathbf{Y}'\mathbf{Y}'}}(\mathbf{Y}' - \mathbb{E}\{\mathbf{Y}'\}) + \mathbb{E}\{\mathbf{G}_r\}\end{aligned} \tag{4.33}$$

where $\mathbf{C}_{\mathbf{G}_r\mathbf{Y}'}$ and $\mathbf{C}_{\mathbf{Y}'\mathbf{Y}'}$ are the covariance matrices. Noting that $\mathbb{E}\{\mathbf{Y}'\}$ and $\mathbb{E}\{\mathbf{G}_r\}$ is zero, we get

$$\hat{\mathbf{G}}_r = \frac{\mathbf{C}_{G_rY'}}{\mathbf{C}_{\mathbf{Y}'\mathbf{Y}'}}[\mathrm{Y}']. \tag{4.34}$$

The covariance matrix of $\mathbf{Y}'$ is calculated as

$$\begin{aligned}\mathbf{C}_{\mathbf{Y}'\mathbf{Y}'} &= \mathbb{E}\{\mathbf{Y}'(\mathbf{Y}')^H\} \\ &= p_p\mathbb{E}\{\mathbf{G}_r\mathbf{G}_r^H\} + \mathbb{E}\{\boldsymbol{\mathcal{N}}(\mathbf{Z}^H\mathbf{Z})^*\boldsymbol{\mathcal{N}}^H\} \\ &= p_p\mathbf{D} + \mathbf{I}_N.\end{aligned} \tag{4.35}$$

And the covariance matrix of $\mathbf{C}_{G_rY'}$ is calculated as

$$\begin{aligned}\mathbf{C}_{G_rY'} &= \mathbb{E}\{\mathbf{G}_r(Y')^H\} \\ &= \mathbb{E}\{\mathbf{G}_r(\sqrt{p_p}\mathbf{G}_r + \boldsymbol{\mathcal{N}}\mathbf{Z}^*)^H\} \\ &= \sqrt{p_p}\,\mathbf{D}.\end{aligned} \tag{4.36}$$

Substituting (4.36) and (4.35) into (4.34), we get

$$\begin{aligned}\hat{\mathbf{G}}_r &= \frac{\sqrt{p_p}\,\mathbf{D}}{p_p\mathbf{D} + \mathbf{I}_N}[\mathrm{Y}'] \\ &= \frac{\sqrt{p_p}\,\mathbf{D}}{p_p\mathbf{D} + \mathbf{I}_N}\mathbf{Y}_{\mathrm{p},r}\mathbf{Z}^* \\ &= \frac{1}{\sqrt{p_p}}\mathbf{Y}_{\mathbf{p},r}\mathbf{Z}^*\tilde{\mathbf{D}} \\ &= \left(\mathbf{G}_r + \frac{1}{\sqrt{p_p}}\mathbf{W}\right)\tilde{\mathbf{D}}\end{aligned} \tag{4.37}$$

where $\tilde{\mathbf{D}} \triangleq (\frac{1}{p_p}\mathbf{D}^{-1} + \mathbf{I}_{\mathrm{N}})^{-1}$ and $\mathbf{W} \triangleq \boldsymbol{\mathcal{N}}\boldsymbol{Z}^*$. This concludes the proof.

Appendix 4.2

Proof of Equation (4.25).

For a central complex Wishart distribution, $\hat{\mathbf{W}} \sim \mathcal{W}_N(M, \hat{\boldsymbol{\Sigma}})$, $\gamma_n = \frac{1}{[(\hat{\mathbf{H}}^{\mathrm{H}}\hat{\mathbf{H}})^{-1}]_{\mathrm{nn}}}$ is a Chi-square random variable [76] with probability density function (pdf) given by [83]

$$f(\gamma_n) = \frac{[\hat{\boldsymbol{\Sigma}}^{-1}]_{\mathrm{nn}}}{\Gamma(M-N+1)} \exp\{-\gamma_n[\hat{\boldsymbol{\Sigma}}^{-1}]_{\mathrm{nn}}\} \left(- \gamma_n[\hat{\boldsymbol{\Sigma}}^{-1}]_{\mathrm{nn}} \right)^{\text{M-N}} \tag{4.38}$$

To calculate the moment of the inverse real Wishart distribution, $\mathbb{E}\{[(\hat{\mathbf{H}}^{\mathrm{H}}\hat{\mathbf{H}})^{-1}]_{\mathrm{nn}}\}$, let us express the integral $\int_0^\infty \frac{1}{\gamma_n} f(\gamma_n)\mathrm{d}\gamma_n$ as

$$\int_0^\infty \frac{1}{\gamma_n} f(\gamma_n) d\gamma_n = \frac{\mathbf{a}}{\mathbf{c}} \int_0^\infty \frac{e^{-\mathbf{a}x}(\mathbf{a}x)^d}{x} dx \tag{4.39}$$

where $x = \gamma_n$, $\mathbf{a} = [\hat{\boldsymbol{\Sigma}}^{-1}]_{\mathrm{nn}}$, $\mathbf{c} = \Gamma(M-N+1)$, and $\mathrm{d} = M-N$. Let $y = \mathbf{a}x$, then $dy = \mathbf{a}dx$. Substitute y and $dy/\mathbf{a}$ in place of x and dx we get

$$\begin{aligned} \frac{\mathbf{a}}{\mathbf{c}} \int_0^\infty \frac{e^{-ax}(ax)^d}{x} dx = \frac{\mathbf{a}}{\mathbf{c}} \int_0^\infty e^{-y} y^{d-1} dy &= \frac{\mathbf{a}}{\mathbf{c}} \Gamma(d) \\ &= [\hat{\boldsymbol{\Sigma}}^{-1}]_{\mathrm{nn}} \frac{\Gamma(M-N)}{\Gamma(M-N+1)} \\ &= \frac{[\hat{\boldsymbol{\Sigma}}^{-1}]_{\mathrm{nn}}}{M-N} \end{aligned} \tag{4.40}$$

Where $\Gamma(M) = (M-1)!$ is the Gamma function [83] and $\int_0^\infty e^{-1}t^{z-1}dt = \Gamma(z)$ for $z \in \mathbb{R}$. Hence, (4.40) concludes our proof and thus we get

$$\mathbb{E}\{[(\hat{\mathbf{H}}^{\mathrm{H}}\hat{\mathbf{H}})^{-1}]_{\mathrm{nn}}\} = \frac{[\hat{\boldsymbol{\Sigma}}^{-1}]_{\mathrm{nn}}}{M-N}. \tag{4.41}$$

Appendix 4.3

Appendix 4.3.1: Proof of Equations (4.10).

The variance of the elements of the channel estimation error is expressed interms of $\hat{\mathbf{g}}_{mi}$ and $\mathbf{g}_{mi}$ as [79]

$$\mathrm{var}\{\tilde{\mathbf{g}}_{mi}\} = \mathbb{E}\{|\mathbf{g}_{mi}|^2\} - \mathbb{E}\{|\hat{\mathbf{g}}_{mi}|^2\} \tag{4.42}$$

where

$$\begin{aligned} \mathrm{var}\{\mathbf{g}_{mi}\} &= \mathbb{E}\{|\mathbf{g}_{mi}|^2\} \\ &= \frac{\beta_i}{\mathcal{K}_i + 1}. \end{aligned} \tag{4.43}$$

and the variance of the elements of the channel estimate is calculated as

$$\begin{aligned}\mathbb{E}\{|\hat{\mathbf{g}}_{mi}|^2\} &= \mathbb{E}\{\hat{\mathbf{g}}_{mi}\hat{\mathbf{g}}_{mi}^{\mathrm{H}}\} \\ &= \frac{1}{(\mathcal{K}_i+1)}(\frac{p_p\beta_i}{p_p\beta_i+1})^2(\beta_i+\frac{1}{p_p}) \\ &= \frac{p_p\beta_i^2}{(\mathcal{K}_i+1)(p_p\beta_i+1)}.\end{aligned} \tag{4.44}$$

Substituting (4.43) and (4.44) to (4.42) , we get

$$\begin{aligned}\mathrm{var}\{\tilde{\mathbf{g}}_{mi}\} &= \mathbb{E}\{|\mathbf{g}_{mi}|^2\} - \mathbb{E}\{|\hat{\mathbf{g}}_{mi}|^2\} \\ &= \frac{\beta_i}{(\mathcal{K}_i+1)} - \frac{p_p\beta_i^2}{(\mathcal{K}_i+1)(p_p\beta_i+1)} \\ &= \frac{\beta_i}{(1+p_{\mathrm{p}}\beta_i)(\mathcal{K}_i+1)}\end{aligned} \tag{4.45}$$

where is $\mathcal{K}_i$ is the Rician $\mathcal{K}$-factor for each user.

Appendix 4.3.2: Proof of Equation (4.11).

Let us start from the estimated Rican channel equation from (4.5)

$$\hat{\mathrm{G}} = [\Omega(\Omega+\mathbf{I}_N)^{-1}]^{\frac{1}{2}}\bar{\mathrm{G}} + [(\Omega+\mathbf{I}_N)^{-1}]^{\frac{1}{2}}\hat{\mathrm{G}}_r. \tag{4.46}$$

From this, the elements of the estimated channel matrix is formulated as

$$\hat{\mathrm{G}}_{mn} = (\frac{\mathcal{K}_n}{\mathcal{K}_n+1})^{\frac{1}{2}}\bar{\mathrm{G}}_{mn} + (\frac{1}{\mathcal{K}_n+1})^{\frac{1}{2}}[\hat{\mathrm{G}}_r]_{mn}. \tag{4.47}$$

From (4.5), the elements of $\hat{\mathrm{G}}_r$ is given by

$$[\hat{\mathrm{G}}_r]_{mn} = \eta_n(\sqrt{\beta_n}q_{mn} + \frac{1}{\sqrt{p_p}}w_{mn}) \tag{4.48}$$

where $\eta_n = \frac{p_p\beta_n}{p_p\beta_n+1}$, and let $q_{mn} = s_{mn} + jt_{mn}$, $w_{mn} = x_{mn} + jy_{mn}$ be independent random variables with zero mean and the variance of each elements of q_{mn} and w_{mn} is 0.5. Let us also assume that q_{mn} and w_{mn} are independent. Now, the inner product of the channel estimate is formulated as

$$\frac{1}{M}\hat{\mathbf{g}}_n^{\mathrm{H}}\hat{\mathbf{g}}_i \xrightarrow{\text{a.s}} \frac{1}{M}\sum_{m=1}^{M}\mathbb{E}\{[\hat{\mathbf{G}}]_{mn}^*[\hat{\mathbf{G}}]_{mi}\} \tag{4.49}$$

where the elements of $[\hat{\mathbf{G}}]_{mn}^*$ and $[\hat{\mathbf{G}}]_{mi}$ is derived from (4.47) and (4.48) as

$$\begin{aligned}[\hat{\mathbf{G}}]_{mn}^* &= \left([\frac{\mathcal{K}_n\beta_n}{\mathcal{K}_n+1}]^{\frac{1}{2}}\sigma_{mn} + [\frac{1}{\mathcal{K}_n+1}]^{\frac{1}{2}}\eta_n(\sqrt{\beta_n}q_{mn} + \frac{1}{\sqrt{p_p}}w_{mn})\right)^* \\ [\hat{\mathbf{G}}]_{mi} &= [\frac{\mathcal{K}_i\beta_i}{\mathcal{K}_i+1}]^{\frac{1}{2}}\sigma_{mi} + [\frac{1}{\mathcal{K}_i+1}]^{\frac{1}{2}}\eta_i(\sqrt{\beta_i}q_{mi} + \frac{1}{\sqrt{p_p}}w_{mi}).\end{aligned} \tag{4.50}$$

Substituting (4.50) to (4.49) and neglecting the zero values of the expectation, we get

$$\frac{1}{M}\hat{\mathbf{g}}_n^{\mathrm{H}}\hat{\mathbf{g}}_i \xrightarrow{\text{as}} \frac{1}{M}\sum_{m=1}^{M}\mathbb{E}\{[\frac{\mathcal{K}_n\mathcal{K}_i\beta_n\beta_i}{(\mathcal{K}_n+1)(\mathcal{K}_i+1)}]^{\frac{1}{2}}\sigma_{mn}^*\sigma_{mi} + \eta_n\eta_i[\frac{\beta_i\beta_n}{(\mathcal{K}_n+1)(\mathcal{K}_i+1)}]^{\frac{1}{2}}\, q_{mn}^* q_{mi} + \frac{\eta_n\eta_i}{p_p}[\frac{1}{(\mathcal{K}_n+1)(\mathcal{K}_i+1)}]^{\frac{1}{2}}\, w_{mn}^* w_{mi}\} \tag{4.51}$$

Equation (4.51) is evaluated for the cases $i = n$ and $i \neq n$ as follows.

Case for $i = n$:

For $i = n$, $\sigma_{mn}^*\sigma_{mi} = e^{j\pi(m-1)(\sin(\theta_n)-\sin(\theta_n))} = 1$, $\mathbb{E}\{q_{\mathrm{mn}}^* q_{\mathrm{mn}}\} = \mathbb{E}\{q_{\mathrm{mn}}^2\} = 1$ and $\mathbb{E}\{w_{\mathrm{mn}}^* w_{\mathrm{mn}}\} = \mathbb{E}\{w_{\mathrm{mn}}^2\} = 1$. Thus, (4.51) is simplified to

$$\frac{1}{M}\hat{\mathbf{g}}_n^{\mathrm{H}}\hat{\mathbf{g}}_i \xrightarrow{\text{a.s}} \frac{1}{M}\sum_{m=1}^{M}[\frac{\mathcal{K}_n\beta_n}{\mathcal{K}_n+1} + \frac{\eta_n^2}{\mathcal{K}_n+1}(\beta_n + \frac{1}{p_p})] = \frac{\beta_n}{\mathcal{K}_n+1}(\mathcal{K}_n+\eta_n). \tag{4.52}$$

Case for $i \neq n$:

For $i \neq n$, the expectation of the last two terms in (4.51) will be zero and thus

$$\begin{aligned}\frac{1}{M}\hat{\mathbf{g}}_n^{\mathrm{H}}\hat{\mathbf{g}}_i &\xrightarrow{\text{as}} \frac{1}{M}\sum_{m=1}^{M}[\frac{\mathcal{K}_n\mathcal{K}_i\beta_n\beta_i}{(\mathcal{K}_n+1)(\mathcal{K}_i+1)}]^{\frac{1}{2}}\mathbb{E}\{\sigma_{mn}^*\sigma_{mi}\} \\ &\xrightarrow{\text{as}} [\frac{\mathcal{K}_n\mathcal{K}_i\beta_n\beta_i}{(\mathcal{K}_n+1)(\mathcal{K}_i+1)}]^{\frac{1}{2}}\frac{1}{M}\sum_{m=1}^{M} e^{j\pi(m-1)(\sin(\theta_n)-\sin(\theta_i))}\end{aligned} \tag{4.53}$$

But, based on [79]the summation term in (4.53) can be further simplified as

$$\sum_{m=1}^{M} e^{j\pi(m-1)(\sin(\theta_n)-\sin(\theta_i))} = \frac{\sin(\frac{M\pi}{2}[\sin(\theta_n)-\sin(\theta_i)]}{\sin(\frac{\pi}{2}[\sin(\theta_n)-\sin(\theta_i)])}e^{j\pi\frac{M-1}{2}(\sin(\theta_n)-\sin(\theta_i))}. \tag{4.54}$$

Noting that the sinusoid and exponential functions are a bounded function, thus M becomes very large [79]

$$\frac{\sin(\frac{M\pi}{2}[\sin(\theta_n)-\sin(\theta_i)]}{M}e^{j\pi\frac{M-1}{2}(\sin(\theta_n)-\sin(\theta_i))} \to 0. \tag{4.55}$$

Hence, for $i \neq n$ and when M is very large, $\frac{1}{M}\hat{\mathbf{g}}_n^{\mathrm{H}}\hat{\mathbf{g}}_i \to 0$.

Finally, combining the results in (4.52) and (4.53), and generalizing for the matrix $\hat{\mathbf{G}}$, we get

$$\frac{1}{M}\hat{\mathbf{G}}^{\mathrm{H}}\hat{\mathbf{G}} \xrightarrow{\text{a.s}} \mathrm{diag}\{\frac{\beta_n}{\mathcal{K}_n+1}(\mathcal{K}_n+\eta_n)\} \tag{4.56}$$

and this concludes our proof.

Chapter 5

Energy Efficient Power Control in Massive MIMO Systems

5.1 Introduction

It is expected that the number of connected mobile devices will grow exponentially in the coming few years [4]. This exponential increment in connected devices will cause huge data traffic, and mobile data traffic is expected to increase substantially. Improving the network capacity via increasing the spectral efficiency is one of the key recommendations to support this huge surge in data traffic. The spectral efficiency can be improved by increasing the transmitter power; introducing additional processing (such as deploying massive multiple antenna systems) in transceiver pairs that help to harvest energy, minimize multiuser-interference and reduce losses; and implement innovative wireless planning and operation strategies that minimize losses or save energy [4, 14, 21].

Focusing on the transmit power in multi-user massive MIMO systems, we cannot increase the power indefinitely to improve the spectral efficiency. This is because power is a scarce resource and also both the desired and interfering users may opportunistically increase their transmit power so that the resulting interference will prohibit the spectral efficiency improvement. Moreover, increasing the transmit power does not seem realistic due to operational, economical and environmental challenges resulting from the exponential growth of the number of connected devices and networks [50]. The above and other facts stimulate to consider energy efficiency as another main design criterion for 5G and beyond networks [4, 21]. The main goal is to design novel technologies and network architectures, employ efficient resource allocation techniques, networking planning and operation strategies that help to achieve the capacity demand with similar or even lower power consumption

as current networks [4, 50].

Resource allocation techniques are employed to allocate the system radio resources (such as transmit power, spectrum, users, antennas) in a way that maximize the energy efficiency of massive MIMO systems. Resource allocation provides considerable energy efficiency gains while operating at minimum levels of power consumption [4, 14, 21, 23, 50]. Based on these facts, many research directions have been proposed to investigate energy efficient resource allocation techniques in massive MIMO systems [21, 22, 51, 53, 84–90].

With the intention of maximizing the energy efficiency in multi-user MIMO systems, joint allocation of transmit power, number of BS antennas and number of users is proposed in [22]. An iterative algorithm is formulated under a practical system power consumption model. Assuming uniform data rates at each user, the algorithm aims to maximize the network's energy efficiency in the coverage area. Joint power allocation and user scheduling that improve energy efficiency in orthogonal frequency division multiple access (OFDMA) downlink multiuser MIMO systems are provided in [85]. The results show that energy efficiency optimization problem is non-convex but can be transformed into a convex fractional programming problem. To solve the non-convex energy efficiency optimization problem, an iterative algorithm is employed based on fractional programming theory. But, optimization is done only via Monte-Carlo simulations and analytical closedform bound is not formulated. Energy efficient power optimization algorithms are proposed in [53] for 5G systems. Global and multi-objective optimization frameworks are proposed for energy efficiency maximization under transmit power and minimum rate constraints at the users. Closed-form feasibility condition is derived and then fractional programming theory is employed to develop power control algorithms that converges to the optimal point with affordable computational complexity. A standard energy efficiency optimization algorithm that exploits the hidden monotonic structure of energy efficiency maximization problem is proposed in [53]. Tools from fractional programming theory, sequential convex optimization and monotonic optimization are utilized to develop sub-optimal energy efficient optimization algorithms and to characterize the global energy efficiency in interference-limited networks. The results show that an interaction between fractional programming and sequential convex programming helps to develop practical power control algorithms that maximize the energy efficiency.

This work builds on our previously published results in [28, 31, 32]. Specifically, energy efficient power control algorithms are proposed for uplink massive MIMO systems

equipped with zero forcing detection and assuming imperfect CSI at the BS. MMSE based channel estimation is considered at the BS. Large system analysis technique is employed to derive closed-form lower bound achievable sum rate expression. Methods from fractional programming theory and sequential convex programming are utilized to derive energy efficient power control algorithms. In line with these, the main contributions of this work are summarized as follows [31–33]:

- We first derive analytical closed-form lower bound achievable sum rate expression and analyze the system performance when the number of BS antennas becomes very large. Due to channel hardening phenomena in massive MIMO systems, the impact of small scale fading (SSF) on the spectral efficiency is asymptotically averaged out and analytical formulation depends only on the system parameters and the large scale fading (LSF) channel coefficients of the users. As a result, calculations that involve large-dimensional matrices from SSF channel coefficients are avoided. This saves computational resources from SSF based signal processing.

- By employing tools from fractional programming theory and sequential convex programming, we formulate energy efficient power control algorithms under maximum transmit power and minimum data rate constraints at each user. An algorithm from fractional programming theory is utilized to solve the fractional energy efficiency optimization problem. Logarithm lower bound approximation and sequential convex programming methods are employed to derive the convex/concave approximation of the objective function and minimum rate constraint. The energy efficiency of both approximations are analyzed theoretically.

- Validate the effectiveness of the proposed algorithms via numerical simulation. The feasibility of the optimization problem has been evaluated. Further, the impacts of system parameters, maximum transmitter power and minimum data rate constraints on energy efficiency are analyzed.

5.1.1 Spectral Efficiency in Massive MIMO Systems

We reconsider a single cell uplink massive MIMO system as shown in Figure 2.2 where the BS is equipped with M antennas to serve K single antenna users in the same time-frequency resource. The system model and channel model, and the channel estimate are taken from Chapter 2 Section 2.3. We formulate the spectral efficiency of the user and

derive a closed-form achievable sum rate expression for uplink massive MIMO systems with ZF detection and imperfect CSI at the BS. We employ ZF detection since it is convenient to derive the lower bound achievable rate in closed-form and give near optimal performance when $M \gg K$ [3, 30]. Let an $M \times K$ matrix $\mathbf{W}$ be the model for a ZF detector which depends on the channel estimate, $\hat{\mathbf{G}}$, and is given by $\mathbf{W} = \hat{\mathbf{G}}(\hat{\mathbf{G}}^H\hat{\mathbf{G}})^{-1}$ [3], then the BS processes the received signal by premultiplying with $\mathbf{W}^{\mathrm{H}}$ as [2, 3]

$$\hat{\mathbf{x}} = \mathbf{W}^{\mathrm{H}}\mathbf{y} = \mathbf{W}^{\mathrm{H}}(\mathbf{G}\mathbf{x} + \mathbf{n}) = \mathbf{W}^{\mathrm{H}}(\hat{\mathbf{G}}\mathbf{x} - \bar{\mathbf{G}}\mathbf{x}) + \mathbf{W}^{\mathrm{H}}\mathbf{n} \tag{5.1}$$

where $\mathbf{y}$ is the received signal vector at the BS. Then, the detected signal for user k is expressed as [2, 3]

$$\hat{x}_k = \sqrt{p_k}\mathbf{w}_k^{\mathrm{H}}\hat{\mathbf{g}}_k x_k + \sum_{i=1, i\neq k}^{K} \sqrt{p_i}\mathbf{w}_k^{\mathrm{H}}\hat{\mathbf{g}}_i x_i - \sum_{i=1}^{K} \sqrt{p_i}\mathbf{w}_k^{H}\tilde{\mathbf{g}}_i x_i + \mathbf{w}_k^{H}\mathbf{n} \tag{5.2}$$

where $\mathbf{w}_k$ is the detector for user k and p_k is the transmit power allocated to the kth user. Then, the signal to interference plus noise ratio (SINR) of the kth user is given by [2, 3]

$$\gamma_k(\mathbf{p}) = \frac{p_k|\mathbf{w}_k^H\mathbf{g}_k|^2}{\sum_{i=1, i\neq k}^{K} p_i|\mathbf{w}_k^H\mathbf{g}_i|^2 + ||\mathbf{w}_k||^2 \sum_{i=1}^{K} \frac{p_i\beta_i}{\tau_p p_p \beta_i + 1} + \sigma^2||\mathbf{w}_k||^2} \tag{5.3}$$

where $\mathbb{E}\{\mathbf{x_k}\mathbf{x_k}^H\} = p_k\mathbf{I}_K$. With SINR in (5.3), the spectral efficiency of the kth user is given by

$$R_k = \mathbb{E}\left\{ \log_2\left(1 + \frac{p_k|\mathbf{w}_k^H\mathbf{g}_k|^2}{\sum_{i=1, i\neq k}^{K} p_i|\mathbf{w}_k^H\mathbf{g}_i|^2 + ||\mathbf{w}_k||^2 \sum_{i=1}^{K} \frac{p_i\beta_i}{\tau_p p_p \beta_i + 1} + \sigma^2||\mathbf{w}_k||^2}\right)\right\} \tag{5.4}$$

and uplink achievable sum rate (in bits/sec) of the system is given by [2]

$$R_s = B\left(1 - \frac{\tau_p}{\tau_c}\right) \sum_{k=1}^{K} \mathbb{E}\left[\log_2\left(1 + \frac{p_k|\mathbf{w}_k^H\mathbf{g}_k|^2}{\sum_{i=1, i\neq k}^{K} p_i|\mathbf{w}_k^H\mathbf{g}_i|^2 + ||\mathbf{w}_k||^2 \sum_{i=1}^{K} \frac{p_i\beta_i}{\tau_p p_p \beta_i + 1} + \sigma^2||\mathbf{w}_k||^2}\right)\right] \tag{5.5}$$

where B is the bandwidth of the system, $(1 - \frac{\tau_p}{\tau_c})$ accounts for the pilot overhead and τ_c is the coherence interval [88]. The achievable sum rate in (5.5) is calculated by approximating the total interference as additive Gaussian noise. Since the total interference is the sum of Gaussian distributed terms that incorporate the channel estimation error and a number of independent multiuser interference terms, the central limit theorem guarantees the accuracy of this approximation, especially for a large number of BS antennas. Thus, (5.5) is

expected to be sufficiently tight and tractable to derive closed-form lower-bound achievable sum rate expression [2]. Therefore, in this work we use analytical closedform lower bound that is derived from (5.5) to formulate energy efficient power control algorithms.

5.1.2 Closedform Lower-bound Achievable Sum Rate Formulation

By considering a massive MIMO system equipped with large number of BS antennas and users, a closedform lower bound achievable sum rate expression is derived from (5.5) and formulated in Theorem 5.1.1.

Theorem 5.1.1 *When both the number of BS antennas and the number of users become very large and satisfy $M \geq K+1$, a closed-form lower bound for the achievable sum rate in (5.5) is given by*

$$R_s \approx B\Big(1-\frac{\tau_p}{\tau_c}\Big)\sum_{k=1}^{K}\log_2\left(1+\frac{p_k(M-K)\hat{\beta}_k}{\sum_{j=1}^{K}p_j\tilde{\beta}_j+\sigma^2}\right) \tag{5.6}$$

where $\hat{\beta}_k$ and $\tilde{\beta}_j$ are the variance of the channel estimate and the channel estimation error, respectively that are given in (2.7). The proof is shown in Appendix 5.1.

The result in Theorem 5.1.1 shows that when the number of BS antennas become very large, the achievable sum rate depends only on the large scale fading channel coefficients and the system parameters. As a result, complicated calculations that involve large dimensional matrices from small scale fading channel coefficients are avoided. This saves computational resources from small scale fading based signal processing. For analysis purpose, we represent the SINR in (5.6) in compact form as

$$\gamma_k(\mathbf{p}) = \frac{p_k b_k}{\sigma^2+\sum_{j=1}^{K}p_j w_j} \tag{5.7}$$

where $b_k = (M-K)\hat{\beta}_k$, $w_j = \tilde{\beta}_j$, and $\mathbf{p} = (p_1, p_2, \cdots, p_K)^T$ is the power allocation vector of the users. We use (5.6) with (5.7) to formulate the proposed energy efficient optimization algorithms.

5.1.3 Power Consumption Model in Massive MIMO Systems

Accurate modeling of the transmitted power and internal dissipated power consumption of the massive MIMO system is required to formulate the energy efficiency expression

and to get reliable guidelines on energy efficiency optimization with respect to the system parameters [22, 54, 91]. Hence, the total power consumption of the proposed uplink massive MIMO system is given by the sum of transmitted power and circuit power (CP) consumption as [22]

$$P_{\text{tot}} = P_{\text{tx}} + P_{\text{cp}} \tag{5.8}$$

where P_{tx} is the power consumed by the power amplifier. It accounts for the power used for uplink pilot and data transmission which is expressed as [22]

$$P_{\text{tx}} = \left(1 - \frac{\tau_p}{\tau_c}\right) \sum_{k=1}^{K} \frac{1}{\eta_k} p_k + \frac{\tau_p}{\tau_c} \frac{1}{\eta_k} K p_p \tag{5.9}$$

where $\eta_k \in (0, 1)$ is the power amplifier efficiency of user k. P_{cp} represents the circuit power consumption of the system given by

$$P_{\text{cp}} = \rho_a M + \sigma_{\text{sc}} \bar{R}_0 + \Theta_0 \tag{5.10}$$

where $\rho_a \triangleq \chi(P_{\text{TC}} + P_{\text{CE}} + P_{\text{LP}})$ denotes the circuit power consumption per BS antenna, χ represents the impact of cooling and other effects at the BS, P_{LP} represents the power consumption for linear processing, P_{TC} accounts for the power consumption of transceiver chains and P_{CE} denotes the power consumption for channel estimation [2, 22]. The term $\sigma_{\text{sc}} \bar{R}_0$ accounts for the power consumption that increases with the uplink data rate with scaling factor σ_{sc} which includes the power consumption for coding and decoding and backhaul transmission. To simplify our analysis, the rate dependent power consumption is assumed to be fixed [22]. Θ_0 shows a static circuit power consumption for control signaling and load independent base-band processing and it is mostly assumed as fixed [22].

Finally, plugging (5.9) and (5.10) into (5.8), the total system power consumption for uplink massive MIMO system is expressed as [51]

$$P_{\text{tot}}(\mathbf{p}) = \sum_{k=1}^{K} \mu_k p_k + P_0 \tag{5.11}$$

where p_k is the power allocated for user k, $\mu_k = (1 - \frac{\tau_p}{T})\frac{1}{\eta_k}$ and P_0 is the sum of the pilot power consumption and circuit power consumption of the system. The typical values of $\eta_k, \rho_a, \sigma_{\text{sc}}$ and Θ_0 depend on the types of the cellular system such as MIMO, macro cell, remote radio head and micro cell [54, 91]. In this work, we assume that the pilot is transmitted at maximum power and optimization is done with respect to the power allocation for data transmission.

5.2 Energy Efficiency in Massive MIMO Systems

The energy efficiency (in bits/Joule) of a wireless communication system is usually defined as the number of bits that can be sent over a unit of power consumption. It is commonly defined as a benefit-cost ratio where the achievable rate is compared with the associated energy consumption of the wireless system [2]. One of the well established metrics to measure this benefit-cost ratio is the global energy efficiency (GEE) which is given by [52]

$$\mathrm{GEE}(\mathbf{p}) = \frac{B\left(1-\frac{\tau_p}{\tau_c}\right)\sum_{k=1}^{K}\log_2(1+\gamma_k(\mathbf{p}))}{\sum_{k=1}^{K}\mu_k p_k + P_0}. \tag{5.12}$$

Equation (5.12) shows that the GEE is the ratio between the total amount of data that can be reliably transmitted per unit of time and the total amount of consumed power. Based on the expression in (5.12), an energy efficient power control optimization problem for uplink massive MIMO system is formulated as [53]

$$\begin{aligned} \max_{\mathbf{p}} \ \mathrm{GEE}(\mathbf{p}) &= \frac{B\left(1-\frac{\tau_p}{\tau_c}\right)\sum_{k=1}^{K}\log_2(1+\gamma_k(\mathbf{p}))}{\sum_{k=1}^{K}\mu_k p_k + P_0} \\ \text{subject to:} \quad & 0 \le p_k \le P_{\max,\,k} \qquad \forall k \\ & \log_2(1+\gamma_k(\mathbf{p})) \ge R_{0,\,k} \ \forall k \end{aligned} \tag{5.13}$$

where $P_{\max,k}$ is the maximum transmit power constraint and $\log_2(1+\gamma_k(\mathbf{p})) \ge R_{0,k}$ is the minimum rate constraint or quality of service (QoS) requirement at each user. The optimization problem in (5.13) aims to calculate the optimal transmit power that maximizes the global energy efficiency under maximum transmit power and minimum rate constraints. But, due to the nonconcave objective function and the nonconvex minimum rate constraint, (5.13) is a nonlinear fractional programming problem and intractable to solve analytically [52, 53]. It requires an exhaustive search algorithm to obtain the global solution. However, exhaustive search algorithm has exponential complexity and is computationally intensive even for small number of BS antennas [22,53]. Therefore, to tackle these challenges, we utilize methods from fractional programming theory such as the Dinkelbach algorithm [92] to solve the problem. The Dinkelbach algorithm is a tool that helps to solve concave-convex fractional programming (CCFP) problems by solving a sequence of easier problems [92]. To employ the Dinkelbach algorithm for energy efficiency maximization, we first summarize the fundamental concepts as follows [92].

5.2.1 Introduction to Fractional Programming

By exploiting the relationship between nonlinear fractional programming and nonlinear parametric programming, Dinkelbach developed an algorithm that solve nonlinear fractional programming problems by successively solving a sequence of simplified nonlinear programming problems [92, 93]. The idea of the Dinkelbach algorithm is built on the relation between a fractional program

$$\max_{\boldsymbol{x}\in\mathcal{S}} \frac{f(\boldsymbol{x})}{g(\boldsymbol{x})} \tag{5.14}$$

and an equivalent substructive function

$$F(\lambda) = \max_{\boldsymbol{x}\in\mathcal{S}} \Big(f(\boldsymbol{x}) - \lambda g(\boldsymbol{x}) \Big) \tag{5.15}$$

where $\mathcal{S}$ denotes the set defined by the constraints and $F(\lambda)$ is an auxiliary function with parameter λ [92]. If we assume that $f(\boldsymbol{x})$ and $g(\boldsymbol{x})$ are continuous, $g(\boldsymbol{x})$ is positive and $\mathcal{S}$ is compact, then $F(\lambda)$ exists and is continuous. Besides, $F(\lambda)$ is monotonic decreasing and has a unique root at λ^* as shown in Figure 5.1.

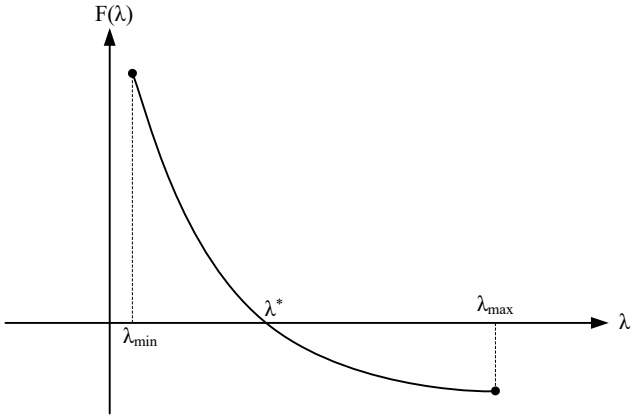

Figure 5.1: Graph of the auxiliary function $F(\lambda)$.

If we consider $\boldsymbol{x}^* \in \mathcal{S}$ and $\lambda^* = \frac{f(\boldsymbol{x}^*)}{g(\boldsymbol{x}^*)}$, then $\boldsymbol{x}^*$ is a solution of (5.14) if and only if [92]

$$\boldsymbol{x}^* = \arg\max_{\boldsymbol{x}\in\mathcal{S}} \Big(f(\boldsymbol{x}) - \lambda^* g(\boldsymbol{x}) \Big). \tag{5.16}$$

As a result, solving a fractional programming problem is equivalent to finding the unique zero of the auxiliary function $F(\lambda)$ which is achieved through the Dinkelbach method shown in Algorithm 1. If $f(\boldsymbol{x})$ is concave, $g(\boldsymbol{x})$ is convex and all constraints are also convex, then the Dinkelbach algorithm converges to the global optimum solution. Moreover, the update rule for λ follows Newton's method applied to the function $F(\lambda)$; hence the Dinkelbach algorithm exhibits a super-linear convergence rate [52, 92, 93].

Algorithm 1 Dinkelbach algorithm to solve the CCFP problem.

A. Initialization

1. Initialize iteration index $n = 0$, tolerance $\epsilon > 0$ and $\lambda_n \geq 0$.

B. Iterative Operation

while $(F(\lambda_n) > \epsilon)$ **do**

$\boldsymbol{x}_n^* = \arg\max_{\boldsymbol{x}\in\mathcal{S}} \Big(f(\boldsymbol{x}) - \lambda_n g(\boldsymbol{x})\Big)$;

$F(\lambda_n) = f(\boldsymbol{x}_n^*) - \lambda_n g(\boldsymbol{x}_n^*)$;

$\lambda_{n+1} = \frac{f(\boldsymbol{x}_n^*)}{g(\boldsymbol{x}_n^*)}$;

$n = n + 1$;

end while

Output: $\boldsymbol{x}^*$

5.3 Energy Efficient Power Control Algorithm Formulation

As stated in Section 5.2.1, fractional programming is an efficient tool to maximize a fractional function when the numerator is a concave function, the denominator is a convex function and the constraint set is convex. If any of these properties are not met, fractional programming could not give low-complex optimization methods for the problem [92]. But, due to the multiuser interference term in (5.6), the objective function in (5.13) does not have a concave numerator, and therefore finding the global solution of (5.13) with affordable complexity is difficult. To tackle this issue, we utilize two techniques to derive the concave approximation of the numerator on the objective function and the convex approximation of the minimum rate constraint in (5.13).

- The first method employs a lower bound on the logarithm to approximate the objective function and the minimum rate constraint in (5.13) [85].
- The second method integrates fractional programming theory with sequential convex programming [51] to approximate the objective function and the minimum rate constraint in (5.13). This allows to develop a computationally efficient algorithm which is guaranteed to converge to a first-order optimal solution [52].

5.3.1 Energy Efficient Power Control Power Control via Logarithm Function Approximation

In this section, the GEE maximization algorithm is formulated by leveraging a lower bound on the logarithm function [85]. Specifically, for all $\gamma_k(\mathbf{p}), \bar{\gamma} \geq 0$, we get the following logarithmic inequality [85]

$$\log_2(1+\gamma_k(\mathbf{p})) \geq \alpha_k \log_2 \gamma_k(\mathbf{p}) + \beta_k \tag{5.17}$$

that is tight at $\gamma_k(\mathbf{p}) = \bar{\gamma}$ when α_k and β_k are calculated adaptively as [85]

$$\begin{aligned} \alpha_k &= \frac{\bar{\gamma}}{\bar{\gamma}+1} \\ \beta_k &= \log_2(1+\bar{\gamma}) - \frac{\bar{\gamma}}{\bar{\gamma}+1}\log_2 \bar{\gamma}. \end{aligned} \tag{5.18}$$

By using the approximations in (5.18), a lower bound for the objective function in (5.13) is formulated as

$$\mathrm{GEE}(\mathbf{p}) \geq \frac{B\left(1-\frac{\tau_p}{\tau_c}\right)\sum_{k=1}^{K}[\alpha_k \log_2(\gamma_k(\mathbf{p})) + \beta_k]}{\sum_{k=1}^{K}\mu_k p_k + P_0}. \tag{5.19}$$

Assuming $p_k = 2^{q_k}$, where $\mathbf{q} = (q_1, q_2, \cdots, q_K)^T \in \mathbb{R}$, (5.19) is further simplified as

$$\begin{aligned} h(\mathbf{q}) \triangleq & \frac{B\left(1-\frac{\tau_p}{\tau_c}\right)\sum_{k=1}^{K}[\alpha_k \log_2(b_k) + \alpha_k q_k + \beta_k]}{\sum_{k=1}^{K}\mu_k 2^{q_k} + P_0} \\ & - \frac{B\left(1-\frac{\tau_p}{T}\right)\sum_{k=1}^{K}[\alpha_k \log_2(\sigma^2 + \sum_{i=1}^{K} w_i 2^{q_i})]}{\sum_{k=1}^{K}\mu_k 2^{q_k} + P_0}. \end{aligned} \tag{5.20}$$

By using (5.20), the optimization problem in (5.13) is reformulated as

$$\begin{aligned} & \max_{\mathbf{q}} \; h(\mathbf{q}) \\ & \text{subject to:} \quad 0 \leq 2^{q_k} \leq P_{\max,k} \qquad \forall k \\ & \qquad\qquad \log_2(1+\gamma_k(\mathbf{p})) \geq R_{0,k} \;\; \forall k. \end{aligned} \tag{5.21}$$

It is shown in [85] that for any given α_k and β_k, both the numerator and denominator of (5.20) are differentiable, and concave and convex in q_k, respectively. Besides, the minimum rate constraint can be reformulated as

$$2^{q_k} b_k + (1-2^{R_{0,k}})\left(\sigma^2 + \sum_{i=1}^{K} w_i 2^{q_i}\right) \geq 0 \tag{5.22}$$

which is convex in q_k [94]. As a result, (5.21) is a fractional programming optimization problem which can be solved by means of fractional programming tools such as the Dinkelbach algorithm [92]. Finally, the complete iterative procedure for the proposed energy

efficient power optimization is summarized in Algorithm 2. This power control algorithm is feasible if it is possible to satisfy the SINR requirements for all users simultaneously under a given power allocation vector [95]. But, this is not always possible and a feasibility condition evaluation should be done before running Algorithm 2. Hence, in the simulation section, we analyze the feasibility conditions for the proposed power control algorithm [95].

Algorithm 2 Energy efficient power control algorithm via logarithm lower bound approximation.

A. Initialization

1. Set maximum iterations N, tolerance ϵ and $n = 0$.
2. Initialize a power allocation $\mathbf{p}^{(0)}$ with a feasible value.
3. Set $\bar{\gamma}_k^{(0)} = \gamma_k^{(0)}(\mathbf{p})$ and compute $\alpha_k^{(0)}$ and $\beta_k^{(0)}$ from (5.18).

B. Iterative Operation

1: $n = n + 1$
2: Solve (5.21) via Dinkelbach method with $\alpha_k^{(n-1)}$ and $\beta_k^{(n-1)}$.
3: Set $\mathbf{q}^{(n)} = \arg\max h(\mathbf{q})$ and then $\mathbf{p}^{(n)} = 2^{\mathbf{q}^{(n)}}$.
4: Set $\bar{\gamma}_k^{(n)} = \gamma_k^{(n)}(\mathbf{p})$ and update $\alpha_k^{(n)}$ and $\beta_k^{(n)}$ from (5.18).
5: Until converegence of $\mathbf{p}^\star$ or $n = N$.

Output: $\mathbf{p}^\star$

5.3.2 Energy Efficient Power Control via Sequential Convex Programming

In this section, to calculate the concave/convex approximation for the objective function and the minimum rate constraint in (5.6), we integrate fractional programming theory with sequential convex programming (SCP) [51,94]. This allows us to formulate computationally efficient optimization algorithm to solve (5.6) that can converge to the optimal solution. Sequential convex programming helps to find the local optimum of a difficult problem with objective f, by solving a sequence of easier problems with objectives $\{\hat{f}_i\}_i$. In each step of the sequence, the following three conditions need to hold [53, 94]:

i. $\hat{f}_i(\mathbf{x}) \leq f(\mathbf{x})$, for all x

ii. $\hat{f}_i(\mathbf{x}^{(i-1)}) = f(\mathbf{x}^{(i-1)})$

iii. $\nabla\hat{f}_i(\mathbf{x}^{(i-1)}) = \nabla f(\mathbf{x}^{(i-1)})$

where i denotes the iteration index and $\mathbf{x}^{(i-1)}$ denotes the maximizer of f_{i-1} [94]. Thus, the difficult task of this approach is to find suitable approximations, $\{\hat{f}_i\}_i$ which fulfill the above conditions while at the same time results in simpler optimization problems [94]. These conditions can be satisfied when the approximate function is a concave or pseudo-concave maximization subject to convex constraints [94]. In this work, we utilize a first order Taylor series approximation [94] to approximate the achievable sum rate and the minimum rate constraint in (5.6).

To employ sequential convex programming algorithm, we first express the spectral efficiency of the user in difference of two functions as $\log_2(1+\gamma_k(\mathbf{p})) = c_k(\mathbf{p}) - d_k(\mathbf{p})$. The particular expressions for $c_k(\mathbf{p})$ and $d_k(\mathbf{p})$ are shown in Appendix III. By using these expressions, the energy efficiency optimization problem in (5.13) is reformulated as [51]

$$\begin{aligned} \max_{\mathbf{p}} \quad & \frac{B\left(1-\frac{\tau_p}{\tau_c}\right)\sum_{k=1}^{K}\left[c_k(\mathbf{p})-d_k(\mathbf{p})\right]}{\sum_{k=1}^{K}\mu_k p_k + P_0} \\ \text{subject to:} \quad & 0 \le p_k \le P_{\max,k} \qquad \forall k \\ & c_k(\mathbf{p}) - d_k(\mathbf{p}) \ge R_{0,k} \ \forall k. \end{aligned} \tag{5.23}$$

The numerator of the objective function in (5.23) becomes a valid concave function iff it is the difference of a concave and a convex expression [94]. Thus, to guarantee a valid concave expression for the numerator function in (5.23), $d_k(\mathbf{p})$ is approximated by the first order Taylor series approximation as shown in Theorem 5.3.1. Then, the corresponding sequential convex programming based energy efficient power control algorithm is formulated by using this approximation.

Theorem 5.3.1 *Let $\boldsymbol{p}^i$ be the value of $\boldsymbol{p}$ in iteration i, then the first-order Taylor series approximation of $d_k(\boldsymbol{p})$ at $\boldsymbol{p}^i$ is expressed as*

$$d_k(\boldsymbol{p}) \le d_k\left(\mathbf{p}^i\right) + \nabla d_k\left(\mathbf{p}^i\right)^T\left(\mathbf{p}-\mathbf{p}^i\right) \tag{5.24}$$

where $\nabla d_k(\boldsymbol{p}^i)$ is the gradient of $d_k(\mathbf{p})$ at $\mathbf{p}^i$. This shows that the first order Taylor series approximation is a global upper bound of a concave function. The derivation of the gradients

are shown in Appendix 5.2. With this approximation, the optimization problem in (5.23) is reformulated as

$$\begin{aligned} \max_{\boldsymbol{p}} \; & \frac{B\left(1-\frac{\tau_p}{\tau_c}\right)\sum_{k=1}^{K}\left[c_k(\boldsymbol{p})-\left(d_k\left(\mathbf{p}^i\right)+\nabla d_k\left(\mathbf{p}^i\right)^T\left(\mathbf{p}-\mathbf{p}^i\right)\right)\right]}{\sum_{k=1}^{K}\mu_k p_k+P_0} \\ & \textit{subject to:} \quad 0\le p_k\le P_{\max,\,k} \qquad\qquad \forall k \\ & \qquad c_k(\boldsymbol{p})-\left(d_k\left(\mathbf{p}^i\right)+\nabla d_k\left(\mathbf{p}^i\right)^T\left(\mathbf{p}-\mathbf{p}^i\right)\right)\ge R_{0,\,k}\;\forall k. \end{aligned} \tag{5.25}$$

It is noteworthy that the objective function in (5.25) has a concave numerator and affine denominator, while the constraint functions are affine and convex. Thus, the first order optimal solution of (5.6) can be achieved by solving the approximate problem in (5.25) with available convex optimization packages in polynomial time [94]. By reformulating (5.25) into (5.26) as shown below, we can find the global solution by employing fractional programming methods [52, 92].

$$\begin{aligned} \max_{\mathbf{p}} \; & B\left(1-\frac{\tau_p}{\tau_c}\right)\sum_{k=1}^{K}\left[c_k(\mathbf{p})-\left(d_k\left(\mathbf{p}^i\right)+\nabla d_k\left(\mathbf{p}^i\right)^T\left(\mathbf{p}-\mathbf{p}^i\right)\right)\right]-\lambda_n\left[\sum_{k=1}^{K}\mu_k p_k+P_0\right] \\ & \text{subject to}: \quad 0\le p_k\le P_{\max,\,k} \qquad \forall k \\ & \qquad c_k(\mathbf{p})-\left(d_k\left(\mathbf{p}^i\right)+\nabla d_k\left(\mathbf{p}^i\right)^T\left(\mathbf{p}-\mathbf{p}^i\right)\right)\ge R_{0,\,k}\;\forall k \end{aligned} \tag{5.26}$$

where λ_n is the auxiliary parameter for the Dinkelbach algorithm. To solve this problem, we employ the Dinkelbach algorithm with Bisection method that is shown in Algorithm 3. Finally, to calculate the optimal power in each Bisection step, we apply the iteration procedure shown in Algorithm 4.

5.3.3 Energy Efficiency Optimization via Equal Power Allocation

When the time and computing resources are limited, it may be difficult to solve the power control optimization problem at low complexity [21, 96, 97]. In this case, it is necessary to use other power allocation techniques with reduced complexity. An intuitive choice is assuming equal power allocation among all users [21, 98, 99]. Specifically, if we consider equal power allocation with $p_k = p_u$ for all K-users, the lower bound spectral efficiency of the user in (5.6) is reformulated as [21]

$$R_k \approx \log_2\left(1+\frac{p_u(M-K)\hat{\beta}_k}{p_u\sum_{j=1}^{K}\tilde{\beta}_j+\sigma^2}\right) \tag{5.28}$$

Algorithm 3 Energy efficient power control with sequential convex programming.

A. Initialization

1. Set iteration index $n = 0$, max iteration N and tolerance ϵ.

2. Set minimum and maximum energy efficiency as $\lambda_{\min}$ and $\lambda_{\max}$ with $\lambda_{\min} \leq \lambda^{\star} \leq \lambda_{\max}$.

B. Iterative Operation

while $n < N$ **do**

  $\lambda_n = \frac{\lambda_{\min}+\lambda_{\max}}{2}$

  With λ_n, solve the optimization problem in (5.26) to get $\mathbf{p}^{(n)}$.

  Calcuate $\mathrm{F}(\lambda_n) = R_s(\mathbf{p}^{(n)}) - \lambda_n P_{\text{tot}}(\mathbf{p}^{(n)})$ where $R_s(\mathbf{p})$ and $P_{\text{tot}}(\mathbf{p})$ are given by

$$\begin{aligned} R_s(\mathbf{p}) &= B\Big(1 - \frac{\tau_p}{\tau_c}\Big) \sum_{k=1}^{K} \Big[c_k(\mathbf{p}) - \Big(d_k\left(\mathbf{p}^i\right) + \nabla d_k\left(\mathbf{p}^i\right)^T \left(\mathbf{p} - \mathbf{p}^i\right)\Big)\Big] \\ P_{\text{tot}}(\mathbf{p}) &= \lambda_n \sum_{k=1}^{K} \mu_k p_k + P_0. \end{aligned} \tag{5.27}$$

  If $|\mathrm{F}(\lambda_n)| \leq \epsilon$

  $\mathbf{p}^{\star} = \mathbf{p}^{(n)},\ \lambda^{\star} = \frac{R_s(\mathbf{p}^{(n)})}{P_{\text{tot}}(\mathbf{p}^{(n)})}$;

  break;

  elseif $\mathrm{F}(\lambda_n) < 0,\ \lambda_{\max} = \lambda_n$;

  else $\lambda_{\min} = \lambda_n$;

  end if

  $n = n + 1$;

end while

Output: $\mathbf{p}^{\star}$

where p_u is a constant power that is allocated to all users equally. Thus, by using this formulation, the optimization problem in (5.13) is reformulated as

$$\begin{aligned} \max_{p_u} \ \mathrm{GEE}(p_u) &= \frac{B\Big(1 - \frac{\tau_p}{\tau_c}\Big) \sum_{k=1}^{K} \log_2(1 + \gamma_k(p_u))}{K p_u \mu_k + P_0} \\ \text{subject to:} \quad & 0 \leq p_u \leq P_{\max,\,k} \qquad \forall k \\ & R_k(p_u) \geq R_{0,\,k} \ \forall k. \end{aligned} \tag{5.29}$$

where $R_k(p_u) = \log_2(1+\gamma_k(p_u))$. To solve this optimization problem, we first determine the feasible region of p_u and then calculate the global optimum. To do this, we first solve the

Algorithm 4 Iterative operation to search the optimal power in each step of Algorithm 3.

A. Initialization

1. Set maximum iteration N, tolerance $\delta > 0$ and $i = 0$.

2. Set initial feasible power allocation $\mathbf{p}^0$ and calculate the Taylor approximation of $d_k(\mathbf{p})$ from (5.24) .

B. Iterative Operation

1: Solve the optimization problem in (5.26) to get the optimal power $\mathbf{p}$.

2: Set $i = i + 1$ and $\mathbf{p}^i = \mathbf{p}$.

3: Calculate $d_k(\mathbf{p})$ from (5.24) with $\mathbf{p}^i$ and go to step 1.

4: Until $|I^i - I^{i-1}| \leq \delta$ or $n = N$ where $I^i = c_k(\mathbf{p}^i) - d_k(\mathbf{p}^i)$

Output: $\mathbf{p}^\star$

equation $R_k(p_u) = R_{0,k}$ and get the solution $p_{u,\,k}$ for all k. It can be noted from (5.28) that $R_k(p_u)$ is a monotonically increasing function in p_u. Hence, the minimum rate constraint in (5.29) can be redefined as $p_u \geq p_{u,\,\max}$ where $p_{u,\,\max} = \max\{p_{u,1}, p_{u,2}, \cdots, p_{u,K}\}$. Then, considering the maximum transmit power constraint, the feasible region of p_u becomes in $[p_{u,\,\max}, P_{\max,\,k}]$. If $p_{u,\,\max} > P_{\max,\,k}$, the optimization problem becomes infeasible and there is no solution that satisfies the minimum rate constraint. Once feasible, the global maximum energy efficiency can be found in $[p_{u,\,\max}, P_{\max,\,k}]$. Besides, the energy efficiency in this region is a quasi-concave function in p_u and has a unique stationary point $p_u^\star$ which coincides with the global maximizer [99]. This stationary point can be found from the first-order derivative of GEE(p_u) with respect to p_u. Therefore, the power allocation solution of (5.29) is given by

$$p_u^\star = \begin{cases} p_{u,\,\max} & p_u^\star \leq p_{u,\,\max} \\ p_u^\star & p_{u,\,\max} < p_u^\star \leq P_{\max,\,k} \\ P_{\max,\,k} & p_u^\star > P_{\max,\,k}. \end{cases} \tag{5.30}$$

Compared to the problem in (5.13) where K variables are optimized, the equal power allocation problem in (5.30) uses only p_u as the optimization variable. Thus, the complexity of equal power allocation is much lower than that of optimal power allocation [21, 99]. Therefore, equal power allocation is mostly considered for further resource allocation, an-

tenna selection and user scheduling algorithm development. In the simulation and analysis section, we include results with equal power allocation as a benchmark to compare the performances of the proposed algorithms.

5.4 Simulation Results and Analysis

In this section, we evaluate the performances of the proposed energy efficient power control algorithms for uplink massive MIMO systems. First, we analyze the accuracy of the derived closed-form lower bound achievable sum rate approximation in (5.6). Then, the feasibility condition for the optimization problem is evaluated. Besides, the impact of system parameters, maximum transmit power and minimum data rate constraints on energy efficiency maximization are analyzed.

5.4.1 Simulation Parameters

For the simulation, we assume that the users are distributed uniformly in a circular cell of radius $r_c = 500\,\text{m}$ except for an exclusion zone ($r_h \leq 35\,\text{m}$) near the BS. The exclusion zone is considered to ensure that forward and reverse link transmission is performed in the far field of the transmitting antennas and plane waves shall be considered at the receivers [3]. The large scale fading is modeled as $\beta_k = z_k(\frac{r_k}{r_h})^{-v}$ where z_k is the log-normal shadow fading random variable with standard deviation $\sigma_{\text{sh}} = 8\,\text{dB}$, $v = 3.8$ is the path loss exponent and $r_k \in [r_c, r_h]$ denotes the Euclidean distance between the kth user and the BS antennas.

The users are considered to have the same maximum transmit power constraints ($P_{\text{max},k} = P_{\text{max}}$) and the same minimum rate constraints ($R_{0,k} = R_0$) for all k. The simulation is run for 1000 Monte-Carlo realizations where in each snapshot, the users are distributed randomly in the cell so that the large scale fading β_k changes. We use the standard system parameters proposed in [22] and [54]. Some of the main simulation parameters are shown in Table 5.1. We deploy CVX with the MOSEK solver [94] to simulate the system.

5.4.2 Analysis of Achievable Sum Rate Approximation

To validate the accuracy of the proposed analytical closedform lower bound formulation, we compare the achievable sum rate in (5.6) with results from Monte-Carlo realization of (5.5) as shown in Figure 5.2. The figure shows that the gaps between results from analytical closedform lower bound and the Monte-Carlo simulation are very small. Thus,

Table 5.1: Some of the simulation parameters.

Parameter	**Value**	**Parameter**	**Value**
τ_c	200	ρ_a	0.002 W
B	20 MHz	Θ_0	0.8 W
(M, K)	(200 , 10)	$\sigma_{\text{sc}}\bar{R}_0$	0.4 W
τ_p	10	η_{BS}	0.39
p_p	30 dBm	η_{UE}	0.3

it is quite reasonable to evaluate the proposed energy efficient power control algorithms by using closed-form lower bound achievable sum rate expression in (5.6).

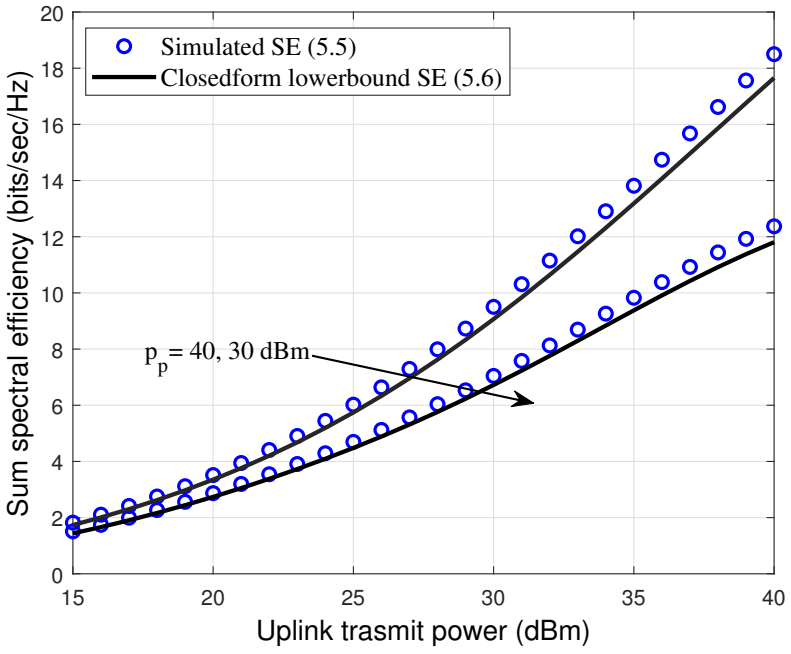

Figure 5.2: Spectral efficiency versus uplink transmitter power. Where p_p is the transmitted pilot power for channel estimation.

Figure 5.3 shows the energy efficiency in (5.12) with the spectral efficiency results in Figure 5.2. As it is known, the energy efficiency is a unimodal function of the transmit power [52] and thus, it increases until some transmit power and then decrease beyond that power. This is the key feature which allows to save energy through energy efficient resource allocation.

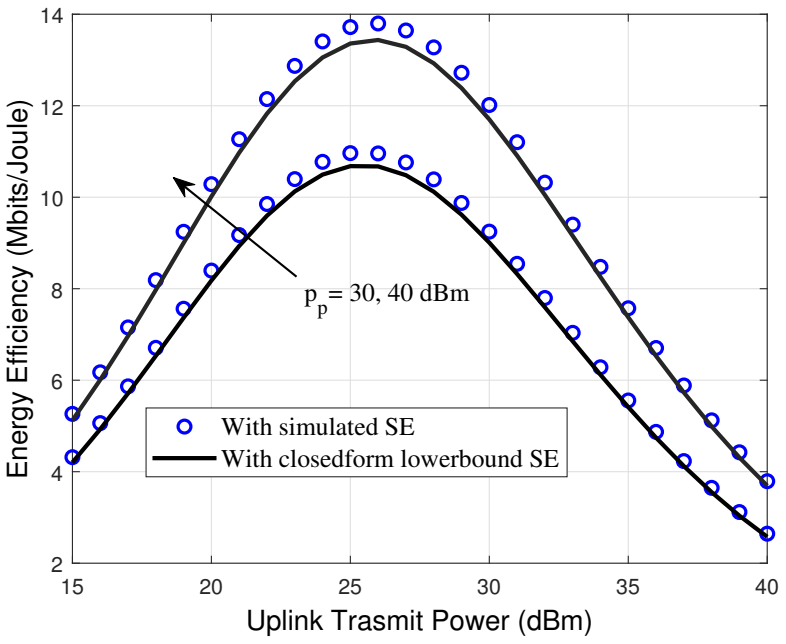

Figure 5.3: Energy efficiency versus uplink transmitter power with spectral efficiency in Figure 5.2.

5.4.3 Feasibility of the Optimization Problem

In cellular systems, each user is active only for some period of time and during this active state it has a quality-of-service (QoS) requirement that must be satisfied by allocating system resources. The QoS requirement changes over time depending on the traffic and the network needs to adapt to these variations. In this work, we assume the QoS requirements are expressed by the minimum rate constraint of each users that is formulated interms of the effective SINR as

$$\text{SINR}_k \geq \gamma_{0,k} \tag{5.31}$$

where $\gamma_{0,k} = 2^{R_{0,k}} - 1$ is the minimum required SINR of user k. It is not always possible to meet this requirements simultaneously. In these cases, the power optimization is infeasible. Whereas, the optimization problem in (5.13) is feasible if it satisfies the required minimum rate constraint of all users simultaneously with a positive power vector $\mathbf{p} = [p_1, p_2, \cdots, p_K]^T \leq P_{\max,k}$. In this work, the system resource to be allocated are the transmit power for given fixed number of users and BS antennas. Thus, from (5.7), the system satisfies the minimum rate constraint if and only if [100, 101]

$$\frac{p_k b_k}{\sigma^2 + \sum_{j=1}^{K} p_j w_j} \geq \gamma_{0,k}. \tag{5.32}$$

where $\gamma_{0,k} = 2^{R_{0,k}} - 1$. By rearranging the terms, we can reformulate (5.32) as

$$\mathbf{p} \geq (\mathbf{I} - \mathbf{F})^{-1}\mathbf{s} \tag{5.33}$$

where $\mathbf{s} = \frac{\sigma^2\gamma_{0,k}}{b_k}$, $\mathbf{F} \in \mathbb{C}^{K\times K}$ is a rank one matrix given by $[\mathbf{F}]_{kj} = \frac{\gamma_{0,k}w_k}{b_k}$ for all k, j and $\mathbf{I}$ is the identity matrix. Then, the necessary condition for proposed optimization algorithm to be feasible is given by [95, 101]

$$\rho(\mathbf{F}) < 1 \text{ and } \mathbf{p} \geq (\mathbf{I} - \mathbf{F})^{-1}\mathbf{s}. \tag{5.34}$$

where $\rho(\mathbf{F})$ is the spectral radius of $\mathbf{F}$. We evaluate the feasibility condition at different minimum rate constraints and given numbers of BS antennas as shown in Figure 5.4. The results are obtained by averaging over 5000 independent scenarios of user drops and large scale fading channel coefficients. The result shows that when the required minimum rate constraint increases, the feasibility probability decreases and most users could not satisfy the minimum rate constraint under the given maximum transmit power constraint.

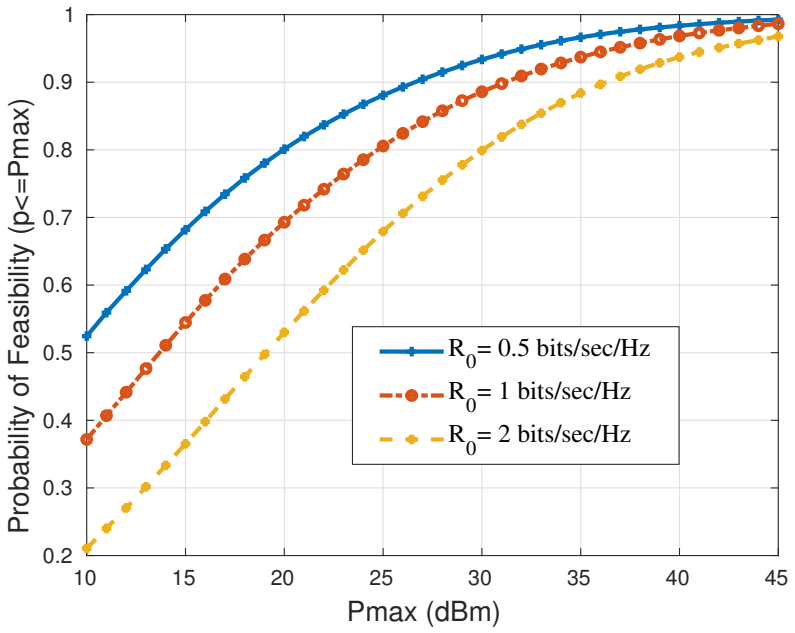

Figure 5.4: Feasibility probability of the proposed energy efficient power control algorithm.

5.4.4 Impact of Increasing the Number of BS Antennas

Figure 5.5 shows the required maximum transmit power of a user with the number of BS antennas that satisfy a minimum data rate constraint of $R_k \geq 1$bits/sec/Hz for different numbers of uniformly distributed users. The result shows that when the number of BS

antennas increases, the power required to achieve the minimum data rate constraint at the user is decreased. The result also shows that when the number of scheduled users are large, the required transmission power to achieve a minimum data rate constraint of $R_k \geq 1$bits/sec/Hz increases. This is because when the number of scheduled users are large, the multiuser interference term becomes very high and thus more power is required to achieve the minimum data rate constraint.

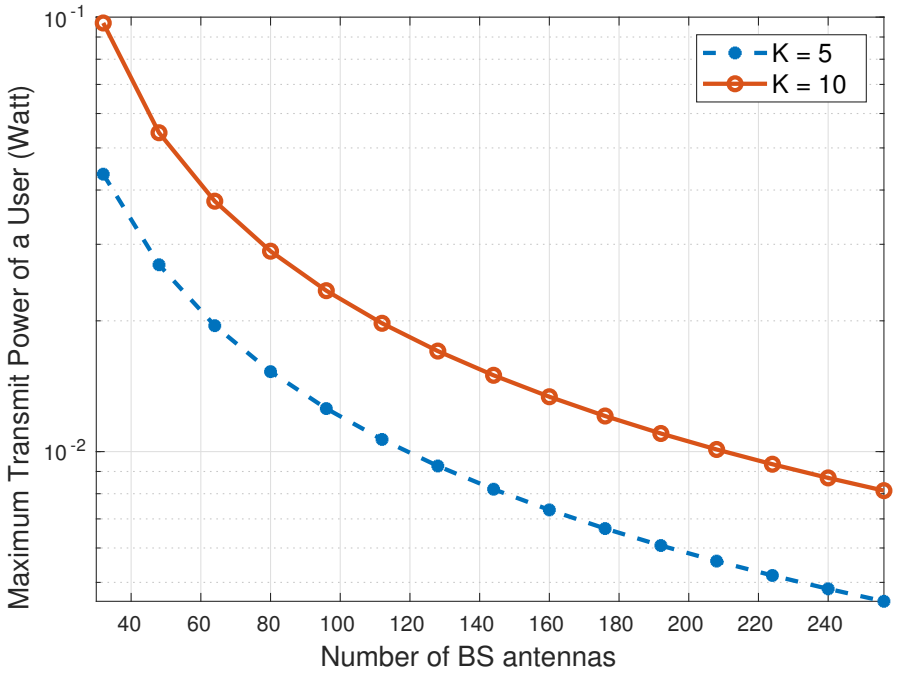

Figure 5.5: Maximum required transmit power of a user versus number of BS antennas to achieve a minimum rate constraint of $R_k \geq 1$bits/sec/Hz to all users.

5.4.5 Impact of the Maximum Transmit Power Constraint on Energy Efficiency

Figure 5.6 shows the impact of the maximum transmit power constraint on the global energy efficiency achieved by the proposed optimization algorithms. The result shows that in a low transmit power regime, increasing the maximum transmit power is energy efficient. Whereas, when the transmitter power grows large, the global energy efficiency saturates at a certain level. This is because once $P_{\max}$ is large enough to achieve maximum energy efficiency, excess fraction of the transmit power is no longer used and increasing the transmitter power further cannot improve the energy efficiency. The result also shows that energy efficiency achieved by sequential convex programming is nearly equal to energy efficiency obtained from the logarithm approximation. As expected, equal power allocation achieves lower energy efficiency than other algorithms.

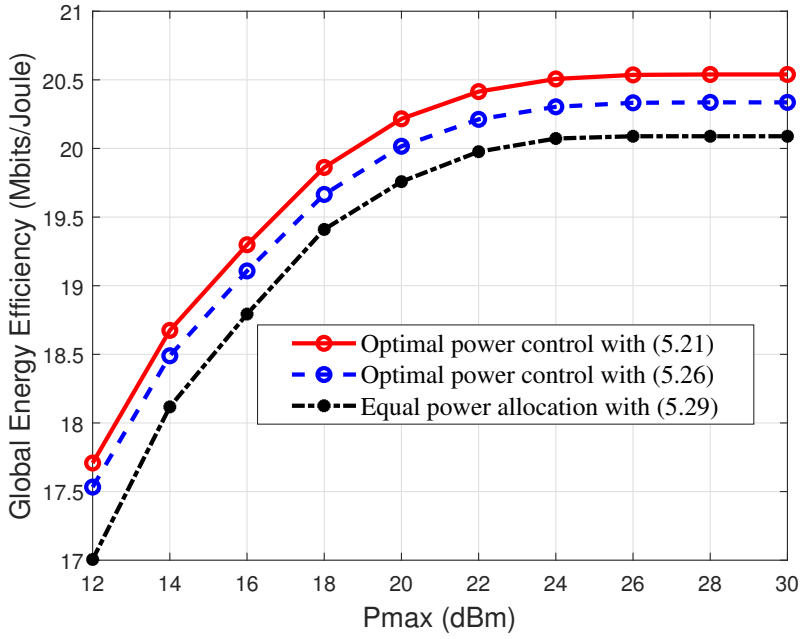

Figure 5.6: Impact of maximum transmit power constraint on global energy efficiency.

5.4.6 Impact of the Minimum Rate Constraint on Energy Efficiency

Finally, Figure 5.7 shows the impact of the minimum rate constraint on global energy efficiency of the proposed power control algorithm. The result shows that when R_0 is small, the global energy efficiency remains unchanged. This is because when R_0 takes a small value, the power optimization solution that maximizes the energy efficiency can also satisfy the minimum rate requirements of each user. Meanwhile, when R_0 increases, the energy efficiency decreases. This is because when the minimum required rate of each user increases, an excess fraction of the power should be allocated to the users that have the worst links to achieve the required rate and which results in a lower energy efficiency in the system. Besides, the energy efficiency achieved by sequential convex programming is nearly equal to the energy efficiency obtained from the logarithm lower bound approximation.

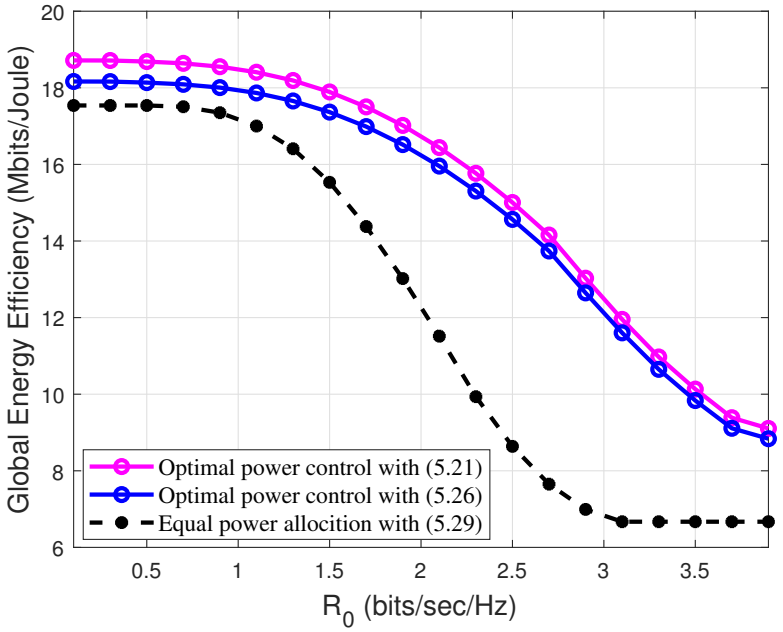

Figure 5.7: Impact of the minimum rate constraint on global energy efficiency. Here $P_{\max}$ =20 dBm .

5.5 Summary

In this work, we have investigated and evaluated power control algorithms that maximize energy efficiency in uplink massive MIMO systems. We consider the system is equipped with zero forcing detection and assuming imperfect channel state information, MMSE based channel estimation is done at the BS. Tools from from fractional programming theory and sequential convex programming is utilized to derive power optimization algorithms that maximize the energy efficiency. Numerical results have been presented to illustrate the effectiveness of the proposed algorithms. The feasibility condition for the optimization problem has been evaluated. The effects of maximum transmitter power and minimum data rate constraints of the users on global energy efficiency have been analyzed. The results show that the global energy efficiency increases with the maximum transmitter power constraint and decreases with the minimum data rate constraint.

Appendix

Appendix 5.1: Proof of Theorem 5.1.1

Applying the Jensen inequality, the spectral efficiency expression in (5.5) can be reformulated as

$$R_{_k} \triangleq \log_2\left(1+\frac{p_k|\mathbb{E}\{\mathbf{w}_k^H\mathbf{g}_k\}|^2}{p_k\mathrm{Var}\left(\mathbf{w}_k^H\mathbf{g}_k\right)+\sum_{i=1,i\neq k}^{K}p_i\mathbb{E}\{|\mathbf{w}_k^H\mathbf{g}_i|^2\}+\sigma^2\mathbb{E}\{||\mathbf{w}_k||^2\}}\right) \tag{5.35}$$

where Var(.) is the variance of a random variable. Thus, to get the achievable sum rate expression shown in (5.6), we derive closed-form results for $\mathbb{E}\{\mathbf{w}_k^H\mathbf{g}_k\}$, $\mathrm{Var}\{\mathbf{w}_k^H\mathbf{g}_k\}$, $\mathbb{E}\{|\mathbf{w}_k^H\mathbf{g}_i|^2\}$ and $||\mathbf{w}_k||^2$as follows.

- $\mathbf{W}^H\mathbf{G} = \mathbf{W}^H(\hat{\mathbf{G}}+\tilde{\mathbf{G}}) = \mathbf{I}_K + \mathbf{W}^H\tilde{\mathbf{G}}$. Thus,

$$\mathbf{w}_k^H\mathbf{g}_k = 1 + \mathbf{w}_k^H\tilde{\mathbf{g}}_k. \tag{5.36}$$

  But, as $\mathbf{w}_k$ and $\tilde{\mathbf{g}}_k$ are independent, we get

$$\mathbb{E}\{\mathbf{w}_k^H\mathbf{g}_k\} = 1. \tag{5.37}$$

- $\text{Var}\{\mathbf{w}_k^H \mathbf{g}_k\} = \mathbb{E}\{|\mathbf{w}_k^H \mathbf{g}_k|^2\} - \left(\mathbb{E}\{\mathbf{w}_k^H \mathbf{g}_k\}\right)^2 = \mathbb{E}\{|\mathbf{w}_k^H \tilde{\mathbf{g}}_k|^2\}$. As $\mathbf{w}_k$ and $\tilde{\mathbf{g}}_k$ are independent,

$$\mathbb{E}\{|\mathbf{w}_k^H \tilde{\mathbf{g}}_k|^2\} = \mathbb{E}\{\tilde{\mathbf{g}}_k \mathbf{w}_k^H \mathbf{w}_k \tilde{\mathbf{g}}_k^H\} \overset{a.s}{\to} \tilde{\beta}_k \mathbb{E}\{||\mathbf{w}_k||^2\}. \tag{5.38}$$

  By using the closed-form approximation in Appendix I and by employing properties in [24: Lemma 2.10] when $M \to \infty$, we get

$$\mathbb{E}\{||\mathbf{w}_k||^2\} = \mathbb{E}\{\text{tr}(\mathbf{w}_k \mathbf{w}_k^H)\} \overset{a.s}{\to} \frac{\hat{\beta}_k^{-1}}{M-K}. \tag{5.39}$$

  Combining the results from (5.38) and (5.39), we get

$$\text{Var}\{\mathbf{w}_k^H \mathbf{g}_k\} \overset{a.s}{\to} \frac{\tilde{\beta}_k \hat{\beta}_k^{-1}}{M-K}. \tag{5.40}$$

- Derive $\mathbb{E}\{|\mathbf{w}_k^H \mathbf{g}_i|^2\}$: as $\mathbf{w}_k$ and $\tilde{\mathbf{g}}_i$ are independent, we have

$$\mathbb{E}\{|\mathbf{w}_k^H \mathbf{g}_i|^2\} = \mathbb{E}\{|\mathbf{w}_k^H \tilde{\mathbf{g}}_i|^2\}. \tag{5.41}$$

  Thus, similar to the previous approach

$$\mathbb{E}\{|\mathbf{w}_k^H \tilde{\mathbf{g}}_i|^2\} \overset{a.s}{\to} \frac{\tilde{\beta}_i \hat{\beta}_k^{-1}}{M-K}. \tag{5.42}$$

  The interuser interference term becomes,

$$\sum_{i=1, i\neq k}^{K} p_i \mathbb{E}\{|\mathbf{g}_k^H \mathbf{w}_i|^2\} \overset{a.s}{\to} \frac{\hat{\beta}_k^{-1} \sum_{i=1, i\neq k}^{K} p_i \tilde{\beta}_i}{M-K}. \tag{5.43}$$

Substituting the results in (5.37), (5.39), (5.40) and (5.43) into (5.35), we get the result in (5.6).

Appendix 5.2: Derivation of the gradient equation for (5.25)

The achievable rate of a user in (5.6) can be expressed as a difference of two functions as

$$\begin{aligned} R_k(\mathbf{p}) &= \log_2\left(1 + \frac{p_k b_k}{\sigma^2 + \sum_{j=1}^{K} p_j w_j}\right) \\ &= \log_2\left(\sigma^2 + p_k b_k + \sum_{j=1}^{K} p_j w_j\right) - \log_2\left(\sigma^2 + \sum_{j=1}^{K} p_j w_j\right) \end{aligned} \tag{5.44}$$

and from (5.44), we can express $c_k(\mathbf{p})$ and $d_k(\mathbf{p})$ as

$$\begin{aligned} c_k(\mathbf{p}) &= \log_2\left(\sigma^2 + p_k b_k + \sum_{j=1}^{K} p_j w_j\right) \\ d_k(\mathbf{p}) &= \log_2\left(\sigma^2 + \sum_{j=1}^{K} p_j w_j\right). \end{aligned} \tag{5.45}$$

Thus, the first derivative of $d_k(\mathbf{p})$ is given by

$$\frac{\partial d_k(\mathbf{p})}{\partial p_k} = \frac{w_k}{\ln 2 \left(\sigma^2 + \sum_{j=1}^{K} p_j w_j \right)} \tag{5.46}$$

an the gradient is calculated from (5.46).

Chapter 6

Joint Energy Efficient Resource Allocation in Massive MIMO Systems

6.1 Introduction

The spectral efficiency and energy efficiency gains of massive MIMO systems cannot be fully exploited without employing efficient resource allocation techniques [84]. Specifically, developing optimization algorithms that select the optimal number of BS antennas, users and transmit power allocation to maximize given utility function is the main focus of resource allocation in massive MIMO systems. Hence, in this chapter, we propose joint energy efficient resource allocation algorithms for downlink single cell massive MIMO systems. In particular, the user selection, number of BS antennas and transmit power allocation are jointly optimized. To do this, similar to the previous section, MMSE based channel estimation and ZF precoding are assumed at the BS. Then, we derive analytical lower bound spectral efficiency in-terms of the large scale fading parameters. Next, we formulate a tractable objective function for the energy efficiency optimization. Applying this optimization formulation, we propose an energy-efficient resource allocation scheme based on the large scale fading channel coefficients. The optimization algorithm aims to calculate the optimal transmit power, the number of scheduled users and number of BS antennas. Finally, numerical simulation results are provided to consolidate the theoretical analysis. In line with these, the main contributions of this work are summarized as follows [31, 32]:

- derive analytical closedform lower bound spectral efficiency in-terms of the large scale fading parameters;
- formulate and analyze joint energy efficiency resource allocation algorithms;

- validate the proposed joint resource allocation algorithm via numerical simulation.

6.2 Downlink Massive MIMO System and Channel Model

In this chapter, we consider a single cell downlink massive MIMO system shown in Figure 2.1 where the BS is equipped with M antennas to serve N single antenna user equipments in the same time frequency resource. A user set Ω that consists of $K = |\Omega| < N$ users is selected for simultaneous transmission at each coherence block composed of τ_c symbols [84]. If $\mathbf{x}$ denotes the complex valued $M \times 1$ simultaneously transmitted signal vector from the BS antennas, the $K \times 1$ received signal vector $\mathbf{y}$ at the user is given by [17]

$$\mathbf{y} = \mathbf{G}\mathbf{x} + \mathbf{n} \tag{6.1}$$

where $\mathbf{G}$ represents a $K \times M$ Rayleigh fading channel matrix between the BS and the K users with $\mathrm{g}_{mk} \triangleq [\mathbf{G}]_{mk}$ being the channel coefficient between the mth antenna of the BS and the kth user. $\mathbf{n}$ represents the model for additive white Gaussian noise vector with zero mean and unit variance elements at each user [3]. To facilitate our analysis, we first redefine the channel model in Chapter 2 for downlink massive MIMO systems.

6.2.1 Downlink Rayleigh Fading Channel Model

Considering all the propagation effects, the massive MIMO channel model in downlink communication is expressed as [3]

$$\mathbf{G} = \mathbf{D}^{\frac{1}{2}}\mathbf{H} \tag{6.2}$$

where the diagonal matrix $\mathbf{D} = \mathrm{diag}\{\beta_1, \beta_2, \cdots, \beta_K\} \in \mathbb{R}^{K \times K}$ represents the large scale fading effect that show pathloss and shadowing effects with elements $\beta_k = c\mathrm{d}_k^{-\alpha}$, d_k is the Euclidean distance between the BS antenna and the kth user, α is the pathloss exponent and c is the pathloss at a reference distance [2, 3]. The matrix $\mathbf{H} \in \mathbb{C}^{\mathrm{K} \times \mathrm{M}}$ represents the multipath fading effect which is assumed to be Rayleigh distributed in this section [2]. In practical systems, perfect knowledge of $\mathbf{H}$ is not possible; hence we consider the MMSE based channel estimation shown in Chapter 2 Section 2.3.2.

6.2.2 Precoding in Massive MIMO Systems

Precoding is a generalization of beamforming to support multi-stream transmission in massive MIMO systems. In conventional single-stream beamforming, the same signal is emitted from each transmit antennas with appropriate weighting (phase and gain) such that the signal power is maximized at the receiver output [3]. Both linear and non-linear precoding techniques are proposed for point to pint MIMO systems. Compared with linear precoding techniques, non-linear techniques such as dirty-paper-coding (DPC), vector perturbation (VP) and lattice-aided methods give better performance although they have high implementation complexity. However, when the number of antennas at the BS increases, linear precoders such as MRT, ZF and MMSE can achieve near optimal performance with low complexity. Thus, it is proposed to use linear precoding techniques in massive MIMO systems [3].

In [102], a survey of linear precoding techniques for downlink transmission for both single-cell and multicell scenarios is provided. Also, the effects of pilot contamination and BS coordination are reviewed and analyzed. In [103], the performance of linear precoding techniques is studied for measured massive MIMO downlink channels. It is shown that when the BS antennas increases, the system performance improves [103]. In [104], the author propose a novel hybrid beamforming techniques and examines the relation between hybrid and digital beamforming for downlink multiuser massive MIMO systems. The hybrid beamforming is designed by considering a weighted sum mean square error (WSMSE) minimization problem incorporating the solution of digital beamforming that is obtained from block diagonalization technique. To address the difficulty of limited number of RF chains, [105] considers a two-stage hybrid beamforming architecture in which the beamformer is constructed by integrating a low-dimensional digital beamformer and RF beamformer implemented using phase shifters.

In this chapter, we consider ZF precoding where the precoding matrix at BS is given by [3]

$$\mathbf{W} = \hat{\mathbf{G}}^{\mathrm{H}}(\hat{\mathbf{G}}\hat{\mathbf{G}}^{\mathrm{H}})^{-1} \tag{6.3}$$

where $\hat{\mathbf{G}}$ is the MMSE based estimate of the channel that is derived in Chapter 2 Section 2.3.2. Then, the $M \times 1$ precoded signal vector at the BS is given by [99]

$$\mathbf{x} = \mathbf{W}\mathbf{p}^{\frac{1}{2}}\mathbf{s} \tag{6.4}$$

where $\mathbf{p} = \mathrm{diag}\{p_1, p_2, \cdots, p_K\}$ is the power allocation matrix, $\mathbf{s} = [s_1, s_2, \cdots, s_K]^T \in$

$\mathbb{C}^{K\times 1}$ is information signal vector of the users with power constraint $\mathbb{E}\{\mathbf{s}\mathbf{s}^H\} = \mathbf{I}_K$. The total transmit power constraint at the BS is given by [99]

$$P_t \triangleq \mathbb{E}\{\mathrm{tr}(\mathbf{x}\mathbf{x}^{\mathrm{H}})\} \leq P_{\max} \tag{6.5}$$

where $P_{\max}$ is the maximum allowable transmit power at the BS [99].

6.3 Downlink Spectral Efficiency Formulation

By using the channel estimation matrix and the precoded vector in (6.4), the received signal in (6.1) is reformulated as [99]

$$\mathbf{y} = (\hat{\mathbf{G}} + \tilde{\mathbf{G}})\mathbf{x} + \mathbf{n} = \mathbf{p}^{\frac{1}{2}}\mathbf{s} + \tilde{\mathbf{G}}\hat{\mathbf{G}}^{\dagger}\mathbf{p}^{\frac{1}{2}}\mathbf{s} + \mathbf{n}. \tag{6.6}$$

Then, the received signal of the kth user is expressed as [99]

$$y_{_k} = \sqrt{p_{_k}}s_k + \tilde{\mathbf{g}}_k\mathbf{x} + n_k. \tag{6.7}$$

And the signal-to-interference plus noise ratio (SINR) at the kth user is given by [99]

$$\gamma_{_k} = \frac{p_{_k}}{\tilde{\mathbf{g}}_k\mathbf{x}\mathbf{x}^H\tilde{\mathbf{g}}_k^H + \sigma^2} \tag{6.8}$$

where $\tilde{\mathbf{g}}_k$ is the kth row of the channel estimation error matrix, $\tilde{\mathbf{G}}$. Then, the downlink sum spectral efficiency of the system is given by [2]

$$R_s = B\Big(1 - \frac{\tau_p}{\tau_c}\Big)\sum_{k=1}^{K}\log_2(1+\gamma_{_k}) \tag{6.9}$$

where B is the transmission bandwidth and τ_p is the pilot symbol length for channel estimation and τ_c is the coherence interval of the system.

6.3.1 Closedform Lower-bound Achievable Rate

Assuming that both $(M, K) \to \infty$ with a finite ratio $M/K \geq 1$, employing large system analysis techniques, the SINR of the user is formulated in terms of the large scale fading parameters [99]. Based on the large scale fading approximation, the achievable sum rate in (6.9) is reformulated as

$$\tilde{R}_s(\mathbf{p}, M, \Omega) = B\left(1 - \frac{\tau_p}{\tau_c}\right)\sum_{k=1}^{K}\log_2(1+\tilde{\gamma}_k) \tag{6.10}$$

where

$$\tilde{\gamma}_k = \frac{p_k}{P_t d_{2k}^2 + \sigma^2} \tag{6.11}$$

and when the large scale fading approximation of the channel estimate and channel estimation error are derived in (2.39) as

$$\begin{aligned} d_{1k} &= \sqrt{\frac{\tau_p \rho_p}{1 + \tau_p \rho_p \beta_k}} \beta_k \\ d_{2k} &= \sqrt{\frac{\beta_k}{1 + \tau_p \rho_p \beta_k}} \end{aligned} \tag{6.12}$$

where τ_p is pilot symbol length, ρ_p is the normalized transmit signal-to-noise ratio of the pilot symbol [2, 3].

6.3.2 Total Power Consumption Formulation

By using the large scale fading approximation, the total power consumption of the system in (5.8) can be reformulated as

$$\tilde{P}_{\text{tot}}(\mathbf{p}, M, \Omega) = \left(1 - \frac{\tau_p}{\tau_c}\right) \frac{P_t}{\eta_{\text{BS}}} + \frac{\tau_p}{\tau_c} \frac{P_p}{\eta_{\text{U}}} + P_{\text{cp}} \tag{6.13}$$

when P_t is the power required for data transmission and is expressed as

$$P_t = \sum_{k=1}^{K} p_k \frac{d_{1k}^{-2}}{M - K} \leq P_{\max} \tag{6.14}$$

where $K = |\Omega|$ and η_{BS}, η_{U} is the power amplifier efficiency at the BS and user, respectively. pP_p is transmit power of the pilot signal.

6.4 Joint Energy Efficient Resource Allocation in Massive MIMO Systems

Based on the spectral efficiency and total power consumption, the energy efficiency of the system is given by

$$\text{GEE}(\mathbf{p}, M, \Omega) = \frac{R_s(\mathbf{p}, M, \Omega)}{P_{\text{tot}}(\mathbf{p}, M, \Omega)}. \tag{6.15}$$

Then, joint energy efficient power allocation, antenna selection and user scheduling optimization problem is formulated as

$$\begin{aligned}
&\max_{\mathbf{p},\, M,\, \Omega} \text{GEE}\,(\mathbf{p}, M, \Omega) = \frac{R_s(\mathbf{p}, M, \Omega)}{P_{\text{tot}}(\mathbf{p}, M, \Omega)} \\
&\quad \text{subject to:} \\
&\qquad P_t \leq P_{\max} \\
&\qquad \Omega \in \mathcal{U} \\
&\qquad M \in \{1, 2, \cdots, M_{\max}\} \\
&\qquad 0 \leq p_k \leq P_{\max} \qquad k = 1, 2, \cdots, |\Omega| \\
&\qquad \gamma_k \geq \gamma_0 \qquad k = 1, 2, \cdots, |\Omega|
\end{aligned} \tag{6.16}$$

where $R_s(\mathbf{p}, M, \Omega)$ represents downlink achievable sum rate as a function of the transmit power allocation, BS antennas and number of users. $P_{\text{tot}}(\mathbf{p}, M, \Omega)$ denotes the total power consumption of the system. $\mathcal{U}$ denotes scheduled user sets and γ_k represents the quality-of-service (QoS) constraints which imply that the SINR of each active user is lower bounded by a minimum rate constraint, γ_0. The energy efficiency optimization problem in (6.16) is non convex and difficult to solve analytically [2, 3, 21, 22, 90, 106, 107]. Thus, to formulate analytical expression for the energy efficiency, we propose a suboptimal and low-complex power allocation, antenna selection and user scheduling algorithm based on the large scale fading approximations in (6.10) and (6.13). For this, we decompose the optimization problem into two parts such as allocation of the transmit power; and optimal selection of active users and number of BS antennas.

Based on the large scale fading approximation in (6.10) and (6.13), the energy efficiency maximization problem in (6.16) is reformulated as

$$\begin{aligned}
&\max_{\mathbf{p},\, M,\, \Omega} \text{GEE}\,(\mathbf{p}, M, \Omega) = \frac{\tilde{R}_s(\mathbf{p}, M, \Omega)}{\tilde{P}_{\text{tot}}(\mathbf{p}, M, \Omega)} \\
&\quad \text{subject to:} \\
&\qquad P_t = \sum_{k=1}^{K} p_k \frac{d_{1k}^{-2}}{M - K} \leq P_{\max} \\
&\qquad \Omega \in \mathcal{U} \\
&\qquad M \in \{1, 2, \cdots, M_{\max}\} \\
&\qquad 0 \leq p_k \leq P_{\max} \\
&\qquad \gamma_k \geq \gamma_0 \qquad \forall k.
\end{aligned} \tag{6.17}$$

It is shown that (6.10) and (6.13) depends only on large scale fading CSI of the users and system parameters. Hence, we can calculate the system energy efficiency without small scale fading CSI. But, due to non-concave objective function and mixed integer nature of joint optimization variables, (6.17) is intractable to solve optimally. Hence, we employ convex transformation technique to develop suboptimal low-complexity resource allocation algorithm to find near-optimal solution [99]. This method transforms the optimization problem into two sub-problems and solve them sequentially. First, we find the optimal value of (M, Ω) under the assumption of equal power allocation. Then, we perform power allocation algorithm to get the optimal power. Detail steps for optimal power allocation, BS antenna selection and user scheduling are shown in the subsequent sections.

6.4.1 Equal Power Allocation Algorithm

First, assuming the number of users and BS antennas are fixed, we perform equal power allocation to get the power allocation coefficients that is used in the next iterative steps of the optimization framework. If we apply equal power allocation condition in (6.14), the power allocation coefficient is given by

$$p_k = \frac{(M-K)P_t}{\sum_{k=1}^{K} d_{1k}^{-2}}. \tag{6.18}$$

Substituting (6.18) into (6.11), the SINR of user k under equal power allocation is become

$$\gamma_k^{\text{ep}} = \frac{P_t(M-K)}{P_t d_{2k}^2 \sum_{k=1}^{K} d_{1k}^{-2} + \sigma^2 \sum_{k=1}^{K} d_{1k}^{-2}}. \tag{6.19}$$

Then, the achievable sum rate in (6.10) is reformulated as

$$R_s^{\text{ep}}(P_t, M, \Omega) = B\left(1 - \frac{\tau_p}{\tau_c}\right) \sum_{k=1}^{K} \log_2(1 + \gamma_k^{\text{ep}}) \tag{6.20}$$

and the corresponding energy efficiency is formulated as

$$\text{GEE}^{\text{ep}}(P_t, M, \Omega) = \frac{R_s^{\text{ep}}(P_t, M, \Omega)}{P_a(P_t, M, \Omega)}. \tag{6.21}$$

Then, with fixed M and Ω, the resource allocation problem in (6.17) under equal power allocation is given by

$$\begin{aligned} &\max_{P_t} \ \mathrm{GEE}^{\mathrm{ep}}(P_t) \\ &\quad \text{subject to:} \\ &\quad\quad 0 \leq P_t \leq P_{\max} \\ &\quad\quad \gamma_k^{\mathrm{ep}} \geq \gamma_0 \qquad \forall k. \end{aligned} \tag{6.22}$$

To solve this optimization problem in (6.22), we first find the feasible region of P_t and then find the global extrema. It requires to optimize the total transmit power with respect to equal power allocation. But, to guarantee the SINR constraint the optimization problem is only feasible for some values of P_t. As shown in (6.19), γ_k^{ep} is a monotonically increasing function of P_t. Therefore, the constraint $\gamma_k^{\mathrm{ep}} \geq \gamma_0$ can be interpreted by $P_t \geq P_{t,k}$ for all k. Thus, the lower bound of P_t become $P_t \geq P_{t,\max}$ in which $P_{t,\max} = \max\{P_{t,1}, P_{t,2}, \ldots, P_{t,K}\}$. Hence, the feasible region of P_t for (6.22) is in between $[P_{t,\max}, P_{\max}]$. When it is feasible to solve (6.22), we can find the global maximum of $\mathrm{GEE}^{\mathrm{ep}}(P_t)$. The function $\mathrm{GEE}^{\mathrm{ep}}(P_t)$ and its first order derivative are always continuous with respect to P_t, hence we apply the extreme value theorem to solve (6.22).

6.4.2 Optimal BS Antenna Selection Algorithm

After equal power allocation, we apply antennas selection algorithm. With fixed $\mathbf{p}$ and Ω, the energy efficiency optimization problem in (6.17) is given by

$$\begin{aligned} &\max_{M} \ \mathrm{GEE}(M) \\ &\quad \text{subject to:} \\ &\quad\quad M \in \{1, 2, \cdots, M_{\max}\} \\ &\quad\quad \gamma_k \geq \gamma_0 \qquad \forall k. \end{aligned} \tag{6.23}$$

The feasible region of (6.23) is $\{1, 2, \cdots, M_{\max}\}$ which is discrete and finite. We use bisection method to solve (6.23).

6.4.3 User Scheduling Algorithm

The optimization problem in (6.17) can be solved by performing optimization of the transmit power and number of BS antennas over all possible sets of candidate users and choosing the best set of users through exhaustive searching. However, the total number of possible

user sets may be very large and which results in implementation complexity [108]. Therefore, to reduce the optimization complexity, we sort the candidate users in a descending order with respect to the location d_k and denote the first k user of the sorted set of candidate user as Ω_k. Then, by iteratively selecting user sets one by one, we can get the best user sets that give maximum energy efficiency in the system. The procedure ends when energy efficiency at Ω_k starts to decrease. The last user set is considered as the optimum user allocation. This approach reduces the maximal search space to K. The user scheduling problem is summarized in Algorithm 5.

Algorithm 5 Antenna selection and user scheduling algorithm.

1. Select the users in a descending order with respect to its location, d_k.

   (a) Denote the first n users as Ω_n

   (b) Set $k = 0$, $\text{GEE}^{\text{ep}}(\Omega_0) = 0$

2. For $k < \min\{M, N\}$

   (a) Set $k = k + 1$

   (b) Repeat

      (i) Optimize P_t under fixed M by using (6.25).

      (ii) Optimize M under fixed P_t by using (6.23).

   (c) Calculate $\text{EE}(\Omega_k)$ with (6.15).
   If $(\text{GEE}(\Omega_k) < \text{EE}(\Omega_{k-1}))$
   go to step 3;
   else go to step 2;

3. **Output**: (M^*, Ω^*)

6.4.4 Optimal Power Allocation

After the optimization of users and number of BS antennas, optimal power allocation is performed to get the optimal power. Under fixed M and Ω, the power allocation problem is given by

$$\max_{\mathbf{p}} \text{GEE}(\mathbf{p})$$

$$\text{subject to:}$$

$$P_t = \sum_{k=1}^{K} p_k \frac{d_{1k}^{-2}}{M-K} \leq P_{\max} \tag{6.24}$$

$$0 \leq p_k \leq P_{\max}, \qquad \forall k$$

$$\gamma_k \geq \gamma_0, \qquad \forall k.$$

The optimization problem in (6.24) is a non-linear fractional programming program. It can be solved by using the Dinkelbach methods shown in Section 5.2.1 [92]. At each iteration, we need to solve the optimization problem with given optimization parameter λ as

$$\max_{\mathbf{p}} \tilde{R}_s(\mathbf{p}) - \lambda \tilde{P}_{\text{tot}}(\mathbf{p})$$

$$\text{subject to :}$$

$$\sum_{k=1}^{K} p_k \frac{d_{1k}^{2}}{M-K} \leq P_{\max} \tag{6.25}$$

$$0 \leq p_k \leq P_{\max}, , \forall k$$

$$\gamma_k \geq \gamma_0 \qquad \forall k.$$

Algorithm 6 Optimal power allocation algorithm for (6.25)

Initialization:

1. Initialize maximum number of iterations N and maximum tolerance ϵ.
2. Set the energy efficiency $\lambda = 0$ and iteration index $n = 0$.

Iterative Operation:

1: **while** $(n < N)\, ||\tilde{R}_s(\mathbf{p}) - \lambda \tilde{P}_{\text{tot}}(\mathbf{p}) < \epsilon)$ **do**
2: Solve problem (6.25)
3: Update n and λ as:
4: $n = n + 1$
5: $\lambda = \frac{\tilde{R}_s(\mathbf{p})}{\tilde{P}_{\text{tot}}(\mathbf{p})}$
end
6: **Output**: $\mathbf{p}^*$

It is noteworthy that $\tilde{R}_s$ is concave over $\mathbf{p}$, $\tilde{P}_{\text{tot}}$ is linear over $\mathbf{p}$ and all the constraints are linear. As a result, (6.25) is a convex optimization problem and it can be solved

efficiently by using fractional program theory. The detail of the optimization is summarized in Algorithm 6.

6.5 Joint Energy Efficient Resource Allocation Algorithm

Based on the proposed Algorithms 5 and 6, we perform joint energy efficient resource allocation algorithm, which optimizes the number of antennas, scheduled users and power allocation jointly. The complete optimization process is summarized in Algorithm 7.

Algorithm 7 Joint energy efficient resource allocation formulation.

Step1. Perform equal power allocation with given number of users and BS antennas.

Step 2. Optimize the number of BS antennas and users under equal power allocation to obtain (M^*, Ω^*).

Step 3. By using (M^*, Ω^*), perform the power allocation to get the optimal power, $\mathbf{p}^*$.

Step 4. Calculate the energy efficiency with the final resource allocation solution $(\mathbf{p}^*, M^*, \Omega^*)$.

6.6 Simulation Results and Analysis

We evaluate the performance and feasibility of the proposed joint energy efficient resource allocation algorithm. We used the system and propagation parameters proposed in [22] where part of these parameters are shown in Table 5.1. For the simulation, we assume a uniform user distribution in a circular cell with radius 500 m and minimum distance of 35 m. The BS is assumed to be located at the center of the cell. We deploy CVX with the MOSEK solver [94] to simulate the system.

Figure 6.1 shows the comparative energy efficiency results by using the large scale fading approximation in (6.17) with the sequential simulation results from (6.16). The figure shows that the results from large scale fading based approximation are nearly the same with the sequential simulation even at finite BS antennas. Thus, it is quite reasonable to design resource allocation scheme based on the large scale fading approximation. Besides, as stated before, the energy efficiency is not a monotonic function with the number of BS

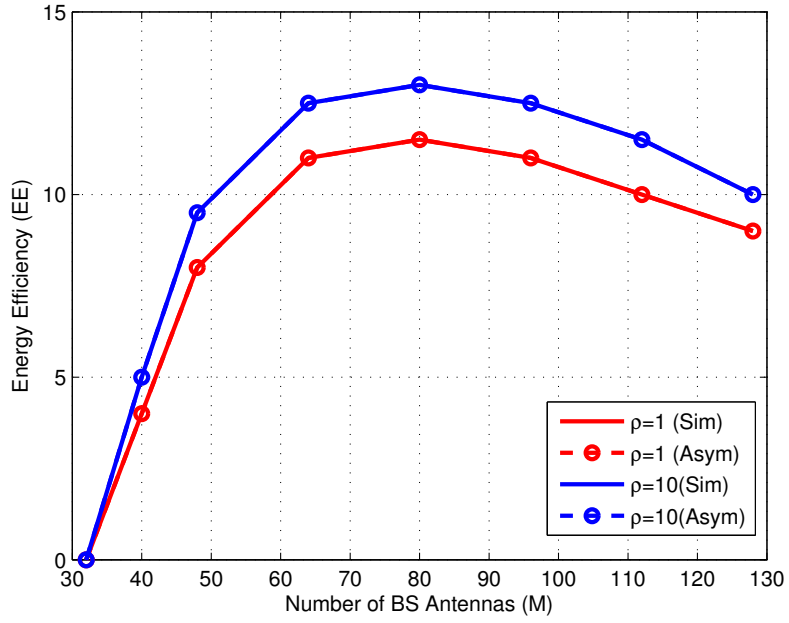

Figure 6.1: Energy efficiency with number of BS antennas. We assume $K = 16$ users and $P_t = 20\,\text{dBm}$. ρ is the SNR of the pilot signal.

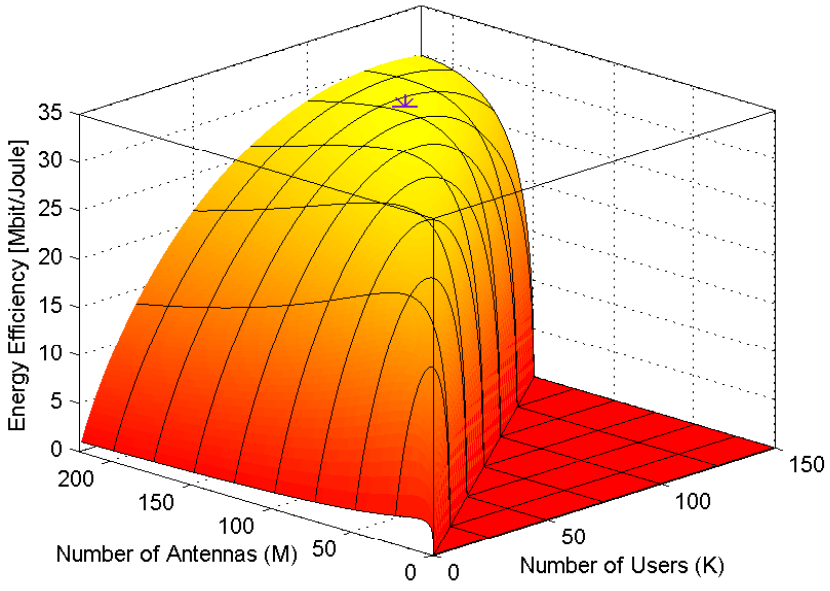

Figure 6.2: Global energy efficiency of massive MIMO system at different combinations of M and K. The global optimum is marked with a star.

antennas. Hence, it increases until some value of the BS antennas and decreases after that value. Furthermore, the result shows that energy efficiency increases with the SNR. This is because, when the SNR increases, channel estimation becomes more robust and that improves the energy efficiency of the system.

Figure 6.2 shows the sets of achievable energy efficiency at different combinations of (M, K) under the assumption of equal power allocation. Each point uses the P_t value in (6.14) to maximize the energy efficiency. The result shows that the surface is concave and smooth. The result indicates a sub-optimal point at $M = 175, K = 75$ which is obtained by iteratively calculate the power allocation and BS antenna selection. The result validates that the optimal energy efficiency calculated based on the large scale fading approximation can be converged to the global optimum.

Figure 6.3 shows the total power that maximizes the energy efficiency with different BS antennas. The result shows that the most energy efficient strategy is to increase the transmit power with the BS antennas. The result also shows that the transmit power per BS antenna decreases with the BS antennas. As shown from the result the required downlink transmit power at the optimal point $(M = 175, K = 75)$ is around 100 mW per antenna. This power is smaller than conventional macro-BS station that consumes around 40 W per antenna [54, 91]. This reveals that energy efficient optimal solution for massive MIMO systems can be deployed with low-power RF amplifiers.

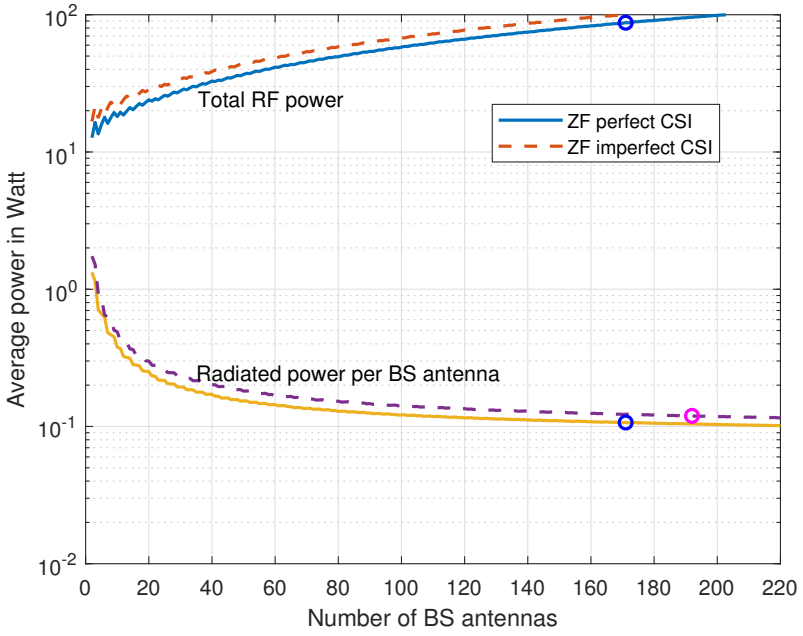

Figure 6.3: Power consumption with the number of BS antennas at maximum energy efficiency point.

Figure 6.4 shows the area throughput that maximizes the energy efficiency versus the number of BS antennas. The result shows that in addition to the energy efficiency there is an improvement in area throughput. Which shows that massive MIMO with proper

interference-suppressing precoding can achieve improvements on both energy efficiency and area throughput.

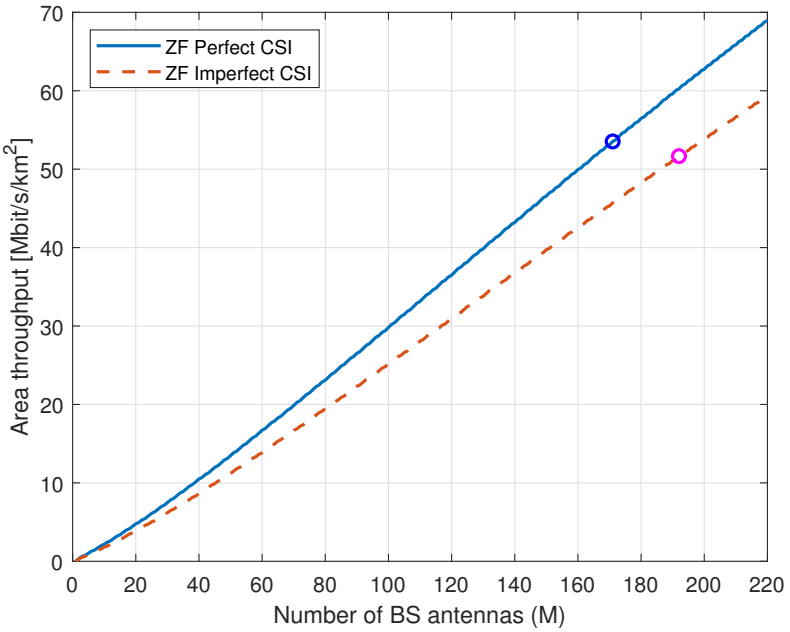

Figure 6.4: Area throughput with the number of BS antennas at maximum energy efficiency point.

6.7 Summary

In this chapter, we analyze joint energy efficient resource allocation techniques for massive MIMO systems. First, analytical closedform lower bound spectral efficiency and accurate system power consumption models are formulated. Besides, a large scale fading based joint energy efficiency resource allocation algorithm is analyzed. The analysis shows that the resource allocation algorithm is tight for massive MIMO systems even at finite BS antennas. The results show that the proposed algorithm converges the optimal value with finite iteration. From the theoretical and simulation results, we proved that large scale fading based energy efficiency optimization can achieve near-optimal performance with low computational complexity.

Chapter 7

Performance Analysis of Multicell Massive MIMO Systems

7.1 Introduction

As can be shown from the rapid generation of mobile communication systems, there is a growing quest to balance between handling the increasing mobile data traffic volume and developing innovative technologies to enhance operational capabilities and network capacity [15]. In this context, various innovative technologies have been proposed for the deployment of 5G networks such as massive MIMO systems, mmWave communication, non-orthogonal multiple access (NOMA) schemes and flexible network deployment along with dynamic nodes [15].

By adopting a very large number of antennas at the base station (BS), called massive MIMO [14, 23], 5G networks can greatly improve the spectral efficiency and energy efficiency [14]. Recent studies show that massive MIMO can increase the spectral efficiency tenfold and simultaneously improve energy efficiency by a factor of 100 as compared to current mobile networks [14]. Practical massive MIMO systems consist of many cells that operate in synchronous TDD protocol and each BS is equipped with $M \gg 1$ antennas to support K-users under the same time-frequency resources. Each BS operates individually and processes the signals using linear receive combining and linear transmit precoding. Thus, a highly spectral efficient massive MIMO systems employ space division multiple access (SDMA) to achieve multiplexing gains, deploy large number of BS antennas to suppress interuser interference (IUI) and to achieve channel hardening, operate in asynchronous time division duplex (TDD) mode to limit CSI acquisition, and use linear processing to reduce signal processing complexity [2, 3, 88].

In multicell massive MIMO systems, due to limitation of the channel coherence interval, we cannot assign orthogonal pilot sequences for users in all cells [3]. Hence, pilot sequences have to be reused from cell to cell. Thus, the channel estimate obtained in a given cell is contaminated by pilots transmitted from users in other cells. This effect is called pilot contamination. It reduces the system performance and is the major limitation of massive MIMO systems [3]. Several pilot contamination mitigation strategies have been made to mitigate the effect of pilot contamination. Eigenvalue-based channel estimation, pilot decontamination and pilot contamination based precoding and covariance aware pilot assignment techniques are proposed in [43, 109–111].

In [112], spectral efficiency maximization algorithms are proposed for multicell massive MIMO systems. Analytical spectral efficiency expression is formulated to evaluate the performance of the system with power control, pilot reuse and random user locations. In [113], energy-efficient resource allocation algorithm is proposed for downlink multicell large-scale distributed antenna systems. A non-convex optimization problem is formulated to maximize the energy efficiency of the system. By using Dinkelbach algorithm, the non-convex optimization problem is transformed into an equivalent convex optimization problem in subtractive form. Then, an iterative algorithm is implemented in which antenna selection, user scheduling and power allocation are implemented separately. To reduce the computational complexity, a norm-based joint antenna and user selection algorithm is proposed to select optimal number of antennas and users. Next, a Lagrangian dual decomposition algorithm is adopted to derive a power allocation that can run independently in each cell. In [114], joint pilot assignment and resource allocation is proposed for energy efficiency maximization in multiuser and multicell massive MIMO system. In [115], pilot allocation optimization problem is formulated to maximize uplink sum rate of the system. A low-complexity pilot allocation algorithm is proposed which decouple the problem into multiple subproblems. At each subproblem, the pilot allocation at a given cell is optimized while the pilot allocation in other cells is assumed fixed.

In this chapter, we analyze the performance of multicell massive MIMO systems in spatially correlated channel model. In this regard correlated based channel modeling, power allocation and resource allocation are analyzed in multicell massive MIMO systems. Besides, we evaluate the impacts of spatial correlation and pilot contamination. Important trade-offs and considerations on design and optimization of multicell massive MIMO systems has been studied. In line with these, the main contributions of this chapter are

summarized as follows:

- Formulate and analyze a correlated based channel model for multicell massive MIMO systems. Specifically, local scattering based spatial channel correlation model is considered.
- Analyze impacts of spatial channel correlation on channel estimation, channel hardening, favorable condition and spectral efficiency in massive MIMO systems.
- Analyze spectrally efficient power optimization algorithms for massive MIMO systems.

7.2 The System and Channel Model

7.2.1 The System Model

We consider a multicell massive MIMO system with L-cells where each cell consists of a BS that is equipped with M-antennas to support K-single antenna users under the same time-frequency resources. A sample cell layout and communication links for a three cell system is shown in Figure 7.1.

In the uplink multicell massive MIMO systems, the received signal at the jth BS is given by

$$\begin{aligned}\mathbf{y}_j &= \sum_{l=1}^{L}\sum_{k=1}^{K}\mathbf{g}_{lk}^{j}x_{lk} + \mathbf{n}_j \\ &= \sum_{k=1}^{K}\mathbf{g}_{jk}^{j}x_{jk} + \sum_{\substack{l=1\\l\neq j}}^{L}\sum_{i=1}^{K}\mathbf{g}_{li}^{j}x_{li} + \mathbf{n}_j\end{aligned} \tag{7.1}$$

where $\mathbf{y}_j \in \mathbb{C}^M$ is the received signal at the jth BS, x_{lk} is the uplink transmitted signal of user k in cell l with power $p_{lk} = \mathbb{E}\{|x_{lk}|^2\}$, $\mathbf{g}_{lk}^{j}$ is the channel between user k in cell l to the BS antennas in cell j and $\mathbf{n}_j \in \mathbb{C}^M$ is additive white Gaussian noise at the jth BS with zero mean and variance σ^2 [2, 3].

7.2.2 The Multicell Massive MIMO Channel Model

In multicell systems, as shown in Figure 7.1 the channel between user k in cell l and the BS in cell j is denoted by $\mathbf{g}_{lk}^{j} \in \mathbb{C}^M$ where each elements corresponds to the channel response from the user to one of the BS antennas. Practical channels are generally spatially

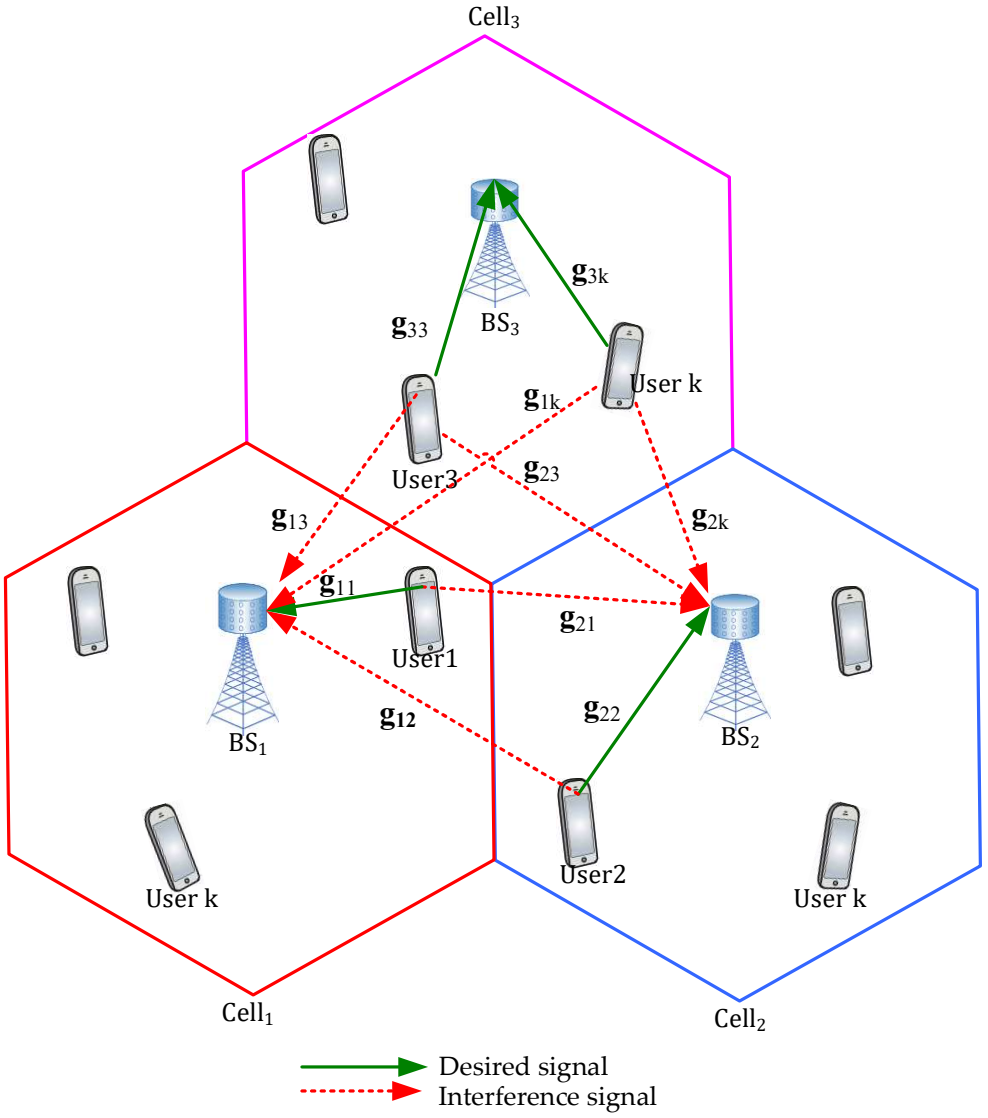

Figure 7.1: Multicell massive MIMO systems model.

correlated since the BS antennas have non-uniform radiation patterns and the physical propagation environment makes some spatial directions more probable to carry strong signals from the transmitter to the receiver than other directions [2, 17]. In this chapter, we assume a spatial correlated Rayleigh fading channel model. Considering pathloss, shadowing, multipath fading and spatial channel correlation, a correlated Rayleigh fading channel model of a user is formulated as

$$\mathbf{g}_{lk}^{j} \sim \mathcal{CN}(\mathbf{0}, \mathbf{R}_{lk}^{j}) \tag{7.2}$$

where $\mathbf{R}_{lk}^{j} \in \mathbb{C}^{M \times M}$ is positive semi-definite spatial channel correlation matrix which represents the model for the large scale fading. The Gaussian distribution is used to model the small-scale fading variations [3, 17].

The spatial channel correlation matrix describes the macroscopic propagation effects including the antenna gains and radiation patterns at the transmitter and receiver. Thus, the average channel gain from the jth BS antenna to user k in cell l is given by [3]

$$\beta_{lk}^{j} = \frac{1}{M}\mathrm{tr}(\mathbf{R}_{lk}^{j}) = \Upsilon - 10\alpha \log_{10}\left(\frac{d_{lk}^{j}}{1\,\mathrm{km}}\right) + \mathrm{F}_{lk}^{j} \tag{7.3}$$

where β_{lk}^{j} the large-scale fading coefficient. d_{lk}^{j} the distance between the transmitter and the receiver, α is the pathloss exponent, and Υ is the median channel gain at the reference distance. F_{lk}^{j} represents a log-normal shadowing with $10\log_{10}\mathrm{F}_{lk}^{j} \sim \mathcal{N}(0, \sigma_{\mathrm{sh}}^{2})$ where σ_{sh} is the standard deviation of the shadow fading model. The shadow fading adds random correction term to obtain a model that better fits with practical channel measurements [17].

In a nutshell, channel models are either deterministic or stochastic [116]. Deterministic channel models depend on a given environment with fixed locations of transmitters, receivers, scatterers and reflectors. These models include deterministic LOS channel model, ray tracing based on 3D-building models and recorded channel measurements [117]. Although, deterministic channel models can provide very accurate performance predictions for specific scenarios, they are only valid for a specific scenario and thus they do not allow for comprehensive conclusions. Besides, due to very few openly accessible databases of channel measurements and 3D-building models, the results cannot be easily reproducible [17, 116, 118, 119]. Stochastic channel models are used to generate a large number of channel realizations with desired statistical properties. These types of channel models are independent of a particular environment. These models include correlation-based, parametric-based and geometry-based channel models. Correlated based Rayleigh fading channel model is one of the correlation-based channel model. The channel responses are all Gaussian distributed with zero mean and entirely defined through the correlation matrices. Parametric channel models represent stochastic distributions of the number of multipath clusters and the delay profile, power, angle of arrival (AoA) and angle of departure (AoD) of the individual multipath components [17, 116, 118, 119]. Since parametric models are independent of the geometry of the propagation environment, they are not feasible for system-level simulations of the channel with time-evolution that is caused by movements of the transmitters and receivers. Stochastic geometry-based channel models represents a distribution of the physical location of scatterers around the transmitters and receivers. Once the locations of all scatterers are chosen, individual propagation paths are modeled in a quasi-deterministic manner. Such models are easy to simulate, agree very well with

measurements, and enable time-evolution [17, 116, 118, 119].

To simplify our analysis, we consider the local scattering based spatial channel correlation model which is described in the subsequent sections.

7.2.3 Local Scattering based Spatial Channel Correlation Model

The local scattering correlation model captures the basic characteristics of spatial channel correlation in terms of the nominal angle and angular standard deviation (ASD). The nominal angle and angular standard deviation of the multipath components are key parameters to model the spatial channel correlation matrix. The ASD shows the random deviation from the nominal angle with given standard deviation. Figure 7.2 shows the scenario of a massive MIMO system under NLOS propagation with the local scattering spatial correlation model where the scattering is localized around the user [2].

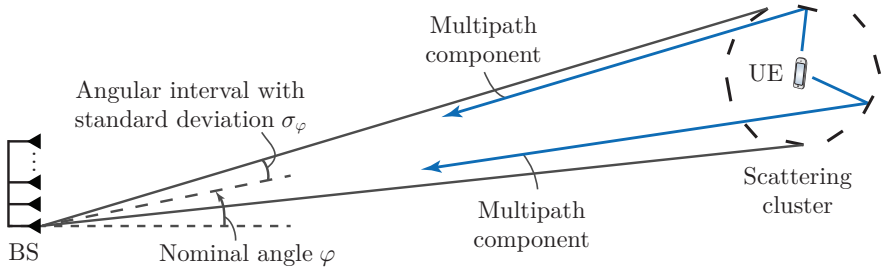

Figure 7.2: NLOS propagation model under local scattering spatial correlation model [2].

This approach helps to develop a model for the spatial correlation matrix for NLOS propagation between the user and the BS equipped with uniform linear array (ULA) antennas. The received signal at the BS is the superposition of N-multipath components. Suppose the scattering is localized around the user and if there is no scatterers in near-field of the BS, each of the multipath components results in a plane wave that reaches the array from a particular angle and gives an array response of [3]

$$\mathbf{a}_n = g_n \left[1,\, e^{j2\pi d \sin(\phi_n)}, \cdots, e^{j2\pi d(M-1)\sin(\phi_n)}\right]^{\mathrm{T}} \tag{7.4}$$

where $\mathbf{a}_n \in \mathbb{C}^M$, $g_n \in \mathbb{C}$ accounts for the gain and phase rotation for this path, ϕ_n is the arrival angle and d is the spacing between the BS antennas. Then, the channel response at the BS is given by the superposition of multipath components as [2]

$$\mathbf{G} = \sum_{n=1}^{N} \mathbf{a}_n \tag{7.5}$$

when the arrival angels ϕ_n are iid random variable with angular probability density function of $f(\phi_n)$ and g_n are iid random variables with zero mean and variance of $\mathbb{E}\{|g_n|^2\}$. The variance represents the average channel gain of the nth path and the total average gain of the multipath components is denoted by $\beta = \sum_{n=1}^{N} \mathbb{E}\{|g_n|^2\}$. When $N \to \infty$, by using the central limit theorem, the channel response converges to [3]

$$\mathbf{G} \to \mathcal{CN}(0, \mathbf{R}) \tag{7.6}$$

where the convergence is in distribution. Besides, the spatial channel correlation is formulated as $\mathbf{R} = \mathbb{E}\{\sum_n \mathbf{a}_n \mathbf{a}_n^{\mathrm{H}}\}$. By using (7.4), the (l, m)th element of the spatial channel correlation can be expressed as [2]

$$\mathbf{R}_{lm} = \beta \int e^{j2\pi d(l-m)\sin(\phi)} f(\phi) d\phi. \tag{7.7}$$

As shown in (7.7), $\mathbf{R}_{lm}$ depends on the difference $l - m$, hence $\mathbf{R}$ is Toeplitz matrix. Assuming that all the multipath components originate from a scattering cluster localized around the user, at the BS antennas $\phi = \varphi + \delta$ where φ is the deterministic nominal angle and δ is the random deviation from the nominal angle with angular standard deviation σ_φ. The ASD is measured in radians and is termed as the angular standard deviation, since it determines how large the deviation from the nominal angle. The random deviation can be modeled as Gaussian distributed, Laplace distributed and Uniformly distributed deviations [2, 3].

In this work, we consider the Gaussian angular standard distribution model. In Gaussian angular distribution with small ASD values, an approximate closedform expression of the spatial channel correlation matrix can be expressed as [2]

$$\mathbf{R}_{lm} = \beta e^{j2\pi d\,(l-m)\sin(\varphi)} e^{-\frac{\sigma_\varphi^2}{2}(2\pi d(l-m)\cos(\varphi))^2}. \tag{7.8}$$

This approximation helps to reduce the computational complexity. It also provides some insights on the structure of the correlation matrix. When $\sigma_\varphi = 0$, $\mathbf{R}_{lm} = \beta e^{j2\pi d\,(l-m)\sin(\varphi)}$ and all multipath components arrive from angle φ and gives rank-one correlation matrix. Whereas, for $\sigma_\varphi > 0$, the diagonal elements are the same, but off-diagonal elements decrease with $e^{-\frac{\sigma_\varphi^2}{2}(2\pi d(l-m)\cos(\varphi))^2}$ and goes to zero as σ_φ grows to large [3, 17].

7.3 Pilot based Channel Estimation in Multicell Massive MIMO Systems

7.3.1 Uplink Pilot Transmission

In pilot based channel estimation, each user transmits a pilot sequence that spans τ_p samples. In multicell systems, the pilot sequence of user k in cell j is denoted by $\phi_{jk} \in \mathbb{C}^{\tau_p}$ where $||\phi_{jk}||^2 = \tau_p$. ϕ_{jk} are scaled by uplink transmit power $\sqrt{p_{jk}}$ and transmitted over τ_p samples. Thus, the received signal at the jth BS is given by [3]

$$\mathbf{Y}_j = \sum_{k=1}^{K} \sqrt{p_{jk}} \mathbf{G}_{jk}^{j} \phi_{jk}^{\mathrm{T}} + \sum_{l=1, l\neq j}^{L} \sum_{i=1}^{K} \sqrt{p_{li}} \mathbf{G}_{li}^{j} \phi_{li}^{\mathrm{T}} + \mathrm{N}_j \tag{7.9}$$

where $\mathbf{Y}_j \in \mathbb{C}^{M \times \tau_p}$, $\mathrm{N}_j \in \mathbb{C}^{M \times \tau_p}$ is the noise at the jth BS with iid $\mathcal{CN}(0, \sigma^2)$ elements. To estimate the channel of a particular user, the BS needs to know the transmit pilot sequence of the user. Hence, the pilots should be deterministic sequences and pilot assignment is made when the user connects to the BS. If the jth BS wants to estimate the channel $\mathbf{G}_{li}^{j}$ from arbitrary user i in cell l, the BS correlates $\mathbf{Y}_j$ with the pilot sequence ϕ_{li} of the user to get the processed pilot signal as

$$\mathbf{y}_{jli}^{p} = \mathbf{Y}_j \phi_{li}^{\star} = \sum_{l=1}^{L} \sum_{i=1}^{K} \sqrt{p_{li}} \mathbf{G}_{li}^{j} \phi_{li}^{\mathrm{T}} \phi_{li}^{\star} + \mathrm{N}_j \phi_{li}^{\star} \tag{7.10}$$

where $\mathbf{y}_{jli}^{p} \in \mathbf{C}^{M}$ and which has the same dimension as $\mathbf{G}_{li}^{j}$. For the kth user in the BS own cell, equation (7.10) can be expressed as

$$\mathbf{y}_{jjk}^{p} = \sqrt{p_{jk}} \mathbf{G}_{jk}^{j} \boldsymbol{\phi}_{jk}^{\mathrm{T}} \boldsymbol{\phi}_{jk}^{\star} + \sum_{\substack{i=1 \\ i\neq k}}^{K} \sqrt{p_{ji}} \mathbf{G}_{ji}^{j} \boldsymbol{\phi}_{ji}^{\mathrm{T}} \boldsymbol{\phi}_{jk}^{\star} + \sum_{l=1, l\neq j}^{L} \sum_{i=1}^{K} \sqrt{p_{li}} \mathbf{G}_{li}^{j} \boldsymbol{\phi}_{li}^{\mathrm{T}} \boldsymbol{\phi}_{jk}^{\star} + \mathrm{N}_j \phi_{jk}^{\star}. \tag{7.11}$$

The second and third terms in (7.11) represent interuser interference, $\phi_{li}^{T} \phi_{jk}^{*}$ is the inner product between the pilot of the desired user and the pilot of other user i in cell l. If the pilot sequences of two users are orthogonal, then $\phi_{li}^{T} \phi_{jk}^{*} = 0$ and interuser interference term in (7.11) vanishes and does not affect the channel estimation quality. Since the pilots are τ_p-dimensional vectors, we can only find a set of at most τ_p-mutually orthogonal sequences. The finite length of the coherence block imposes the constraint $\tau_p \leq \tau_c$ (where τ_c is the coherence interval of the system) that makes impossible to assign mutually orthogonal pilots to all users in practice.

We consider a set of τ_p-mutually orthogonal pilot sequences that is extracted from the columns of uplink pilot book $\mathbf{\Phi} \in \mathbb{C}^{\tau_p \times \tau_p}$ which satisfy $\mathbf{\Phi}^{\mathrm{H}}\mathbf{\Phi} = \tau_p \mathbf{I}$. Since, the strongest interference usually originates from the own cell, it is recommended to have $\tau_p \geq K$ pilots so that each BS can allocate different uplink pilot sequences among the users. For pilot assignment, let us define the set [120]

$$\mathcal{P}_{jk} = \{(l,i) : \phi_{li} = \phi_{jk}, \quad l = 1, 2, \cdots, L, \ i = 1, 2, \cdots, K\} \tag{7.12}$$

with the indices of all users that utilize the same pilot sequence as user k in cell j. Hence, $(l,i) \in \mathcal{P}_{jk}$ implies that user i in cell l uses the same pilot as user k in cell j. By using the notation in (7.12), the expression in (7.10) is reformulated as [3, 120]

$$\mathbf{y}_{jjk} = \sqrt{p_{jk}}\tau_p \mathbf{G}_{jk}^{j} + \sum_{(l,i)\in\mathcal{P}_{jk}\setminus(j,k)} \sqrt{p_{li}}\tau_p \mathbf{G}_{li}^{j} + \mathrm{N}_j \phi_{jk}^{\star} \tag{7.13}$$

where the first term is the desired pilot signal, the second term is the interfering pilot signal and the third term is the nose. The processed received signal in (7.13) is a sufficient statistics to estimate $\mathbf{G}_{jk}^{j}$ since there is no loss in useful information as compared to $\mathbf{Y}_j$.

7.3.2 MMSE based Channel Estimation

Assuming that $\mathbf{G}_{li}^{j} \sim \mathcal{CN}(0, \mathbf{R}_{li}^{j})$ and by using a pilot book with mutually orthogonal sequences, the MMSE estimate of the channel $\mathbf{G}_{li}^{j}$ based on the received pilot signal $\mathbf{Y}_j$ is given by

$$\hat{\mathbf{G}}_{li}^{j} = \mathbb{E}\{\mathbf{G}_{li}^{j} | \mathbf{Y}_j\} = \sqrt{p_{li}}\mathbf{R}_{li}^{j}\mathbf{\Psi}_{li}^{j}\mathbf{y}_{jli}^{p} \tag{7.14}$$

where $\mathbf{\Psi}_{li}^{j}$ is the inverse of the normalized correlation matrix given by $\mathbb{E}\{\mathbf{y}_{jli}^{p}(\mathbf{y}_{jli}^{p})^{\mathrm{H}}\}/\tau_p$ and $\mathbf{R}_{li}^{j}$ is the spatial channel correlation matrix. After some calculations and simplifications, the normalized correlation matrix is expressed as [3]

$$\mathbf{\Psi}_{li}^{j} = \left(\sum_{(l,i)\in\mathcal{P}_{li}} p_{li}\tau_p \mathbf{R}_{li}^{j} + \sigma^2 \mathbf{I}_M \right)^{-1}. \tag{7.15}$$

Equation (7.14) shows that to estimate $\mathbf{G}_{li}^{j}$, the BS should correlate the received pilot signal with the pilot sequence used by user i in cell l as $\mathbf{y}_{jli} = \mathbf{Y}_j \phi_{li}^{\star}$ and then multiply the result with $\mathbf{\Psi}_{li}^{j}$ and $\mathbf{R}_{li}^{j}$. These multiplications suppresses interference and noise that do not use the same second-order statistics with $\mathbf{G}_{li}^{j}$.

The error due to channel estimation is expressed as $\tilde{\mathbf{G}}_{li}^{j} = \mathbf{G}_{li}^{j} - \hat{\mathbf{G}}_{li}^{j}$ and its covariance matrix is given by [17]

$$\mathbf{C}_{li}^{j} = \mathbb{E}\{\tilde{\mathbf{G}}_{li}^{j}(\tilde{\mathbf{G}}_{li}^{j})^{\mathrm{H}}\} = \mathbf{R}_{li}^{j} - p_{li}\tau_{p}\mathbf{R}_{li}^{j}\mathbf{\Psi}_{li}^{j}\mathbf{R}_{li}^{j}. \tag{7.16}$$

The channel estimation accuracy can be calculated by using the mean square error (MSE) as $\mathbb{E}\{||\mathbf{G}_{li}^{j} - \hat{\mathbf{G}}_{li}^{j}||^{2}\} = \mathrm{tr}(\mathbf{C}_{li}^{j})$. A good estimation accuracy is represented by small MSE. Similar to the single cell scenario in [21], the estimate $\hat{\mathbf{G}}_{li}^{j}$ and the estimation error $\tilde{\mathbf{G}}_{li}^{j}$ are independent random variables and modeled in Gaussian distribution as [3]

$$\begin{aligned} \hat{\mathbf{G}}_{li}^{j} &\sim \mathcal{CN}\left(\mathbf{0}, \mathbf{R}_{li}^{j} - \mathbf{C}_{li}^{j}\right) \\ \tilde{\mathbf{G}}_{li}^{j} &\sim \mathcal{CN}\left(\mathbf{0}, \mathbf{C}_{li}^{j}\right). \end{aligned} \tag{7.17}$$

To compare the estimation quality of the channel estimation, we use the normalized mean square error (NMSE) which is given by [2]

$$\mathrm{NMSE}_{li}^{j} = \frac{\mathrm{tr}(\mathbf{C}_{li}^{j})}{\mathrm{tr}(\mathbf{R}_{li}^{j})}. \tag{7.18}$$

7.4 Spectral Efficiency in Multicell Massive MIMO Systems

Based on Equation (7.1), let us consider user k in cell j transmits a random data signal $x_{jk} \sim \mathcal{CN}(0, p_{jk})$ where the variance p_{jk} is the transmit power of the users. Each BS detects the desired signal by using linear receive combining. For this, the receiving BS selects the combining vector $\mathbf{v}_{jk} \in \mathbb{C}^{M}$ for the kth user as a function of the estimated channel matrix. Hence, BS_j correlates the received signal $\mathbf{y}_j$ with the combining vector to obtain [2]

$$\mathbf{v}_{jk}^{\mathrm{H}}\mathbf{y}_{j} = \mathbf{v}_{jk}^{\mathrm{H}}\hat{\mathbf{G}}_{jk}^{j}x_{jk} + \mathbf{v}_{jk}^{\mathrm{H}}\tilde{\mathbf{G}}_{jk}^{j}x_{jk} + \sum_{\substack{i=1 \\ i\neq k}}^{K}\mathbf{v}_{jk}^{\mathrm{H}}\mathbf{G}_{ji}^{j}x_{ji} + \sum_{\substack{l=1 \\ l\neq j}}^{L}\sum_{i=1}^{K}\mathbf{v}_{jk}^{\mathrm{H}}\mathbf{G}_{li}^{j}x_{li} + \mathbf{v}_{jk}^{\mathrm{H}}\mathbf{n}_{j}. \tag{7.19}$$

Thus, the signal to interference plus noise ratio (SINR) is given by

$$\mathrm{SINR}_{jk} = \frac{p_{jk}\left|\mathbf{v}_{jk}^{\mathrm{H}}\hat{\mathbf{G}}_{jk}^{j}\right|^{2}}{\sum_{l=1}^{L}\sum_{i=1}^{K_l}p_{li}\left|\mathbf{v}_{jk}^{\mathrm{H}}\hat{\mathbf{G}}_{li}^{j}\right|^{2} + \mathbf{v}_{jk}^{\mathrm{H}}\left(\sum_{l=1}^{L}\sum_{i=1}^{K_l}p_{li}\mathbf{C}_{li}^{j} + \sigma^{2}\mathbf{I}_{M_j}\right)\mathbf{v}_{jk}}. \tag{7.20}$$

and uplink achievable rate of user k in cell j is given by

$$\mathrm{SE}_{jk} = \frac{\tau_d}{\tau_c}\mathbb{E}\left\{\log_2\left(1 + \mathrm{SINR}_{jk}\right)\right\}. \tag{7.21}$$

The spectral efficiency expression in (7.21) applies for any choice of the receive combining vector. Similar to single cell scenarios, we consider equivalent multicell linear detection and precoding techniques such as MRC, ZF and MMSE to analyze the performance of multicell massive MIMO systems. Under imperfect CSI, the mathematical expression for these combining techniques are given by

$$\mathbf{v}_j = \begin{cases} \hat{\mathbf{G}}_j^j & \text{MRC} \\ \hat{\mathbf{G}}_j^j \left(\left(\hat{\mathbf{G}}_j^j \right)^{\mathrm{H}} \hat{\mathbf{G}}_j^j \right)^{-1} & \text{ZF} \\ \hat{\mathbf{G}}_j^j \left(\left(\hat{\mathbf{G}}_j^j \right)^{\mathrm{H}} \hat{\mathbf{G}}_j^j + \sigma^2 \mathbf{P}_j^{-1} \right)^{-1} & \text{MMSE} \end{cases} \tag{7.22}$$

where $\mathbf{v}_j$ is the linear processing matrix and $\mathbf{P}_j$ the power allocation matrix at BS_j, respectively.

7.5 Spectrally Efficient Power Optimization in Multicell Massive MIMO Systems

Equal transmit power allocation is generally not the optimal strategy if we want to maximize the spectral efficiency of the system. Firstly, by exploiting the different propagation conditions of the users, the sum spectral efficiency can be increased by unequal power allocation [88]. Besides, the sum spectral efficiency only measures the aggregated throughput of the network, while ignoring how fairly it is distributed among the users. This can lead to substantial unfairness. In addition to the sum spectral efficiency, there are other utility functions that balance between aggregate throughput and fairness such as max-min fairness and maximum product spectral efficiency [51, 84, 88]. In this section, we formulate these utility functions and provide power allocation schemes that maximize the spectral efficiency of the system.

For analysis purpose, we consider a downlink communication of the proposed multicell massive MIMO system with linear precoding and imperfect CSI. Based on (7.20), the equivalent downlink spectral efficiency of user k in cell j is formulated as

$$\mathrm{SE}_{jk} = \frac{\tau_d}{\tau_c} \log_2 \left(1 + \frac{\rho_{jk} a_{jk}}{\sum_{l=1}^{L} \sum_{i=1}^{K} \rho_{li} b_{lijk} + \sigma^2} \right) \tag{7.23}$$

where τ_d is the data symbol length, τ_c is the coherence interval, ρ_{jk} is the downlink transmitter power allocated to the kth user in cell j. a_{jk} is the average channel gains and b_{lijk}

is the average interference gains that are given by

$$a_{jk} = |\mathbb{E}\{\mathbf{v}_{jk}^{\mathrm{H}}\hat{\mathbf{G}}_{jk}^{j}\}|^2$$

$$b_{lijk} = \begin{cases} |\mathbb{E}\{\mathbf{v}_{li}^{\mathrm{H}}\hat{\mathbf{G}}_{jk}^{l}\}|^2 & (l,i) \neq (j,k) \\ \mathbb{E}\{|\mathbf{v}_{jk}^{\mathrm{H}}\hat{\mathbf{G}}_{jk}^{j}|^2\} - |\mathbb{E}\{\mathbf{v}_{jk}^{\mathrm{H}}\hat{\mathbf{G}}_{jk}^{j}\}|^2 & (l,i) = (j,k). \end{cases} \tag{7.24}$$

Averaging is computed with respect to small-scale fading realizations. Hence, the power allocation is only a function of the channel statistics and the choice of precoding vectors. The spectral efficiency is increasing with ρ_{jk} and decreasing with ρ_{li}. Thus, there is a conflicting relation between the spectral efficiency of two users due to the mutual interference and the limited power of the BS that allocate to the users. This conflicting relation is illustrated by the spectral efficiency region shown in Figure 7.3 which contain all the achievable spectral efficiency combinations [2]. The area under Pareto boundary contains all points that can

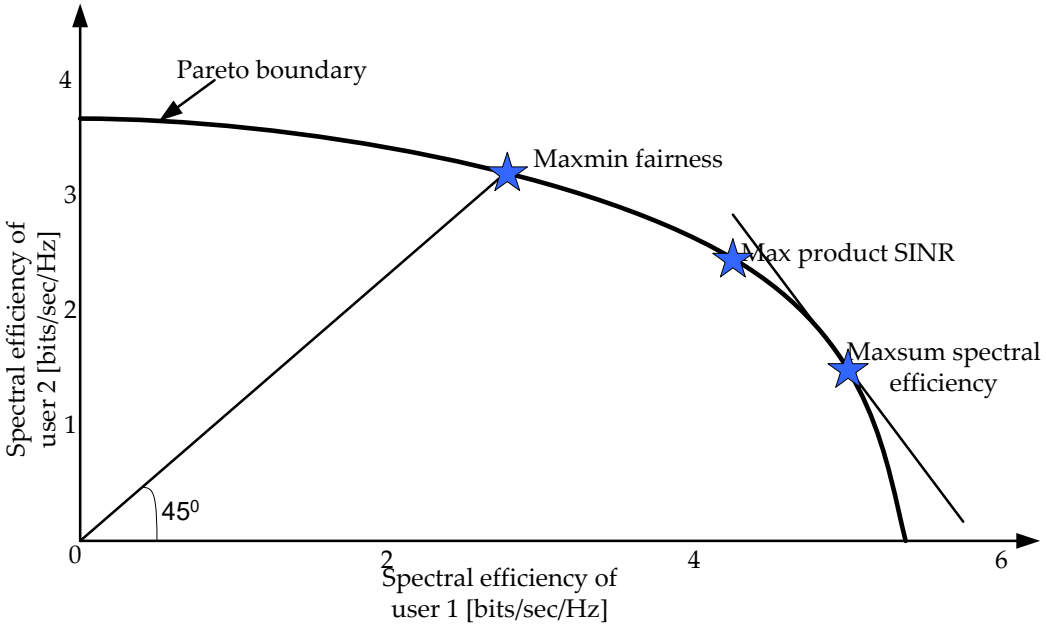

Figure 7.3: Spectral efficiency region that is achieved by different power allocation algorithms for a single cell system with two users [2].

be achieved by different power allocation among the users. Any point in the interior of the spectral efficiency region is strictly suboptimal. Because, it is possible to jointly increase the spectral efficiency of both users by varying the power allocation. Hence, an efficient network should operate on the outer boundary of the spectral efficiency region which is termed as the Pareto boundary. There are many points on the Pareto boundary and we cannot increase the spectral efficiency of a user without decreasing the spectral efficiency

of another user [84]. Thus, we need to find a subjective balance between the individual goals of the users by defining a network utility function that takes the spectral efficiency of all users as the input and gives the utility function as the output. The utility functions are formulated as [2, 52]

$$\mathrm{U}\left(\mathrm{SE}\right) = \begin{cases} \max \sum_{j=1}^{L} \sum_{k=1}^{K} \mathrm{SE}_{jk} & \text{Max sum SE} \\ \max \min_{j,k} \mathrm{SE}_{jk} & \text{Maxmin fairness} \\ \max \prod_{j=1}^{L} \prod_{k=1}^{K} \mathrm{SINR}_{jk} & \text{Max-product SINR} \end{cases} \tag{7.25}$$

where SINR_{jk} is the effective SINR of user k in cell j. The utility functions aim to maximize the sum spectral efficiency, minimum spectral efficiency, and the product SINR of the system, respectively. The max-sum utility function gives the highest aggregate spectral efficiency, but without any fairness guarantees where some users with bad channel conditions might get zero spectral efficiency. The maximization of the product of the SINR leads to high spectral efficiency for the weakest users as compared to maximizing the sum spectral efficiency. The max-product SINR utility also guarantees that every user gets a non-zero spectral efficiency and this utility function provides more fairness than the sum spectral efficiency function. The maxmin fairness utility function provides complete fairness by improving the spectral efficiency achieved by the weakest user in the network. Maximizing this utility function results in the same spectral efficiency for every user, thus a user has no benefit of having a good channel condition [3]. In the next sections, we formulate algorithms for maxmin fairness and max-product power allocation algorithms that maximizes the spectral efficiency of the system [52, 84].

7.5.1 Maxmin Fairness Power Allocation Algorithm

The maxmin fairness power allocation algorithm provides complete fairness by considering the spectral efficiency achieved by the weakest user in the network. As stated before, maximizing this utility function results in equal spectral efficiency for every user. Thus, a user has no benefit of having a good channel condition. By using the value of a_{jk} and b_{lijk} in (7.23) and applying epigraph form [94], the maxmin fairness power allocation is given

by [2,3,52]

$$\begin{aligned} &\max_{\rho_{jk}\geq 0,\ \gamma\geq 0} \ \gamma \\ &\text{subject to:} \quad \frac{\rho_{jk}a_{jk}}{\sum_{l=1}^{L}\sum_{i=1}^{K}\rho_{li}b_{lijk}+\sigma^2} \geq \gamma \qquad \forall k,\ l \\ &\qquad\qquad \sum_{k=1}^{K}\rho_{jk} \leq P_{\max} \qquad\qquad \forall l \end{aligned} \tag{7.26}$$

where γ is the auxiliary variable which satisfies the constraint $\text{SINR}_{jk} \geq \gamma$ for all j, k. The constraints in (7.26) are linear with the transmit power parameters. Hence, we can solve the problem as linear feasibility problem when γ is fixed. A linear search is done over γ to find the largest value for which all power constraints are satisfied when solving the feasibility problem. The global optimal solution can be obtained by Bisection method to a predefined tolerance limit over a search range between $[0, \gamma = \min_{j,k} P_{\max}a_{jk}/\sigma^2]$. This approach solves a sequence of linear feasibility problems. Each subproblem finds the minimum power that satisfies given SINR constraints [51,52,84].

7.5.2 Maximum Product Power Allocation Algorithm

The maximum product SINR utility function seeks to maximize a lower bound on the sum spectral efficiency where the plus one term is neglected inside the logarithm. Removing the plus one term has very small effect on users that support high SINR, but underestimates the spectral efficiency of the weakest users. Hence, maximization of the product of the SINR leads to higher spectral efficiency for the weakest users as compared to maximizing the sum spectral efficiency. The maximum product SINR utility function also guarantees that every user gets non-zero spectral efficiency. Thus, it provides more fairness than the sum spectral efficiency function. For given value of a_{jk} and b_{lijk} the maximum product SINR power allocation is expressed as [2,3,52,114]

$$\begin{aligned} &\max_{\rho_{jk}\geq 0,\ c_{jk}\geq 0} \ \prod_{j=1}^{L}\prod_{k=1}^{K} c_{jk} \\ &\text{subject to:} \quad \sum_{l=1}^{L}\sum_{i=1}^{K}\frac{c_{jk}\rho_{li}b_{lijk}}{\rho_{jk}a_{jk}} + \frac{c_{jk}\sigma^2}{\rho_{jk}a_{jk}} \leq 1 \qquad \forall k,l \\ &\qquad\qquad \sum_{k=1}^{K}\rho_{jk} \leq P_{\max} \qquad \forall l \end{aligned} \tag{7.27}$$

where c_{jk} is the auxiliary variable that satisfy the constraint $c_{jk}\left(\sum_{l=1}^{L}\sum_{i=1}^{K}\rho_{li}b_{lijk}+\sigma^2\right) \leq \rho_{jk}a_{jk}$. Equation (7.27) is a geometric programming optimization problem which can be

solved efficiently by using a geometric programming algorithms [52, 53].

7.6 Simulation Results and Analysis

7.6.1 Simulation Setup and Parameters

We perform numerical simulation to analyze the performances of the proposed multicell massive MIMO systems in spatially correlated channel model. For this, we consider a seven cell hexagonal network setup shown in Figure 7.4. We assume M-antennas at each BS and K-users in each cell. Depending on the analysis, the values of M and K may

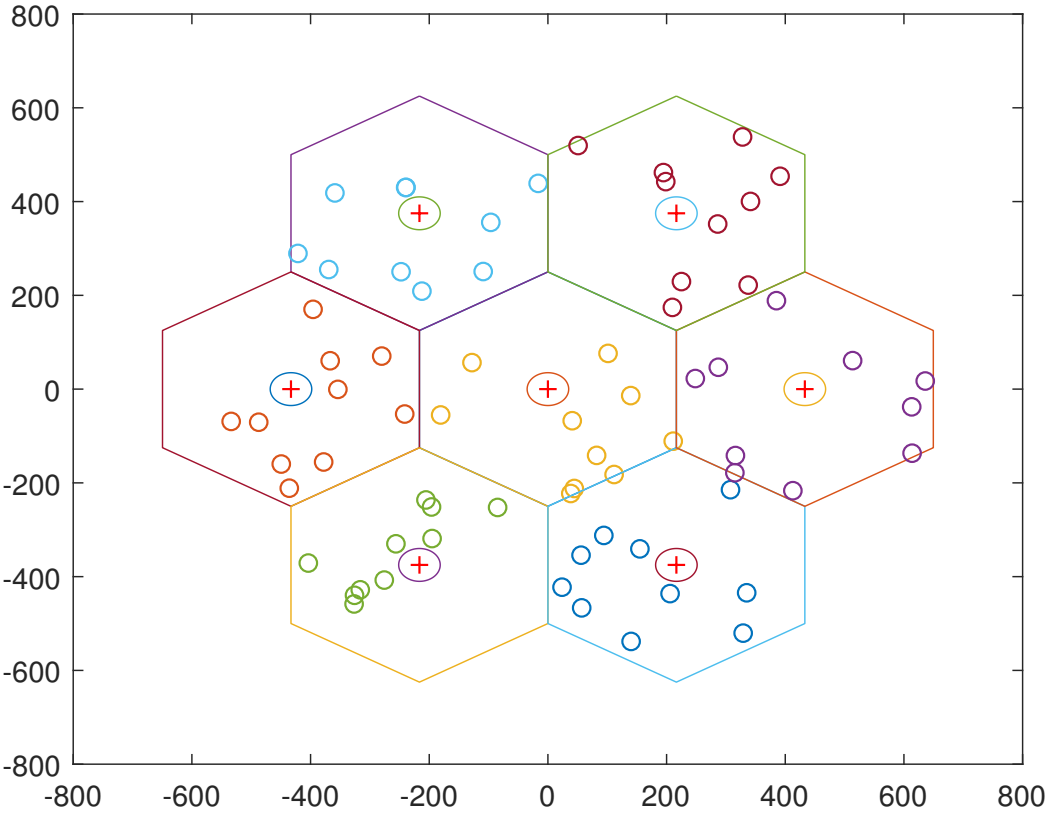

Figure 7.4: A snapshot of seven cell hexagonal network setup with ten uniformly distributed users in each cell.

be changed. We consider a communication bandwidth of 20 MHz and an uplink transmit power of 20 dBm per user and each BS allocates 20 dBm downlink transmit power. The pilot signal length is $\tau_p = \alpha K$ where the integer α is the pilot reuse factor. Thus, there are α-times more pilots than users per cell [2, 120]. The pilots are randomly assigned

to the users in every cell in the sense that the kth user in two cells that belong to the same pilot group uses the same pilot. We consider a Rayleigh fading channel under local scattering spatial channel correlation model with given nominal arrival angle and Gaussian angular standard deviation, σ_φ. As stated before, MMSE based channel estimation is done to estimate the true channel statistics at the BS. To simulate the power allocation algorithms, we deploy CVX with the MOSEK solver [94]. Based on the above system and propagation parameters, we perform numerical simulation to analyze the impacts of spatial channel correlation on channel estimation, channel hardening, favorable condition and spectral efficiency in multicell massive MIMO systems. Besides, the performance of spectrally efficient power optimization algorithms are analyzed.

7.6.2 Impact of Spatial Correlation on Channel Estimation

To analyze the channel estimation quality under spatially correlated channel model, we plot the normalized mean square error in (7.18) with respect to the SNR and angular standard deviation spatial correlation. The spatial channel correlation matrices are generated by using the local scattering model with Gaussian angular standard distribution. Figure 7.5 shows the normalized MSE versus the SNR. The result shows the impact of spatial channel correlation on channel estimation. The result shows that normalized MSE of the channel estimation error is monotonically decreasing with the SNR. This is because when the SNR increases, the eigenvalue of the channel estimation error decreases and this intern improves channel estimation quality. The result also shows that normalized MSE decreases with the number of BS antennas. An NMSE of 10^{-2} is achieved at 20 dB SNR which indicates that the estimation error variance is only 1 % of the original variance of the channel.

Figure 7.6 shows the normalized MSE with respect to angular standard deviation. The result shows that the error is small at low ASD. This is because at low ASD, spatial channel correlation is very high and most of the channel variance lies in few eigenvalues.Thus, when most eigenvalues lie in few eigenspaces and it becomes easier to estimate these strong eigen directions than weaker ones. The figure shows that for strong spatially correlated channels, the channel estimation error is two times smaller than uncorrelated channel.

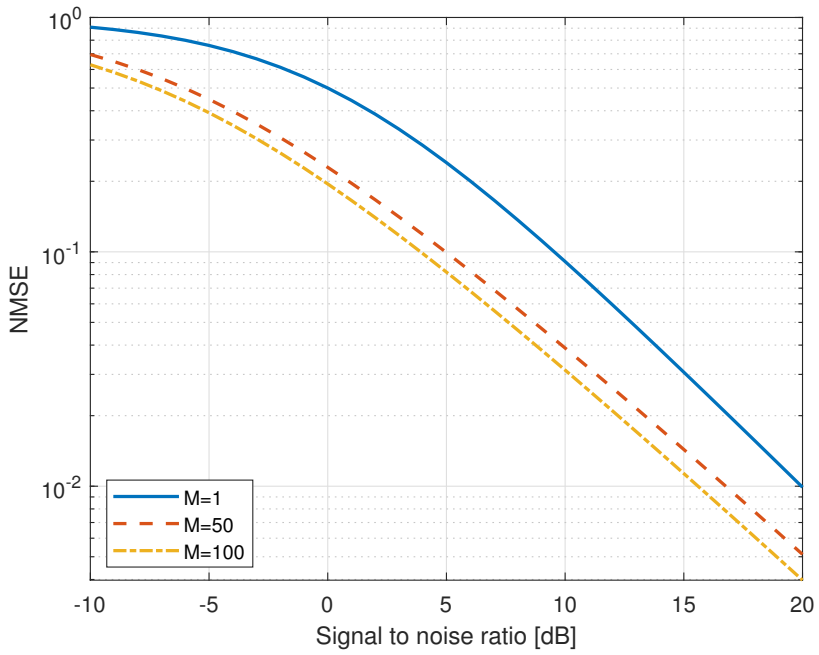

Figure 7.5: Normalized MSE versus SNR of the channel estimate for a spatially correlated channel under local scattering based spatial channel correlation model. We consider $\sigma_\varphi = 10°$.

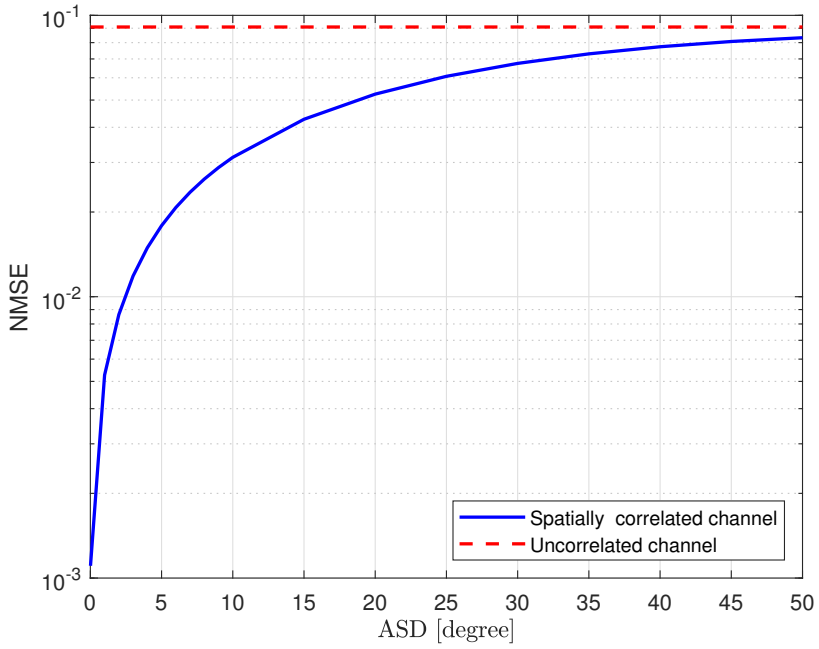

Figure 7.6: Normalized MSE versus ASD of the channel estimate for a spatially correlated channel under local scattering based spatial channel correlation model. We consider SNR $= 10\,\mathrm{dB}$, $M = 200$.

7.6.3 Impact of Spatial Channel Correlation on Channel Hardening and Favorable Condition

As stated in Section 2.1, when the number of antennas at the BS is becoming large, the channel becomes nearly deterministic. Hence, the effect of small scale fading is averaged out. For massive MIMO systems, this property is termed as channel hardening. Figure 7.7 shows the variance of the channel hardening with respect to the numbers of BS antennas. It is noteworthy that the smaller the variance, the more the channel is hardened. The figure shows the results from a correlated Rayleigh fading channel with the local scattering spatial correlation channel model under a Gaussian angular standard deviation with ASD $\in \{10°, 30°\}$. The results from uncorrelated fading channel model is included as a benchmark.

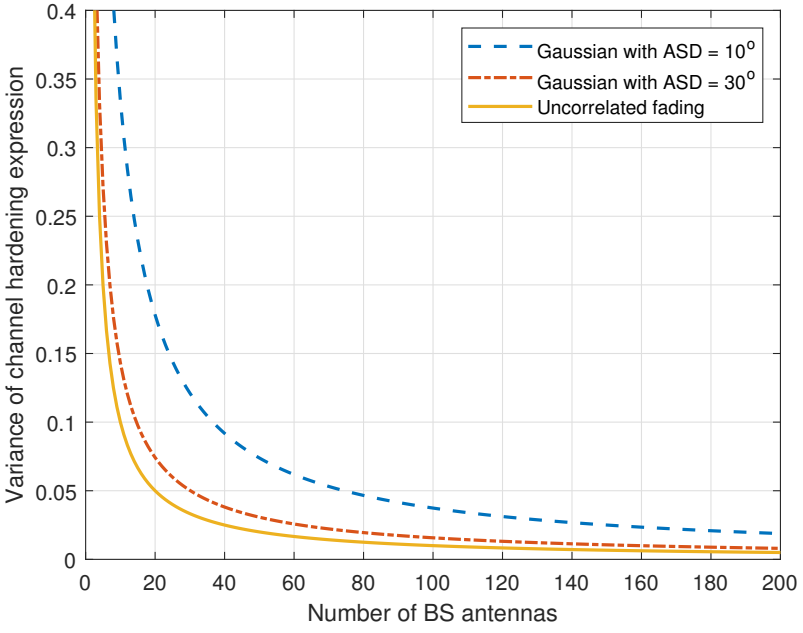

Figure 7.7: Variance of the channel hardening of a correlated channel under local scattering spatial channel correlation model. We assume the nominal angle is $\varphi = 30°$ and Gaussian angular standard deviation spatial correlation model.

As expected, smaller variance is obtained with uncorrelated Rayleigh fading channel whereas the spatial correlation shifts the curve to the right. With ASD $= 30°$, which represents moderate spatial channel correlation, the difference from uncorrelated Rayleigh fading is small. Whereas, with ASD $= 10°$, the spatial channel correlation is strong and which results a loss in channel hardening.

We also analyze the cumulative distribution function (CDF) of the variance of the chan-

nel hardening of a spatially correlated channel for different detection techniques. Figure 7.8 shows the CDF of both uncorrelated Rayleigh fading and spatially correlated channels under Gaussian local scattering model with ASD $= 10°$. The result shows that spatial channel correlation has significant impact on channel hardening. Whereas the choice of detection techniques has small effect on the CDF results. Under local scattering spatial correlation channel model, the channel hardening of all users is less. Because, in this case only some percent of the eigenvalues of the spatial correlation matrix are non-negligible values. This shows that spatial channel correlation reduces the channel hardening due to large variations in effective channel after detection. In contrast, the type of detection techniques has negligible impact on channel hardening.

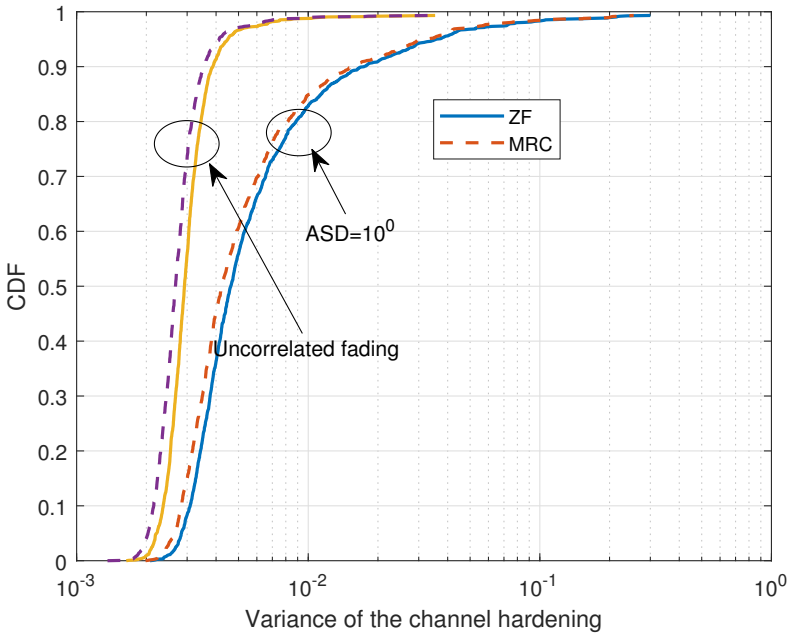

Figure 7.8: CDF of the channel hardening with different detection techniques. We assume $M = 200$, $K = 10$.

Figure 7.9 shows the variance of favorable propagation under local scattering channel model with a Gaussian angular standard deviation. To plot the result, we assume a desired user is found at the center BS and other users interfere with this user. The desired user is assumed to have a fixed nominal angle of 30° and the nominal angle of the interfering user is varied between $-180°$ and 180°. A smaller variance implies that the users channel directions are closer to be orthogonal. As expected with uncorrelated fading, the variance is independent of the user angles. In contrast, under spatial channel correlation, the variance depends strongly on user angles.

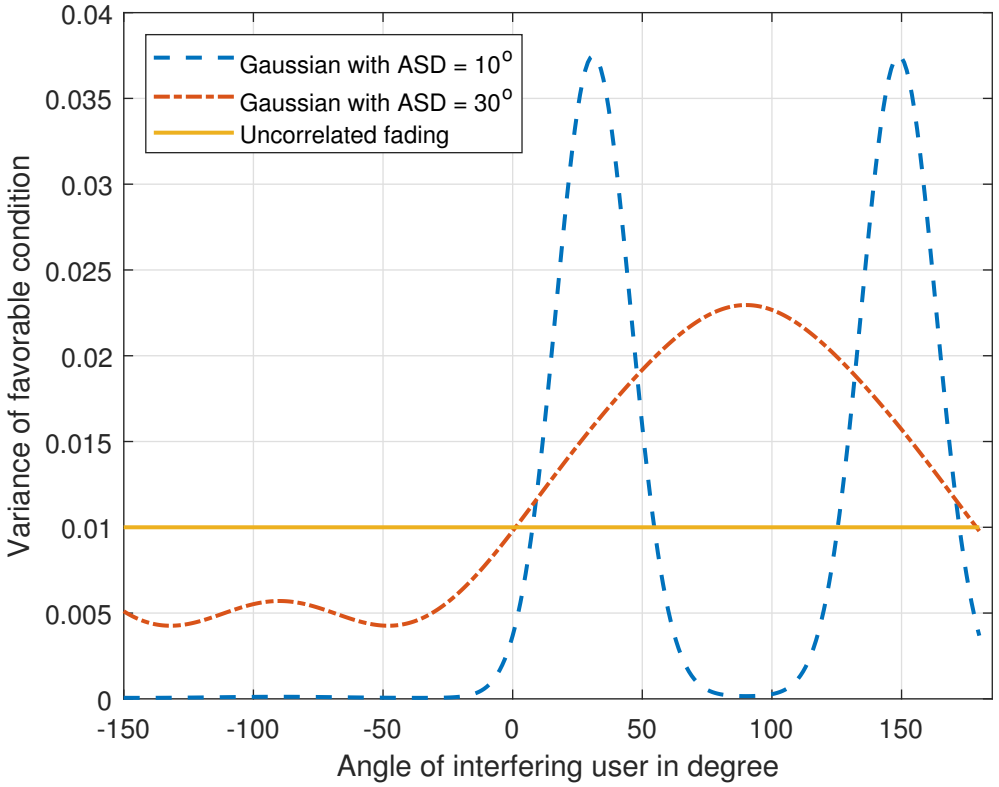

Figure 7.9: Variance of the favorable propagation under local scattering spatial channel correlation model with Gaussian angular standard deviation.

When the ASD is small, there are visible peaks at 30° and 150°. When the ASD increases, these peaks widen and merge to a single peak at ASD = 30°. In that case, the largest variance actually occurs when the users have different angles. When the interfering user has the same nominal angle as the desired user, the variance is substantially larger than uncorrelated fading. This represents the case when the users have similar spatial correlation matrices. When the users have well-separated angles, the variance is substantially smaller than uncorrelated fading. This shows that spatial channel correlation is good if the users have different correlation-eigenspaces; whereas it is a negative effect when the users have similar correlation-eigenspaces.

7.6.4 Spectral Efficiency Analysis in Multicell Massive MIMO Systems

We first show the uplink sum spectral efficiency of multicell massive MIMO system under spatial correlation channel model. Figure 7.10 shows the uplink spectral efficiency of multicell massive MIMO systems with the number of BS antennas. The result shows that the

spectral efficiency increases with the number of BS antennas. Besides, the result shows that ZF detection gives better spectral efficiency than MRC detection.

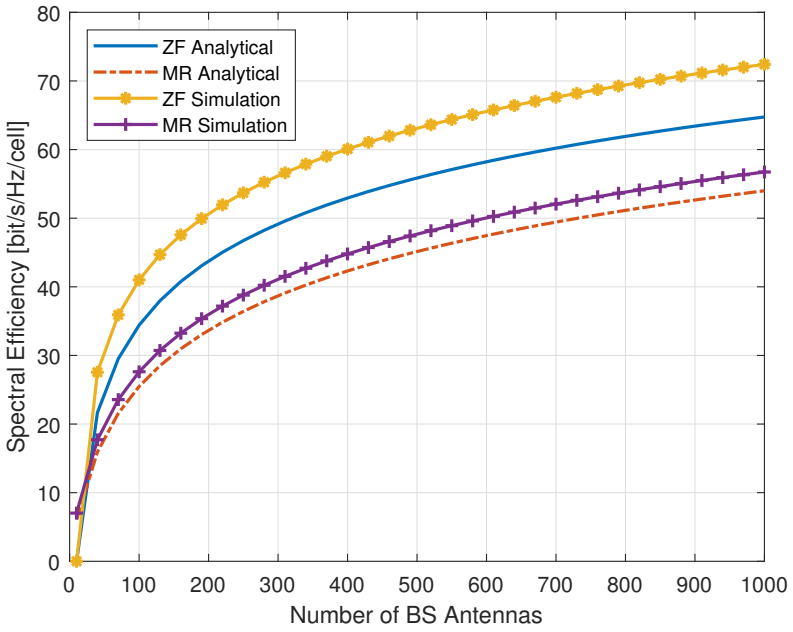

Figure 7.10: Uplink sum spectral efficiency of multicell massive MIMO system under spatial correlation channel model.

We also analyze the CDF of the spectral efficiency of a user for the proposed multicell massive MIMO systems. Figure 7.11 shows the CDF of the variations of the spectral efficiency of a user. The results are given for uncorrelated Rayleigh fading channel and spatially correlated channel with Gaussian local scattering channel model at ASD = 10°. The result shows that the spatial channel correlation improves the sum spectral efficiency. Hence, all users statistically have high spectral efficiency since the CDF curves with spatial channel correlation are to the right of the corresponding curves with uncorrelated fading.

We also analyze the impact of the ASD on the spectral efficiency of the system. Figure 7.12 shows the uplink sum spectral efficiency as a function of the ASD. The result shows that the spectral efficiency decreases with ASD. This is because at low ASD, the spatial channel correlation is high and this reduces the interference between users that have sufficiently different spatial correlation matrices.

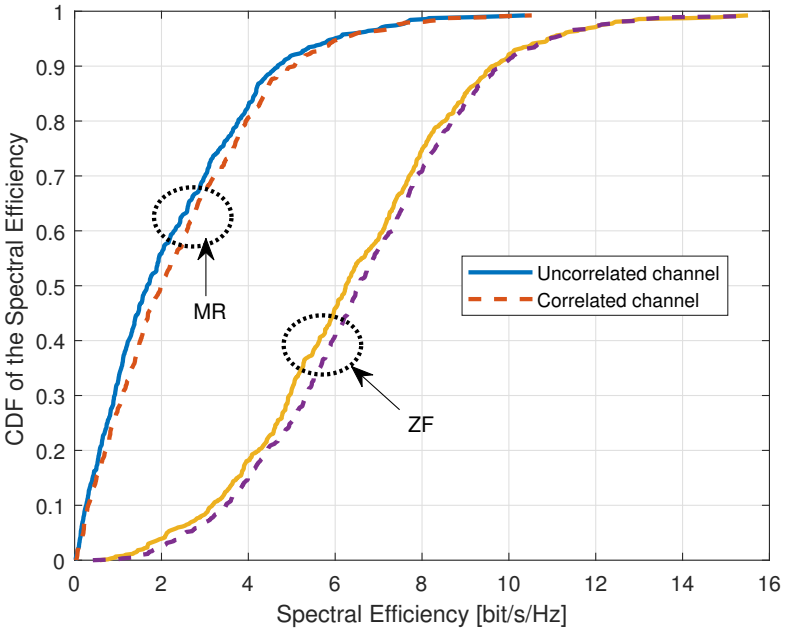

Figure 7.11: CDF of spectral efficiency of a user under spatial correlated channel model and with MRC and ZF detection techniques.

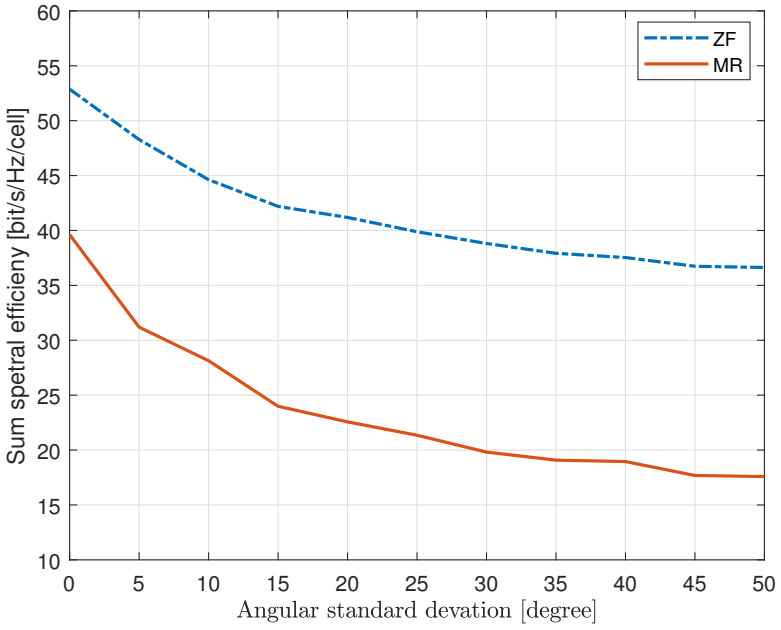

Figure 7.12: Uplink sum spectral efficiency with angular standard deviation under Gaussian local scattering spatial channel correlation model.

7.6.5 Analysis of Power Allocation Optimization in Multicell Massive MIMO Systems

To analyze the effect of power allocation optimization on spectral efficiency in multicell massive MIMO systems, we plot the simulation results of (7.26) and (7.27). For the

simulation we consider a pilot reuse factor of two and spatially correlated channel based on Gaussian local scattering spatial correlation model with ASD = 30°. Figure 7.13 shows the CDF of the spectral efficiency of the user under maxmin fairness and max-product SINR based power allocation. Simulation results from the equal power allocation algorithm are included as a benchmark.

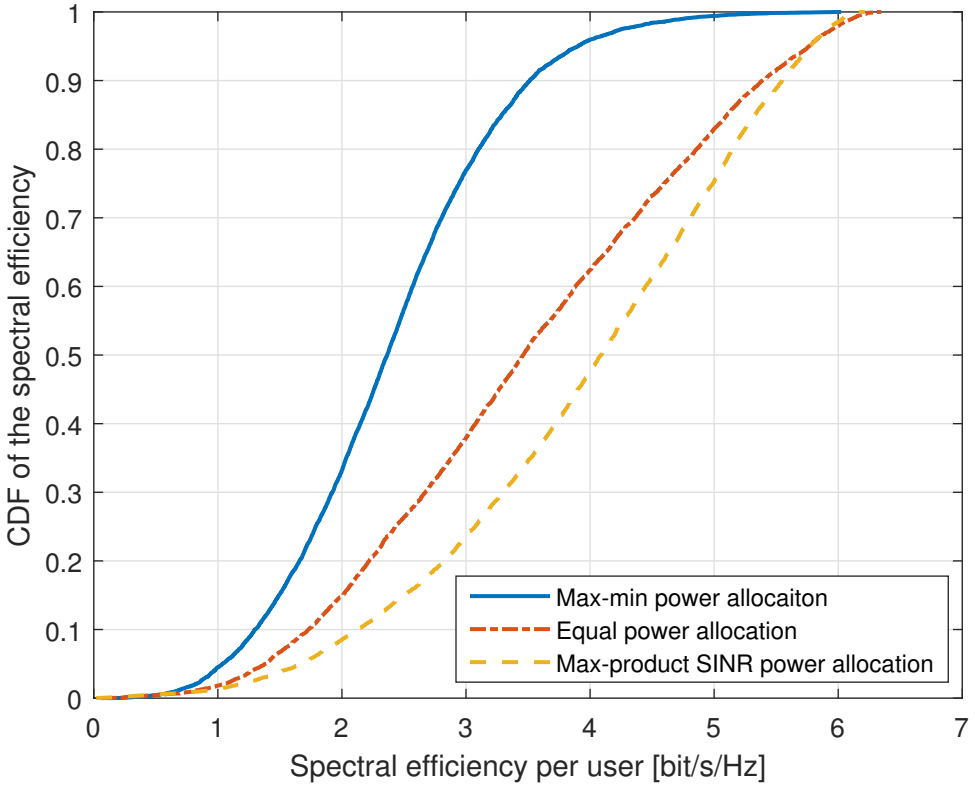

Figure 7.13: CDF of the spectral efficiency of a user with different power allocation algorithms. We consider a downlink multicell massive MIMO system equipped with ZF precoding and imperfect CSI. We assume $M = 100$ and $K = 10$.

The result shows that the CDF curve with maximum product SINR is to the right of equal power allocation curve which in-turn is to the right of the max-min fairness power allocation curve. This indicates that a user achieves better performance with max-product SINR power allocation than with other power allocation algorithms. But, this is not always true at the tails of the CDF curve. For instance a user with 10% strongest channel could achieve higher spectral efficiency with equal power allocation.

7.7 Summary

In this work, we evaluate the performances of multicell massive MIMO systems under spatially correlated channel model. In this regard, we review fundamentals of multicell massive MIMO systems and analyze impacts of spatial correlation on massive MIMO systems. In this regard spatially correlated channel modeling, channel estimation and power allocation in multicell massive MIMO systems are considered. Important trade-offs and considerations on design and optimization of multicell massive MIMO systems has been studied. The results show that spatial channel correlation has a major impact on channel hardening, favorable propagation and channel estimation quality. The estimation quality improves under spatial correlation and users with different spatial characteristics have better favorable propagation and spectral efficiency. But, spatial channel correlation reduces channel hardening property.

Chapter 8

Conclusions and Recommendations

8.1 Conclusions

By adopting very large numbers of antennas at the BS, which is called massive multiple MIMO, we can significantly improve the spectral efficiency of next generation networks. Besides, massive MIMO simplifies transmission processing, improves energy efficiency and reduces the required transmission power of the users. Thus, it is expected to be an enabler for the deployment of next generation mobile networks.

In this PhD research, we study and analyze channel modeling, channel estimation, linear signal processing, resource allocation and optimization techniques in massive MIMO systems. Firstly, recent works on signal processing, channel modeling, channel estimation, resource allocation and optimization techniques are studied and analyzed in Chapter 2. The performances of massive MIMO systems including spectral efficiency, communication reliability and energy efficiency have been analyzed. Detail mathematical formulations are derived and simulation results are provided to validate the theoretical analysis. The results in Figure 2.2, 2.3, 2.4 and 2.7 show that the spectral efficiency increases with the number of BS antennas whereas the required transmit power decreases with the number of BS antennas. On the other side, the energy efficiency increases up to some number of BS antennas and transmit power; and decreases above that BS antennas and transmit power. This is due to the increment on internal power consumption due to increment the number of RF chains of the system. Besides, the result in Figure 2.8 shows that the sum spectral efficiency increases with the number of scheduled users.

The performance of computationally efficient linear detection techniques for massive MIMO systems is analyzed in Chapter 3. Besides, the performances of Truncated Neumann series-based matrix inversion approximation to linear detection techniques are ana-

lyzed. Specifically, the probability of convergence, complexity and error of approximation is evaluated theoretically and via numerical simulation. The results in Figure 3.5, 3.6, 3.9 and 3.10 shows that when the number of BS antennas become very large, the channel becomes more diagonal dominant and Truncated Neumann series-based inverse approximation converges fast and gives nearly the same performance as exact inversion techniques. The achievable sum rate of massive MIMO system under Rician fading channel model is analyzed in Chapter 4. By approximating the non-central Wishart distribution to central Wishart distribution, closed-form lower-bound expression is derived for the achievable sum rate. Detail analysis is done to understand the impact of system and propagation parameters on the achievable rate. The results in 4.1 and 4.2 show that when the LOS factor of the Rician channel increases, channel estimation becomes more robust and the effects of the random component of the Rician fading channel is decreased and thus, the achievable sum rate increases.

Energy efficient resource allocation in massive MIMO systems is analyzed in Chapters 5 and 6. First, in Chapter 5 energy efficient power control algorithms for massive MIMO systems are proposed under maximum transmitter power and minimum data rate constraints of the user. The feasibility condition of the optimization problem is evaluated. The effects of maximum transmitter power and minimum data rate constraints of the user on global energy efficiency have been analyzed. The results in Figure 5.6 and 5.7 show that the global energy efficiency increases with the maximum transmitter power constraint and decreases with the minimum data rate constraint. Then, joint energy efficient resource allocation algorithm is proposed in Chapter 6. The algorithm aims to select optimal number of users, number of BS antennas and transmit power jointly in massive MIMO systems. The results in Figure 6.1 and 6.2 show that the proposed joint energy efficient resource allocation algorithm converges the optimal value with finite iteration. Besides, the radiate power consumption decreases with the number of BS antennas whereas the area throughput increases with number of BS antennas. Hence, at large number of BS antennas, large scale fading based joint energy efficient optimization algorithms can achieve near-optimal performance with low computational complexity.

Finally, in Chapter 7 we analyze the performances of multicell massive MIMO systems. First, we study fundamentals of multicell massive MIMO systems. Besides, we analyze the impacts of spatial correlation and pilot contamination. In this regard correlated based channel modeling, power allocation and resource allocation in multicell massive MIMO

systems are considered. Important trade-offs and considerations on design and optimization of multicell massive MIMO systems has been studied. The results in Figure 7.5, 7.6, 7.7, 7.8 and 7.9 show that spatial channel correlation has a significant impact on channel hardening, favorable propagation and channel estimation quality. The results show that the estimation quality improves under spatial correlation and users with different spatial characteristics has better favorable propagation. But, spatial channel correlation results a slower convergence to asymptotic channel hardening.

8.2 Recommendations

Deploying large number of BS antennas in massive MIMO system allows to get large spatial degrees of freedom to serve multiple users in the same time-frequency resource. Large number of antennas at the BS contributes to achieve favorable propagation and channel hardening. These properties enables a massive MIMO system to spatially separate simultaneous users and provide stable stationary channel conditions even with user dynamics. In this PhD research, we study and analyze channel modeling, resource allocation and optimization techniques in massive MIMO systems. We formulate and analyze detection, precoding, channel modeling, channel estimation, resource allocation and optimization techniques in massive MIMO systems. The spectral efficiency and energy efficiency have been analyzed. Starting from the fundamental concepts in this PhD research, the following interested research directions are recommended for possible area of future work.

- **Cases Studies and Deployment Analysis**: currently, real deployment of 5G networks are on the way all over the world. Massive MIMO is one of the most enabling technologies that is deploying on 5G networks. However, various massive MIMO related challenges and diverse 5G deployment scenarios make the deployment of massive MIMO systems complicated [16, 121, 122]. Hence, performance analysis on case studies and practical deployment scenarios in massive MIMO systems is very interesting direction for future work. This direction of research provides significant insights to understand the local relevance and Techno-Economic aspects of massive MIMO based 5G system deployment in developing countries like Ethiopia.

- **Cell Free Massive MIMO Systems**: in cell free massive MIMO systems, a very large number of distributed access points are connected to a network controller to

simultaneously and jointly serve a number of users [123]. The system is not partitioned into cells and each user is served by all access point antennas simultaneously and jointly. Cell free massive MIMO systems are expected to provide more than ten-fold improvement interms of outage probability and spectral efficiency [123]. But, power control, resource allocation and user association in cell free massive MIMO systems are an active area of research and a promising continual work from this PhD research.

- **Employing Artificial Intelligence in Massive MIMO Systems**: classical algorithms and methods in wireless communications systems exhibit inherent limitations to implement into practical deployment and handle complexity optimization in emerging wireless applications. Artificial intelligence specifically deep-learning has a strong potential to overcome this challenge via data-driven solutions and improve the performance of wireless systems to utilize limited resources [124–126]. Deep learning improves the performance in wireless communication specially when the model-based approaches are failed [124–126]. Hence, employing deep learning in massive MIMO systems for practical channel modeling and estimation, power control and resource allocation is a very good direction of future work in the area.

Bibliography

[1] Cisco, "Cisco visual networking index: Global mobile data traffic forecast update, 2017–2022," 2019.

[2] E. Björnson, J. Hoydis, and L. Sanguinetti, "Massive MIMO networks: Spectral, energy, and hardware efficiency," *Foundations and Trends in Signal Processing*, vol. 11, no. 3, pp. 154–655, 2017.

[3] T. L. Marzetta, E. G. Larsson, H. Yang, and H. Q. Ngo, *Fundamentals of Massive MIMO*. Cambridge University Press, 2016.

[4] A. Osseiran, F. Boccardi, V. Braun, K. Kusume, P. Marsch, M. Maternia, O. Queseth, M. Schellmann, H. Schotten, H. Taoka, H. Tullberg, M. Uusitalo, B. Timus, and M. Fallgren, "Scenarios for 5G mobile and wireless communications: the vision of the METIS project," *IEEE Communications Magazine*, vol. 52, pp. 26–35, May 2014.

[5] G. Liu and D. Jiang, "5G: Vision and requirements for mobile communication system towards 2020," *Chinese Journal of Engineering*, 2016.

[6] C. Wang and et al., "Cellular architecture and key technologies for 5G wireless communication networks," *IEEE Communications Magazine*, vol. 52, pp. 122–130, February 2014.

[7] I. Akyildiz, S. Chun, and M. Chandrasekaran, "5G roadmap: Ten key enabling technologies," *Computer Networks*, vol. 106, pp. 17–48, 2016.

[8] A. Gupta and R. Kumar, "A survey of 5G networks: Architecture and emerging technologies," *IEEE Access*, vol. 3, pp. 1206–1232, 2015.

[9] F. Boccardi, R. Heath, A. Lozano, T. Marzetta, and P. Popovski, "Five disruptive technology directions for 5G," *IEEE Communications Magazine*, vol. 52, no. 2, pp. 74–80, 2014.

[10] L. Lu, G. Y. Li, A. L. Swindlehurst, A. Ashikhmin, and R. Zhang, "An overview of massive MIMO: benefits and challenges," *IEEE Journal of Selected Topics in Signal Processing*, vol. 8, pp. 742–758, Oct 2014.

[11] M. Dryjanski and M. Rahnema, *From LTE to LTE-Advanced Pro and 5G.* Artech House, September 2017.

[12] NGMN Alliance, "5G white paper," *Next Generation Mobile Networks (NGMN)*, 2015.

[13] E. G. Larsson, "Massive MIMO for 5G: Overview and the road a head," *51st Annual Conference on Information Sciences and Systems (CISS)*, pp. 1–10, March 2017.

[14] E. G. Larsson, O. Edfors, F. Tufvesson, and T. L. Marzetta, "Massive MIMO for next generation wireless systems," *IEEE Communications Magazine*, vol. 52, pp. 186–195, February 2014.

[15] A. Osseiran, J. Monserrat, and P. Marsch, *5G mobile and wireless communications technology.* Cambridge University Press, 2016.

[16] R. Chataut and R. Akl, "Massive MIMO systems for 5G and beyond networks: Overview, recent trends, challenges, and future research directions," *Sensors*, vol. 20, no. 10, pp. 27–53, 2020.

[17] T. L. Marzetta, "Noncooperative cellular wireless with unlimited numbers of base station antennas," *IEEE Transactions on Wireless Communications*, vol. 9, no. 11, pp. 3590–3600, 2010.

[18] Amare Kassaw, Fikiraddis Tazeb and Dereje Hailemariam, "Performance analysis of multicarrier modulation techniques for next generation networks," 8*th International Conference on the Advancements of Science and Technology (ICAST2020)*, no. 8, 2020.

[19] Y. Niu, Y. Li, D. Jin, L. Su, and A. V. Vasilakos, "A survey of millimeter wave communications (mmWave) for 5G: opportunities and challenges," *Wireless Networks*, vol. 21, no. 8, pp. 2657–2676, 2015.

[20] W. Xiang, K. Zheng, and X. S. Shen, *5G mobile communications*. Springer, 2016.

[21] H. Q. Ngo, E. G. Larsson, and T. L. Marzetta, "Energy and spectral efficiency of very large multiuser MIMO systems," *IEEE Transactions on Communications*, vol. 61, no. 4, pp. 1436–1449, 2013.

[22] E. Bjornson, L. Sanguinetti, J. Hoydis, and M. Debbah, "Optimal design of energy-efficient multiuser MIMO systems: Is massive MIMO the answer?," *IEEE Transactions on Wireless Communications*, no. 14, pp. 3059–3075, 2015.

[23] F. Rusek, D. Persson, B. K. Lau, E. G. Larsson, T. L. Marzetta, O. Edfors, and F. Tufvesson, "Scaling up MIMO: Opportunities and challenges with very large arrays," *IEEE Signal Processing Magazine*, vol. 30, no. 1, pp. 40–60, 2013.

[24] K. Davaslioglu and R. D. Gitlin, "5G green networking: Enabling technologies, potentials and challenges," *17th IEEE Annual Wireless and Microwave Technology Conference (WAMICON-2016)*, pp. 1–6, 2016.

[25] H. Q. Ngo, E. G. Larsson, and T. L. Marzetta, "Aspects of favorable propagation in massive MIMO," *22nd European Signal Processing Conference (EUSIPCO2014)*, pp. 76–80, 2014.

[26] A. Chockalingam and B. S. Rajan, *Large MIMO systems*. Cambridge University Press, 2014.

[27] E. Bjornson, E. G. Larsson, and T. L. Marzetta, "Massive MIMO: Ten myths and one critical question," *IEEE Communications Magazine*, vol. 54, pp. 114–123, February 2016.

[28] Amare Kassaw, Dereje Hailemarim and Abdelhak Zoubir, "Performance analysis of uplink massive MIMO systems over Rician fading channel," *26th European Signal Processing Conference (EUSIPCO2018)*, 2018.

[29] Tewelgn Kebede, Amare Kassaw, Yihenew Wondie and Johannes Stenibrunn, "Joint evaluation of spectral efficiency, energy efficiency and transmission reliability in massive MIMO systems," 7*th International Conference on the Advancements of Science and Technology (ICAST2019)*, no. 7, 2019.

[30] Amare Kassaw, Dereje Hailemarim and Abdelhak Zoubir, "Review of truncated Neumann series based detection in massive MIMO systems," *1st IEEE Wireless Africa Conference (IEEE WAC-2018)*, 2018.

[31] Amare Kassaw, Dereje Hailemarim and Abdelhak Zoubir, "Review of energy efficient resource allocation techniques in massive MIMO systems," *9th International Conference on Information and Communication Technology Convergence (ICTC2018)*, 2018.

[32] A. Kassaw, D. Hailemarim, and A. Zoubir, "'Fractional programming for energy efficient power control in uplink massive MIMO systems," 27*th European Signal Processing Conference (EUSIPCO2018)*, 2018.

[33] Amare Kassaw, Dereje Hailemarim, Michael Fauß and Abdelhak Zoubir, "'Energy efficient power control in uplink massive MIMO systems: A fractional programming approach," *Submitted to Elsevier Journal of Physical Communication*, 2020.

[34] D. Zhu, B. Li, and P. Liang, "On the matrix inversion approximation based on Neumann series in massive MIMO systems," *IEEE International Conferencein Communications (ICC2015)*, pp. 1763–1769, 2015.

[35] A. Elghariani and M. Zoltowski, "Low complexity detection algorithms in large-scale MIMO systems," *IEEE Transactions on Wireless Communications*, vol. 15, pp. 1689–1702, March 2016.

[36] Q. Zhou and X. Ma, "Element-based lattice reduction algorithms for large MIMO detection," *IEEE Journal on Selected Areas in Communications*, vol. 31, pp. 274–286, February 2013.

[37] Amare Kassaw, Dereje Hailemarim and Abdelhak Zoubir, *Review of massive MIMO systems: Channel capacity, detection and precoding techniques.* Addis Ababa Institute of Technology, 2018.

[38] Amare Kassaw, Zemene Matewos and Dereje Hailemariam , "Digital dividend and its opportunities for long term evolution (LTE) mobile network: The case of Ethiopia," *IEEE AFRICON-2017*, pp. 245–250, 2017.

[39] Yosef Birhanu, Fikreselam Gared and Amare Kassaw, "Performance analysis of hybrid beamforming techniques in large multiuser MIMO systems," 8*th International*

Conference on the Advancements of Science and Technology (ICAST2019), no. 8, 2020.

[40] G. N. Kamga, M. Xia, and S. Aissa, "Channel modeling and capacity analysis of large MIMO in real propagation environments," *IEEE International Conference on Communications (ICC2015)*, pp. 1447–1452, June 2015.

[41] H. Hijazi, E. P. Simon, M. Lienard, and L. Ros, "Channel estimation for MIMO-OFDM systems in fast time-varying environments," *4th International Symposium on Communications, Control and Signal Processing (ISCCSP2010)*, pp. 1–6, 2010.

[42] T. Peken, G. Vanhoy, and T. Bose, "Blind channel estimation for massive MIMO," *Analog Integrated Circuits and Signal Processing*, vol. 91, no. 2, pp. 257–266, 2017.

[43] H. Q. Ngo and E. G. Larsson, "EVD-based channel estimation in multicell multiuser MIMO systems with very large antenna arrays," *IEEE International Conference on Acoustics, Speech and Signal Processing (ICASSP2012)*, pp. 3249–3252, 2012.

[44] A. Hu, T. Lv, and Y. Lu, "Subspace-based semi-blind channel estimation for large-scale multicell multiuser MIMO systems," *77th IEEE Vehicular Technology Conference (VTC2013)*, pp. 1–5, 2013.

[45] C. E. . Shannon, "A mathematical theory of communication," *Bell System Technical Journal*, vol. 27, pp. 379–423, 2014.

[46] M. Matthaiou, C. Zhong, M. R. McKay, and T. Ratnarajah, "Sum rate analysis of ZF receivers in distributed MIMO systems," *IEEE Journal on Selected Areas in Communications*, vol. 31, no. 2, pp. 180–191, 2013.

[47] H. Q. Ngo, E. G. Larsson, and T. L. Marzetta, "The multicell multiuser MIMO uplink with very large antenna arrays and a finite dimensional channel," *IEEE Transactions on Communications*, vol. 61, no. 6, pp. 2350–2361, 2013.

[48] J. Hoydis, S. Ten Brink, and M. Debbah, "Massive MIMO in the uplink-downlink cellular networks: How many antennas do we need?," *IEEE Journal on selected Areas in Communications*, vol. 31, no. 2, pp. 160–171, 2013.

[49] G. N. Kamga, M. Xia, and S. Aïssa, "Spectral efficiency analysis of massive MIMO systems in centralized and distributed schemes," *IEEE Transactions on Communications*, vol. 64, pp. 1930–1941, May 2016.

[50] S. Buzzi, I. Chih-Lin, T. E. Klein, H. V. Poor, C. Yang, and A. Zappone, "A survey of energy efficient techniques for 5G networks and challenges a head," *IEEE Journal on Selected Areas in Communications*, vol. 34, no. 4, pp. 697–709, 2016.

[51] A. Zappone, E. Björnson, L. Sanguinetti, and E. Jorswieck, "Globally optimal energyefficient power control and receiver design in wireless networks," *IEEE Transactions on Signal Processing*, vol. 65, no. 11, pp. 2844–2859, 2017.

[52] A. Zappone and E. Jorswieck, "Energy efficiency in wireless networks via fractional programming theory," *Foundations and Trends in Communications and Information Theory*, vol. 11, no. 4, pp. 185–396, 2015.

[53] A. Zappone, L. Sanguinetti, G. Bacci, E. Jorswieck, and M. Debbah, "Energy-efficient power control: A look at 5G wireless technologies," *IEEE Transactions on Signal Processing*, vol. 64, no. 7, pp. 1668–1683, 2015.

[54] G. Auer, V. Giannini, C. Desset, I. Godor, P. Skillermark, M. Olsson, M. A. Imran, D. Sabella, M. J. Gonzalez, and O. Blume, "How much energy is needed to run a wireless network?," *IEEE Wireless Communications*, vol. 18, no. 5, pp. 40–49, 2011.

[55] S. M. Kay, *Fundamentals of statistical signal processing, Volume I: Estimation theory.* Prentice Hall PTR, 1993.

[56] J. Evans and D. N. C. Tse, "Large system performance of linear multiuser receivers in multipath fading channels," *IEEE Transactions on Information Theory*, vol. 46, no. 6, pp. 2059–2078, 2000.

[57] A. M. Tulino, S. Verdú, *et al.*, "Random matrix theory and wireless communications," *Foundations and Trends in Communications and Information Theory*, vol. 1, no. 1, pp. 1–182, 2004.

[58] K. Zheng, L. Zhao, J. Mei, B. Shao, W. Xiang, and L. Hanzo, "Survey of large scale MIMO systems," *IEEE Communications Surveys and Tutorials*, vol. 17, no. 3, pp. 1738–1760, 2015.

[59] S. Yang and L. Hanzo, "Fifty years of MIMO detection: The road to large-scale MIMOs," *IEEE Communications Surveys and Tutorials*, vol. 17, pp. 1941–1988, November 2015.

[60] B. Lin and C. Jinho, *Low complexity MIMO detection*. Springer Science and Business Media, 2012.

[61] M. Wu, B. Yin, G. Wang, C. Dick, J. R. Cavallaro, and C. Studer, "Large-scale MIMO detection for 3GPP LTE: Algorithms and FPGA implementations," *IEEE Journal of Selected Topics in Signal Processing*, vol. 8, no. 5, pp. 916–929, 2014.

[62] H. Prabhu, J. Rodrigues, O. Edfors, and F. Rusek, "Approximate matrix inverse computations for very large MIMO and applications to linear precoding systems," *IEEE Wireless Communications and Networking Conference (WCNC2013)*, pp. 2710–2715, 2013.

[63] Y. Jiang, M. K. Varanasi, and J. Li, "Performance analysis of ZF and MMSE equalizers for MIMO systems: An in depth study of the high SNR regime," *IEEE Transactions on Information Theory*, vol. 57, no. 4, pp. 2008–2026, 2011.

[64] Y. Xu, W. Zou, and L. Du, "A fast and low-complexity matrix inversion scheme based on CSM method for massive MIMO systems," *EURASIP Journal on Wireless Communications and Networking*, vol. 2, Oct 2016.

[65] L. Dai, X. Gao, X. Su, S. Han, I. Chih-Lin, and Z. Wang, "Low-complexity soft-output signal detection based on Gauss–Seidel method for uplink multiuser large-scale MIMO systems," *IEEE Transactions on Vehicular Technology*, vol. 64, no. 10, pp. 4839–4845, 2015.

[66] X. Gao, L. Dai, Y. Hu, Z. Wang, and Z. Wang, "Matrix inversion-less signal detection using SOR method for uplink large-scale MIMO systems," *IEEE Global Communications Conference (GLOBECOM2014)*, pp. 3291–3295, 2014.

[67] B. Yin, M. Wu, J. R. Cavallaro, and C. Studer, "Conjugate gradient-based soft-output detection and precoding in massive MIMO systems," *IEEE Global communications conference (GLOBECOM2014)*, pp. 3696–3701, 2014.

[68] Y. Hu, Z. Wang, X. Gaol, and J. Ning, "Low-complexity signal detection using CG method for uplink large-scale MIMO systems," *IEEE International Conference on Communication Systems (ICCS2014)*, pp. 477–481, 2014.

[69] X. Gao, L. Dai, Y. Ma, and Z. Wang, "Low-complexity near-optimal signal detection for uplink large-scale MIMO systems," *Electronics letters*, vol. 50, no. 18, pp. 1326–1328, 2014.

[70] L. Shao and Y. Zu, "Joint Newton iteration and Neumann series method of convergence-accelerating matrix inversion approximation in linear precoding for massive MIMO systems," *Mathematical Problems in Engineering*, vol. 2, 2016.

[71] Amare Kassaw, Dereje Hailemarim and Abdelhak Zoubir, *Computationally efficient detection techniques for massive MIMO systems*. Addis Ababa Institute of Technology, 2018.

[72] Amare Kassaw, Dereje Hailemariam and Abdelhak Zoubir, "Performance analysis of multiple antenna based blind spectrum sensing techniques for cognitive radio networks," 5*th International Conference on the Advancements of Science and Technology (ICAST2017)*, no. 5, 2017.

[73] D. Tse and P. Viswanath, *Fundamentals of wireless communication*. Cambridge university press, 2005.

[74] R. Couillet and M. Debbah, *Random matrix methods for wireless communications*. Cambridge University Press, 2011.

[75] P. J. Smith, C. Neil, M. Shafi, and P. A. Dmochowski, "On the convergence of massive MIMO systems," *IEEE International Conference on Communications (ICC2014)*, pp. 5191–5196, 2014.

[76] C. Siriteanu, Y. Miyanaga, S. D. Blostein, S. Kuriki, and X. Shi, "MIMO zero-forcing detection analysis for correlated and estimated Rician fading," *IEEE transactions on Vehicular Technology*, vol. 61, no. 7, pp. 3087–3099, 2012.

[77] D. W. Yue and G. Y. Li, "LOS-based conjugate beamforming and power-scaling law in massive-MIMO systems," *arXiv preprint, arXiv:1404.1654*, 2014.

[78] I. A. Hemadeh, K. Satyanarayana, M. El-Hajjar, and L. Hanzo, "Millimeter-wave communications: Physical channel models, design considerations, antenna constructions and link budget," *IEEE Communications Surveys and Tutorials*, vol. 20, no. 2, pp. 870–913, 2018.

[79] N. Ravindran, N. Jindal, and H. C. Huang, "Beamforming with finite rate feedback for LOS MIMO downlink channels," *IEEE Global Telecommunications Conference (GLOBECOM2007)*, pp. 4200–4204, 2007.

[80] J. Cao, D. Wang, J. Li, Q. Sun, and Y. Hu, "Uplink spectral efficiency analysis of multicell multi-user massive MIMO over correlated Ricean channel," *China Information Sciences*, vol. 61, no. 8, 2018.

[81] Q. Zhang, S. Jin, K.-K. Wong, H. Zhu, and M. Matthaiou, "Power scaling of uplink massive MIMO systems with arbitrary-rank channel means," *IEEE Journal of Selected Topics in Signal Processing*, vol. 8, no. 5, pp. 966–981, 2014.

[82] L. Sanguinetti, A. Kammoun, and M. Debbah, "Asymptotic analysis of multicell massive MIMO over Rician fading channels," *IEEE International Conference on Acoustics, Speech and Signal Processing (ICASSP2017)*, pp. 3539–3543, 2017.

[83] D. K. Nagar and A. K. Gupta, "Expectations of functions of complex Wishart matrix," *Acta applicandae mathematicae*, vol. 113, no. 3, pp. 265–288, 2011.

[84] E. Bjornson, E. A. Jorswieck, M. Debbah, and B. Ottersten, "Multiobjective signal processing optimization: The way to balance conflicting metrics in 5G systems," *IEEE Signal Processing Magazine*, vol. 31, no. 6, pp. 14–23, 2014.

[85] L. Venturino, A. Zappone, C. Risi, and S. Buzzi, "Energy efficient scheduling and power allocation in downlink OFDMA networks with base station coordination," *IEEE transactions on wireless communications*, vol. 14, no. 1, pp. 1–14, 2015.

[86] N. D. Kwan, L. Ernest, and S. Robert, "Energy-efficient resource allocation in OFDMA systems with large numbers of base station antennas," *IEEE Transactions on Wireless Communications*, vol. 11, no. 9, pp. 3292–3304, 2012.

[87] E. Björnson, L. Sanguinetti, J. Hoydis, and M. Debbah, "Designing multi-user MIMO for energy efficiency: When is massive MIMO the answer?," *IEEE Wireless Communications and Networking Conference (WCNC2014)*, pp. 242–247, 2014.

[88] E. Björnson, E. Jorswieck, *et al.*, "Optimal resource allocation in coordinated multicell systems," *Foundations and Trends in Communications and Information Theory*, vol. 9, no. 2–3, pp. 113–381, 2013.

[89] Y. Xin, D. Wang, J. Li, H. Zhu, J. Wang, and X. You, "Area spectral efficiency and area energy efficiency of massive MIMO cellular systems," *IEEE Transactions on Vehicular Technology*, vol. 65, no. 5, pp. 3243–3254, 2016.

[90] Y. Y. Xinhua Wang and J. Sheng, "Energy efficient power allocation for the uplink of distributed massive MIMO systems," *Future Internet*, 2017.

[91] G. Auer, O. Blume, V. Giannini, I. Godor, M. Imran, Y. Jading, E. Katranaras, M. Olsson, D. Sabella, P. Skillermark, *et al.*, "D2. 3: Energy efficiency analysis of the reference systems, areas of improvements and target breakdown," *Earth*, vol. 20, no. 10, 2010.

[92] W. Dinkelbach, "On nonlinear fractional programming," *Management science*, vol. 13, no. 7, pp. 492–498, 1967.

[93] J.-P. Crouzeix and J. A. Ferland, "Algorithms for generalized fractional programming," *Mathematical Programming*, vol. 52, no. 3, pp. 191–207, 1991.

[94] S. Boyd and L. Vandenberghe, *Convex optimization*. Cambridge University Press, 2004.

[95] K. Senel, E. Björnson, and E. G. Larsson, "Adapting the number of antennas and power to traffic load: When to turn on massive MIMO?," *IEEE Wireless Communications and Networking Conference (WCNC2018)*, pp. 1–6, 2018.

[96] E. Castaneda, A. Silva, A. Gameiro, and M. Kountouris, "An overview on resource allocation techniques for multiuser MIMO systems," *IEEE Communications Surveys and Tutorials*, vol. 19, no. 1, pp. 239–284, 2016.

[97] E. Nayebi, A. Ashikhmin, T. L. Marzetta, H. Yang, and B. D. Rao, "Precoding and power optimization in cell-free massive MIMO systems," *IEEE Transactions on Wireless Communications*, vol. 16, no. 7, pp. 4445–4459, 2017.

[98] F. Tan, T. Lv, and S. Yang, "Power allocation optimization for energy-efficient massive MIMO aided multi-pair decode and forward relay systems," *IEEE Transactions on Communications*, vol. 65, no. 6, pp. 2368–2381, 2017.

[99] H. Gao, T. Lv, X. Su, H. Yang, and J. M. Cioffi, "Energy-efficient resource allocation for massive MIMO amplify and forward relay systems," *IEEE Access*, vol. 4, pp. 2771–2787, 2016.

[100] G. Bacci, E. V. Belmega, and L. Sanguinetti, "Distributed energy-efficient power optimization in cellular relay networks with minimum rate constraints," *IEEE International Conference on Acoustics, Speech and Signal Processing (ICASSP2014)*, pp. 7014–7018, 2014.

[101] M. Chiang, P. Hande, T. Lan, and C. W. Tan, "Power control in wireless cellular networks," *Foundations and Trends in Networking*, vol. 2, no. 4, pp. 381–533, 2008.

[102] N. Fatema, G. Hua, Y. Xiang, D. Peng, and I. Natgunanathan, "Massive MIMO linear precoding: A survey," *IEEE Systems Journal*, no. 99, pp. 1–12, 2017.

[103] X. Gao, O. Edfors, F. Rusek, and F. Tufvesson, "Linear precoding performance in measured very large MIMO channels," *IEEE Vehicular Technology Conference (VTC2011)*, pp. 1–5, September 2011.

[104] T. E. Bogale and L. B. Le, "Beamforming for multiuser massive MIMO systems: Digital versus hybrid analog-digital," *arXiv preprint, arXiv:1407.0446*, 2014.

[105] F. Sohrabi and W. Yu, "Hybrid digital and analog beamforming design for large-scale MIMO systems," *IEEE International Conference on Acoustics, Speech and Signal Processing (ICASSP2015)*, pp. 2929–2933, 2015.

[106] Y. Zhang, H. Gao, F. Tan, and T. Lv, "Resource allocation of energy efficient multiuser massive MIMO systems," *IEEE Globecom Workshops (GLOBECOM2016)*, pp. 1–6, 2016.

[107] E. Castaneda, A. Silva, A. Gameiro, and M. Kountouris, "An overview on resource allocation techniques for multiuser MIMO systems," *IEEE Communications Surveys and Tutorials*, vol. 19, no. 1, pp. 239–284, 2016.

[108] R. Hamdi, E. Driouch, and W. Ajib, "Resource allocation in downlink large-scale MIMO systems," *IEEE Access*, vol. 4, pp. 8303–8316, November 2016.

[109] R. R. Muller, L. Cottatellucci, and M. Vehkapera, "Blind pilot decontamination," *IEEE Journal of Selected Topics in Signal Processing*, vol. 8, no. 5, pp. 773–786, 2014.

[110] A. Ashikhmin and T. Marzetta, "Pilot contamination precoding in multicell large scale antenna systems," *IEEE International Symposium on Information Theory Proceedings (ISIT2012)*, pp. 1137–1141, 2012.

[111] H. Yin, D. Gesbert, M. Filippou, and Y. Liu, "A coordinated approach to channel estimation in large-scale multiple-antenna systems," *IEEE Journal on Selected Areas in Communications*, vol. 31, no. 2, pp. 264–273, 2013.

[112] E. Björnson, E. G. Larsson, and M. Debbah, "Massive MIMO for maximal spectral efficiency: How many users and pilots should be allocated?," *IEEE Transactions on Wireless Communications*, vol. 15, no. 2, pp. 1293–1308, 2015.

[113] M. Mahajan and W. Yoon, "Energy efficient resource allocation in multicell large-scale distributed antenna system with imperfect CSI," *IETE Journal of Research*, vol. 66, no. 6, pp. 1–9, 2018.

[114] T. M. Nguyen, V. N. Ha, and L. B. Le, "Resource allocation optimization in multiuser multicell massive MIMO networks considering pilot contamination," *IEEE Access*, vol. 3, pp. 1272–1287, 2015.

[115] W. Hao, O. Muta, H. Gacanin, and H. Furukawa, "Uplink pilot allocation for multicell massive MIMO systems," *IEICE Transactions on Communications*, vol. 102, no. 2, pp. 373–380, 2019.

[116] C.-X. Wang, J. Bian, J. Sun, W. Zhang, and M. Zhang, "A survey of 5G channel measurements and models," *IEEE Communications Surveys and Tutorials*, August 2018.

[117] F. Hossain, T. K. Geok, T. A. Rahman, M. N. Hindia, K. Dimyati, S. Ahmed, C. P. Tso, and N. Z. Abd Rahman, "An efficient 3D ray tracing method: Prediction of indoor radio propagation at 28 GHz in 5G network," *Electronics*, vol. 8, no. 3, p. 286, 2019.

[118] K. Zheng, S. Ou, and X. Yin, "Massive MIMO channel models: A survey," *International Journal of Antennas and Propagation*, vol. 2014.

[119] H. Jiang and G. Gui, *Channel modeling in 5G wireless communication systems*. Springer, 2019.

[120] X. Zhu, Z. Wang, L. Dai, and C. Qian, "Smart pilot assignment for massive MIMO," *IEEE Communications Letters*, vol. 19, no. 9, pp. 1644–1647, 2015.

[121] P. K. Gkonis, P. T. Trakadas, and D. I. Kaklamani, "A comprehensive study on simulation techniques for 5G Networks: State of the art results, analysis, and future challenges," *Electronics*, vol. 9, no. 3, p. 468, 2020.

[122] M. Z. Aslam, Y. Corre, E. Björnson, and E. G. Larsson, "Performance of a dense urban massive MIMO network from a simulated ray-based channel," *EURASIP Journal on Wireless Communications and Networking*, vol. 2019, no. 1, p. 106, 2019.

[123] Z. Chen, E. Björnson, and E. G. Larsson, "Dynamic resource allocation in co-located and cell-free massive MIMO," *IEEE Transactions on Green Communications and Networking*, vol. 4, no. 1, pp. 209–220, 2019.

[124] A. Alkhateeb, "DeepMIMO: A generic deep learning dataset for millimeter wave and massive MIMO applications," *arXiv preprint, arXiv:1902.06435*, 2019.

[125] M. Yao, M. Sohul, V. Marojevic, and J. H. Reed, "Artificial intelligence defined 5G radio access networks," *IEEE Communications Magazine*, vol. 57, no. 3, pp. 14–20, 2019.

[126] V. Bhatia, M. R. Tripathy, and P. Ranjan, "Deep learning for massive MIMO: Challenges and future prospects," *9th International Conference on Communication Systems and Network Technologies (CSNT2020)*, pp. 26–31, 2020.